Understanding the interplay between structure and properties in phase separated copolymer blends prepared by free-radical polymerization

Analyse von Struktur-Eigenschafts-Beziehungen in phasenseparierten, durch radikalische Copolymerisation hergestellten Copolymermischungen

TECHNISCHE UNIVERSITÄT DARMSTADT

From the Department of Chemistry

at the Technischen Universität Darmstadt

to obtain the degree

Doctor rerum naturalium

(Dr.rer.nat.)

Dissertation by

M. Sc. Julien Fage

First reviewer: Prof. Dr. Matthias Rehahn
Second reviewer: Prof. Dr. Rudolf Pfaendner

Darmstadt 2024

Date of submission: 14.12.2023

Day of the oral examination: 19.02.2024

Fage, Julien: Understanding the interplay between structure and properties in phase separated copolymer blends prepared by free-radical polymerization

Darmstadt , Technische Universität Darmstadt

Year thesis published on TUprints: 2024

URN: urn:nbn:de:tuda-tuprints-267052

Date of viva voce: 19.02.2024

Acknowledgements

I would like to begin by expressing my heartfelt gratitude to all those who have contributed to the completion of this Ph.D. thesis. First, I would like to thank Prof. Dr. Matthias Rehahn for providing me opportunity to pursue research at Technical University of Darmstadt Fraunhofer Institute for Structural Durability and System Reliability LBF. I would also like to thank Prof. Dr. Manfred Döring for the rich and constructive discussions during the supervision of my project at Fraunhofer LBF. I would like to express my deepest gratitude to Dr. Frank Schönberger for the guidance and support, his outstanding example of scientific practice, and the great working atmosphere.

Special thanks go to the company INEOS Styrolution for financing the project with the Fraunhofer LBF, within the framework of which the present dissertation could be written. I would like to thank Dr. Niessner for the trust he has placed in me to execute this research. Furthermore, I would like to thank him, Dr Knoll and Dr. Schulz for their outstanding cooperation. The professional and personal exchange within the framework of the project meetings was not only a great pleasure throughout the entire period of the collaboration, but also served as a valuable opportunity to gain insights into the practical implementation of scientific research within an industrial setting.

I would like to thank my former colleagues at the Fraunhofer LBF for the pleasant working atmosphere. Particularly, I thank Maria Stec-Gokhale and Bettina Webber for the friendly atmosphere and coffee breaks. I would like to thank Dr Frank Malz for his assistance in NMR and TEM measurements. I specially thank Dr. Robert Brüll and Dr. Tibor Macko for the guidance in the SEC measurements.

My parents have worked tirelessly to provide me with a good education. Their dedication and love have shaped me into the person I am today, and I am forever grateful for their support. *Maman, Papa sans votre amour, support et dévouement, rien n´aurait été possible.*

Finally, there is no words to describe the unconditional support I received from my wife, Aleksandra. She is always there to discuss my work, offer constructive feedback, and celebrate my successes. I could not have done this without her.

List of publications

Publication:

Fage, J.; Knoll, K.; Niessner, N.; Carstensen, O.; Schulz, T.; Malz, F.; Döring, M.; Schönberger, F. Poly (Butyl Acrylate)-Graft-Polystyrene Synthesis by Free-Radical Polymerization: Interplay between Structure, Morphology, Mechanical, and Optical Properties. Polymers 2019, 11, 1317. https://doi.org/10.3390/polym11081317

Patents:

WO2018033444: Transparent graft copolymers based on acrylate soft phases

WO2018033445: Transparent graft copolymers based on acrylate soft phases

1. Table of content

2. Abstract in English and German

Polystyrene is the 6th most widely produced and used plastic in the world. Easy to produce and cost effective, it is a transparent and glassy polymer. However, it suffers from its inherent brittleness, which limits its use in certain applications. Enhancement of its toughness has been a focus in the last few decades. The incorporation of rubber particles in a polystyrene matrix allows to increase the toughness of the material but results in an opaque material. The development of block copolymer such as styrene-butadiene-styrene allowed to enhance further the flexibility and toughness of styrenic polymer, whilst keeping their excellent transparency. However, the method needed to prepare such polymers is cost intensive due to the infrastructures and purity of the reagents needed.

This work focusses on the development of graft copolymer prepared by free-radical polymerization. Free-radical polymerization offers numerical advantages compared to controlled polymerization as it does not require demanding conditions in terms of reagent and environment purity. Poly(butyl acrylate) is used as backbone polymer as it offers significant advantage in terms of UV stability in comparison to polybutadiene. As poly(butyl acrylate) does not have functionalities available for grafting with free-radical polymerization, butyl acrylate needs to be copolymerized with a comonomer. 2 routes have been explored for the synthesis of PBA-g-PS: Route A uses a copolymer backbone made of butyl acrylate and allyl methacrylate or DCPA whilst route B uses a copolymer backbone made of butyl acrylate and glycidyl acrylate or glycidyl methacrylate. In route A, the backbone can be used directly for grafting polymer with styrene, using the unreacted allyl or vinyl functionalities n the backbone. In route B, the backbone undergoes polymer analogous reaction where the glycidyl function is converted to acryloyl reactive groups using acrylic acid.

The influence of the type of polymerization, emulsion, or solution polymerization is studied for the preparation of the backbone. The graft copolymer blends made of PBA-g-PS and homo-polystyrene are studied in terms of optical and mechanical properties. Transmission electron microscopy is used to determine which type of morphology in the phase separated product is obtained when varying the backbone chemical properties. Finally, the influence of the type of processing, solvent casting or extrusion/injection molding are studied by analyzing the change in mechanical properties as well as the change in morphology.

Polystyrol ist der sechsthäufigst produzierte und verwendete Kunststoff weltweit. Einfach herzustellen und kostengünstig, handelt es sich um ein transparentes und glasartiges Polymer. Allerdings besitzt Polystyrol eine inhärente Sprödigkeit, welche seine Verwendung in bestimmten Anwendungen einschränkt. Die Verbesserung seiner Zähigkeit war daher in den letzten Jahrzehnten ein Schwerpunkt der Forschung. Die Einbindung von Gummipartikeln in eine Polystyrolmatrix ermöglicht die Erhöhung der Zähigkeit des Materials, führt jedoch zu einem undurchsichtigen Material. Die Entwicklung von Blockcopolymeren wie Styrol-Butadien-Styrol ermöglichte es, die Flexibilität und Zähigkeit von Styrolpolymeren zu verbessern, während ihre ausgezeichnete Transparenz erhalten blieb. Der für die Herstellung solcher Polymere erforderliche Prozess der kontrollierten Polymerisation ist jedoch aufgrund der benötigten Infrastruktur und Reinheit der Reagenzien kostenintensiv.

Diese Arbeit konzentriert sich auf die Entwicklung von Pfropfcopolymeren, die durch radikalische Polymerisation hergestellt werden. Die radikalische Polymerisation bietet gegenüber kontrollierter Polymerisation numerische Vorteile, da sie keine anspruchsvollen Bedingungen in Bezug auf Reagenzien- und Umweltreinheit erfordert. Poly(butylacrylat) wird als Grundpolymer verwendet, da es im Vergleich zu Polybutadien erhebliche Vorteile in Bezug auf die UV-Stabilität bietet. Da Poly(butylacrylat) keine für die radikalische Polymerisation verfügbaren Funktionalitäten aufweist, muss Butylacrylat mit einem Comonomeren copolymerisiert werden. Es wurden zwei Routen für die Synthese von PBA-g-PS erforscht: Route A verwendet ein Copolymergrundgerüst aus Butylacrylat und Allylmethacrylat oder DCPA, während Route B ein Copolymergrundgerüst aus Butylacrylat und Glycidylacrylat oder Glycidylmethacrylat verwendet. Bei Route A kann das Grundgerüst direkt für die Pfropfung von Styrol verwendet werden, wobei die nicht reagierten Allyl- oder Vinylfunktionalitäten im Grundgerüst genutzt werden. Bei Route B durchläuft das Grundgerüst zunächst eine polymeranaloge Reaktion, bei der die Glycidylfunktion unter Verwendung von Acrylsäure in die reaktive Acryloyl-Gruppe umgewandelt wird.

Der Einfluss des Typs der Polymerisation, welche für die Herstellung des Grundgerüsts verwendet wird, Emulsions- oder Lösungspolymerisation, wird untersucht. Die Pfropfcopolymerblends aus PBA-g-PS und Homo-Polystyrol werden hinsichtlich optischer und mechanischer Eigenschaften untersucht. Der Einfluss des Typs der Verarbeitung auf die physikalischen Eigenschaften des Materials wird ebenfalls untersucht. Transmissionselektronenmikroskopie wird verwendet, um zu bestimmen, welche Art von Morphologie im phasengetrennten Produkt entsteht, wenn die chemischen Eigenschaften des

Grundgerüsts variiert werden. Schließlich wird der Einfluss des Typs der Verarbeitung, Lösungsgießen oder Extrusion/Spritzgießen, untersucht, indem die Veränderung der mechanischen Eigenschaften sowie die Veränderung der Morphologie analysiert werden.

3. Introduction

Polystyrene (PS) was the first synthetic polymer to be prepared and has reports of its existence as early as 1839 [1]. It is nowadays one of the most widely used plastics with the scale of its production being 9 million tons per year [2]. PS is a glassy, amorphous polymer with outstanding transparency, gloss and processability. However, it suffers from inherent brittleness and poor chemical resistance which restricts its use in application where ability to withstand deformation is required.

In order to enhance the toughness of PS, two approaches are commonly used. The first method is the incorporation of a rubber phase in the PS matrix. The soft (or rubber) phase is dispersed in the hard PS matrix in the form of particles, due to the lack of compatibility between the components. The synthesis of high impact PS (HIPS) for example, is performed by polymerizing styrene in presence of polybutadiene (PB). Due to the chemical structure of PB, containing alkene functional groups, PS chains are partially grafted to it, which enhances the cohesion of the material and therefore its toughness and impact resistance. Similar processes were used to develop acrylonitrile-butadiene-styrene (ABS) and acrylonitrile-styrene-acrylate (ASA) polymers. Due to the mentioned immiscibility between rubber and PS, segregation into domains occurs. The size and organization of the formed domains determines the physical properties of the material, in particular its transparency. Since most of rubber-modified PS have domains size in the range of μm, larger than the wavelength of the visible light (400 nm), they are opaque [5]. In order to combine transparency and impact resistance, the refractive indexes of both phases must match, or the domain sizes must be well below the wavelength of the visible light.

A way to combine the properties of both polymers and reach low domain size is by the synthesis of copolymers. These molecules are known to self-assemble into a variety of ordered structures in the melt and in the solid state by a process called nanophase separation. These nanophase-separated structures endow these copolymers with outstanding mechanical and optical properties [3]. Copolymers also play a crucial role as compatibilizers and impact modifiers in polymer blends [4]. The development of controlled polymerization techniques allowed to design a variety of styrenic copolymers, in which hard and soft phases are segregating in nano-domains with a size as low as 20 nm [5-9].

Although controlled polymerization methods are powerful in the design of well-defined nanostructures of graft copolymers, they have some major drawbacks. Anionic polymerization requires high purity of solvents, monomers and atmosphere, and its application for acrylate-based systems has significant

limitations [10-12]. The use of atom transfer radical polymerization (ATRP) or reversible addition−fragmentation chain-transfer (RAFT) polymerization is advantageous in terms of monomer choice and simplified purification required compared to anionic polymerization. However, reaching high monomer conversion and sufficiently large molecular weight is challenging. Due to the high complexity of the controlled polymerization methods, the cost of their use in industrial production must be justified by high value application.

In contrast, free-radical polymerization offers numerous advantages over the controlled polymerization methods as it does not require demanding conditions in terms of reagent and environment purity. It allows use of a large variety of monomers in a simple, cost-effective, and industrially attractive process. However, the challenge of free-radical method in graft copolymerization process is the lack of selectivity of the grafting reaction. The reaction products are typically mixtures of the targeted graft copolymer and homopolymers by-product, which can lead to undesired macrophase separation and brittle properties. For example, in the synthesis of HIPS and ASA, the use of partially cross-linked PB backbone, in combination with the formation of homopolystyrene (h-PS) leads to large domains, making the product opaque. Therefore, finding the narrow window of synthesis conditions in terms of components ratio and reactivity is essential to reach the desired nanostructure between the graft copolymer and the homopolymer phases.

A method to develop grafting of styrene onto anionically polymerized PB to yield tough and transparent copolymers with nanolamellar morphology was, for example, reported by Portl [13]. It was demonstrated that the size of the PB backbone and PS side chains plays a major role in the formation of domains. Therefore, it also determines the mechanical and optical properties of the obtained material. The obtained product consisted of a blend of PB-g-PS and h-PS as it uses non-selective free-radical polymerization. The dosing of styrene monomer and initiator over the reaction course, instead of their addition at the start of the polymerization, proved to increase the grafting efficiency onto the backbone and avoid macrophase separation between the h-PS and the PB-g-PS.

3.1. Motivation, objectives, and concept of the work

The current applicability of impact-resistant PB-g-PS copolymers is facing the challenge of UV sensitivity due to the intrinsic properties of the PB backbone. A viable alternative to overcome this drawback is to use poly(butyl acrylate) (PBA) as backbone. PBA has similar mechanical characteristics to PB, with the advantage of being resistant to UV degradation [14]. Thus, the production of PBA-g-PS through

free-radical polymerization is of great interest. However, PBA does not contain radically active functionality in its structure, in contrary to PB which have available vinyl groups. Therefore, the approach for the development of PBA-g-PS is to establish synthesis method for incorporation of viable grafting sites into the PBA backbone and subsequently determine the optimal parameters conditions for the graft copolymerization.

The aims of this work are to:

- investigate the influence of the method of polymerization of the PBA-based backbone on the structure of the graft copolymer,
- establish an efficient method for the synthesis of PBA-g-PS/h-PS by successive free-radical polymerization and polymer analogous reaction,
- understand the correlation between the backbone molecular weight and functional groups frequency and the physical and morphological properties of the graft copolymer blend.

For the development of the PBA backbone, two routes are explored, in which butyl acrylate (BA) is copolymerized with a bifunctional comonomer. The first route uses a comonomer with two double bound functional groups having different reactivity. In this case, the more reactive function polymerizes during the synthesis of the backbone, while the less reactive function remains available for the graft polymerization step. The second route uses a comonomer containing a double bound and a different functional group, which is converted into alkene function in polymer analogous reaction. The type and amount of comonomer present in the backbone is expected to influence the backbone synthesis itself but also the grafting process. Consequently, the mechanical and optical properties of the blend as susceptible to be affected.

Independently on the route used for the preparation of backbone and subsequent graft copolymer, the method of their polymerization is an important factor affecting the final product properties. Emulsion and solution polymerization are the two methods used in this work, as each of them present practical advantages. Emulsion polymerization avoids any possible gel effect which can occur during the polymerization and the necessary removal of organic solvents. On the other hand, solution polymerization reduces the probability of cross-linking due to the dilution of the backbone in the solvent. The synthesis media not only influences the reaction kinetics and architecture of the PBA-based backbone and the PBA-g-PS/h-PS blend, but also determines the cost and feasibility for industrial production.

Due to the novelty of the process, a comprehensive investigation was carried out focusing on the method and conditions for the backbone polymerization as well as the grafting step. The influence of the resulting backbone structure is evaluated based on the physical properties of the PBA-g-PS/h-PS blends, as well as on their morphology. An important aspect of this work is to achieve compatibilization effect between PBA-g-PS and h-PS, through the formation of nano-segregated phases yielding mechanical resistance and transparency of the blend. As PBA-g-PS has potential application as compatibilizer or impact modifier, its blending in a PS matrix must be efficient. To study this phenomenon, the sizes of the domains are estimated based on transmission electron microscopy (TEM) images, while the grafting efficiency is analyzed by size exclusion chromatography (SEC).

3.2. Outline

The work presented in this thesis is divided into 6 chapters. The introduction, motivation and concept of this work are presented in chapter 1. Chapter 2 and 3 provide an overview on the theoretical background and state-of-the-art. The chapter 2 details the mechanical behavior of amorphous materials such as PS and the method to improve their flexibility, as well as the interplay between structure, morphology, and properties. Chapter 3 describes the graft copolymerization in the scope of this work and a short overview on the kinetics of the polymerization. Chapter 4 develops and discusses the obtained results. Chapter 5 summarizes the results from this work and gives an outlook on possibility for future development. Finally, chapter 6 describes the experimental methodology of synthesis and characterization used in this work.

4. Theoretical background

The goal of this work is to demonstrate how to synthesize flexible and transparent PBA-g-PS/h-PS blends using facile approach of free-radical polymerization. The strategy to be followed for this purpose is to obtain defined nanomorphology of the material, allowing to reach the desired physical properties and mechanical response.

To understand and develop experimental tools to pursue the objectives of this work, this chapter introduces the fundamental concepts of deformation behavior of amorphous polymers and approaches in overcoming their brittleness. The factors influencing the phase separation phenomenon in copolymer systems are explained. Additionally, an overview is provided on methods of synthesis for graft copolymers.

4.1. Behavior of thermoplastic polymers under deformation

Unlike crystalline polymers, which have a complex structure made of heterogeneous zones, amorphous polymers can be considered a homogeneous entanglement network. The presence of entanglements in the material is an essential prerequisite for mechanical strength. Amorphous materials are deformed in a mechanically reversible manner up to the limit of linear viscoelastic response. This typically corresponds to an elongation at break between 0.1 and 1%. This deformation, called elastic extension, is mainly due to an increase of intersegmental distance, shear displacement and conformational changes. The elastic extension leads to the formation of voids in regions of high tensile stress which relieve the constraints.

The response to the void formation is different depending on the type of polymer studied. In amorphous polymers, two responses are observed: craze formation or homogeneous plastic deformation. The Kausch model as represented in Figure 1 will be used to explain the deformation behavior [15].

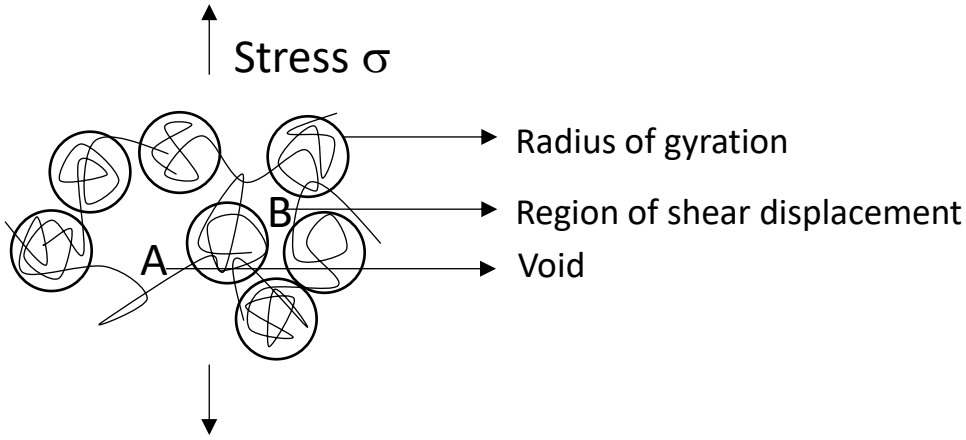

Figure 1. The Kausch model of craze nucleation in amorphous polymer. After [16].

The network of entanglement is schematically represented by statistically coiled subchains of molecular mass Me between entanglements with a radius of gyration represented as circle on the figure. The features essential to craze initiation are: (i) the increase of intersegmental distances, (ii) the increase of free volume and its accumulation in sites of lower entanglement density and (iii) the resulting heterogeneous distribution of local stress. The created stress can be relieved by shear displacement, as in region B, or by the formation of voids which appear preferably in region of low entanglement as in region A. It has been demonstrated that initial voids can be formed without breaking the entanglement network. Therefore, it is considered that a void formed in the early stage of deformation would close upon release of the applied stress. This means that void formation does not necessarily lead to the creation of a craze. However, in case adjacent voids are formed in a perpendicular direction to the largest component of stress σ, the void initiates the formation of crazes.

The microstructure of an amorphous polymer under uniaxial stress is depicted in Figure 2. The lens-shaped cavity shown is a craze with a thickness of 1 to 10 μm and a diameter of 10 to 1000 μm. The different cavities are bridged by fibrils made of several polymer molecules and have a diameter of about 10 to 100 nm.

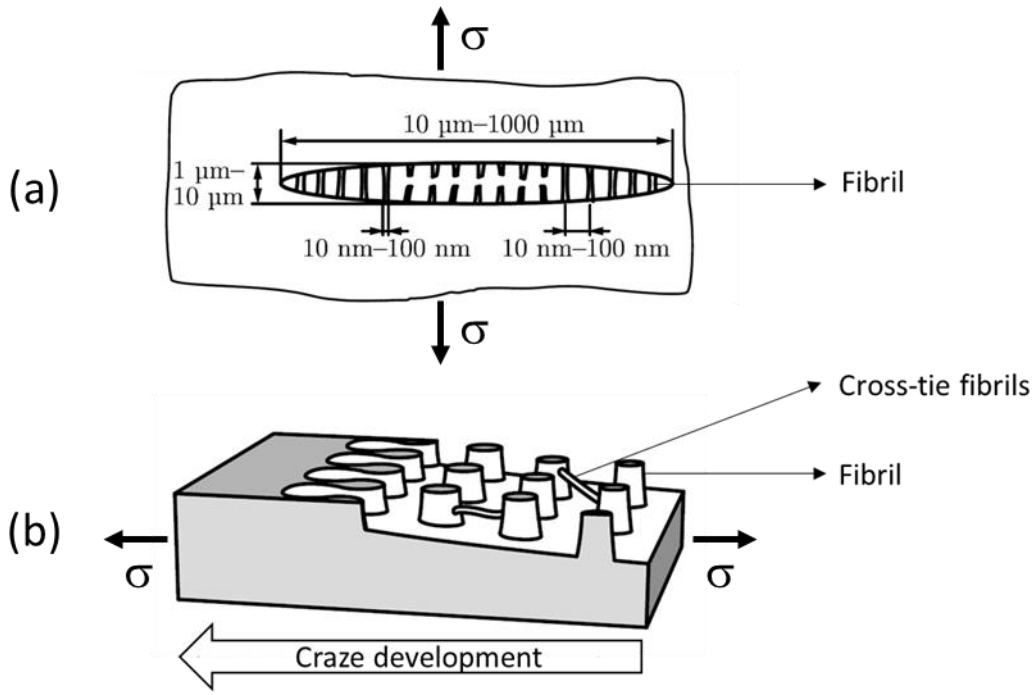

Figure 2. (a) Cross-sectional view of a craze and (b) partial representation of the edge of a craze. After [17].

Although the fibrils in the craze represents only 10 to 50 % in volume, the reduction of the material strength compared to its undeformed state is negligible. Indeed, the chain molecules within the fibrils are elongated and can bare a higher load than when entangled in the bulk material. Despite this load bearing ability of the fibrils, the stress concentration near the edge of the craze causes its propagation. The growth mechanism of a craze is called meniscus instability and is represented in Figure 3. Subsequently, new fibrils are created near the edge of the craze. The fibrils in the center of the craze initially elongate by drawing other chain molecules from the bulk material. Connections between fibrils, called cross tie fibrils, can form when opposite ends of chain molecule are drawn into neighboring fibrils (see Figure 2, (b)). Finally, fibrils in the center of the craze break. The craze then grows at constant load and eventually causes the fracture of the polymer.

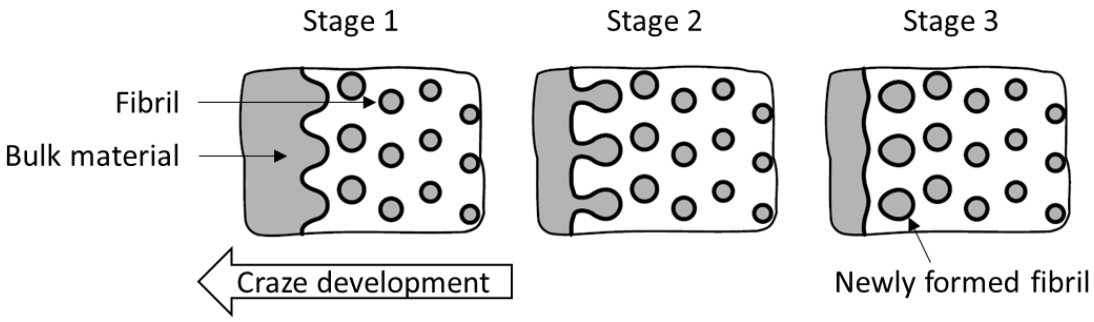

Figure 3. Growth of a craze by a meniscus instability – Top view. After [17].

The formation of initial voids and the possible further development of crazes depends on the type of polymer studied. The creation of additional voids can be affected if the stress transfer between neighboring sites is weakened. This can happen by shear deformation of the coiled sub chains and the resistance to cavitation, due to a high number of entanglements crossing the future craze plane. This effect has been successfully demonstrated by a correlation between the critical craze initiation stress σ_c and the entanglement density ν_e as shown in Figure 4.

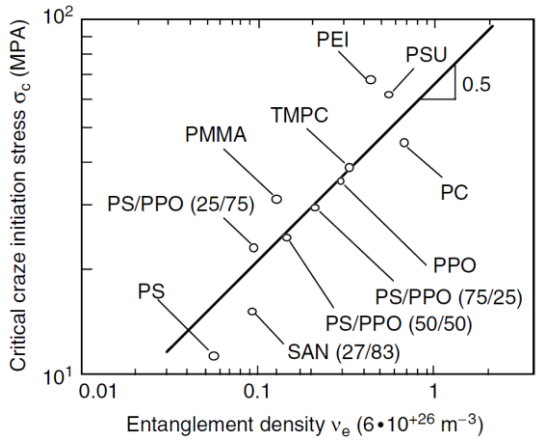

Figure 4. Correlation between entanglement density ν_e and critical craze initiation stress σ_c. After [18]

It is clear that amorphous polymers such as PS, Poly(methyl methacrylate) (PMMA) and polycarbonate (PC) have different ν_e and as a consequence different σ_c. This means that PS is more likely to form crazes in comparison to PMMA, itself more likely to form crazes in comparison to PC. This kind of structural differences between materials influence their mechanical behavior as observed in the Figure 5 with the stress-strain curves of PC and PS.

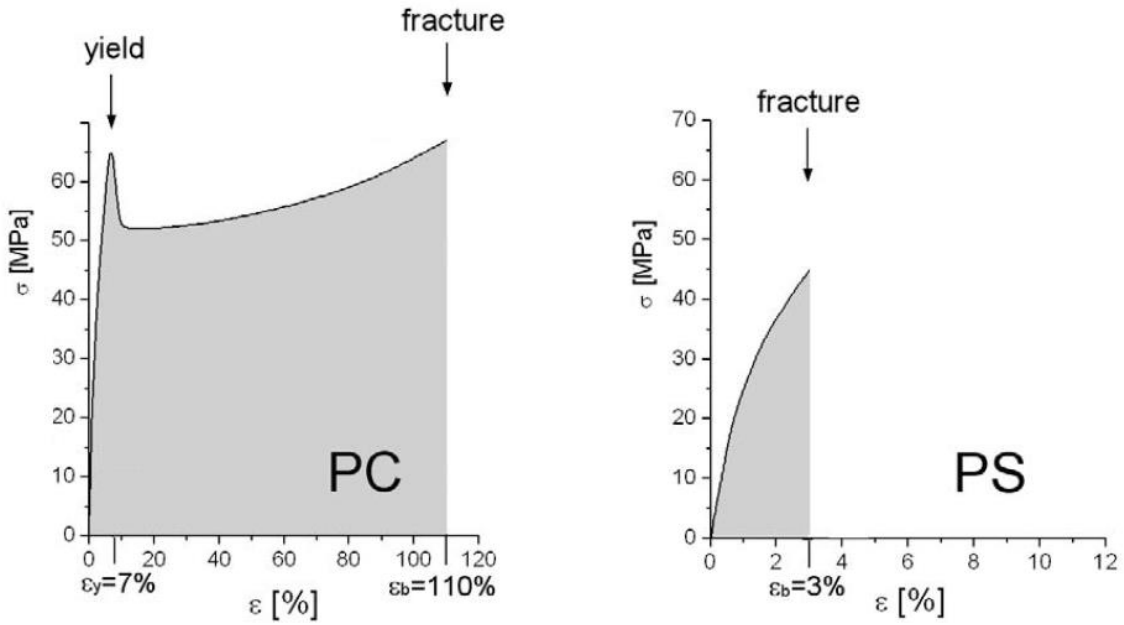

Figure 5. Typical stress-strain curves of PC (left) and PS (right). After [13].

PC is a ductile material that can stretch to an elongation at break of 110 %. On the contrary, PS is a brittle polymer that can absorb only little mechanical energy and have low elongation at break (max 3%). This high difference in mechanical behavior is correlated to the entanglement density of the polymers but also to their deformation mechanism. As already described, PS undergoes deformation by the formation of crazes due to the low value of σ_c [18]. In the contrary, PC has high ν_e and σ_c and deforms elastically, reaching high strain before fracture [19].

4.2. Toughness enhancement of amorphous polymers

Different methods are commonly used to enhance flexibility and toughness of brittle polymer such as PS. A non-exclusive list includes: (i) rubber network yielding, (ii) inclusion yielding, (iii) self-reinforcement, (iv) phase transformation toughness, (v) rubber particle toughening and (vi) thin layer yielding. A focus will be put on the latter two mechanisms as they are the most used in case of PS.

4.2.1. Rubber particle toughening of brittle polymers

The rubber toughening of brittle polymers such as PS or PMMA was introduced in the late 1940s and has been studied extensively since then. It consists of the addition of a small amount of rubber particles in a thermoplastic matrix (usually 5 to 25 %). The rubber particles present in the matrix increases the toughness of the material by:

- Initiating and multiplying the deformation process in the matrix polymer;
- Stabilizing the crack propagation by bridging developing cracks;
- Blunting the crack tip by reducing the detrimental dilatational stress field in the matrix by internal voiding (limitation of the free crack length in the matrix).

It was first used when PB was added/grafted to PS or styrene-acrylonitrile (SAN) matrix, leading to high impact PS (HIPS) and acrylonitrile-butadiene-styrene copolymer (ABS) [6]. The deformation of this kind of material proceeds through three-stage mechanism of toughening as depicted in Figure 6.

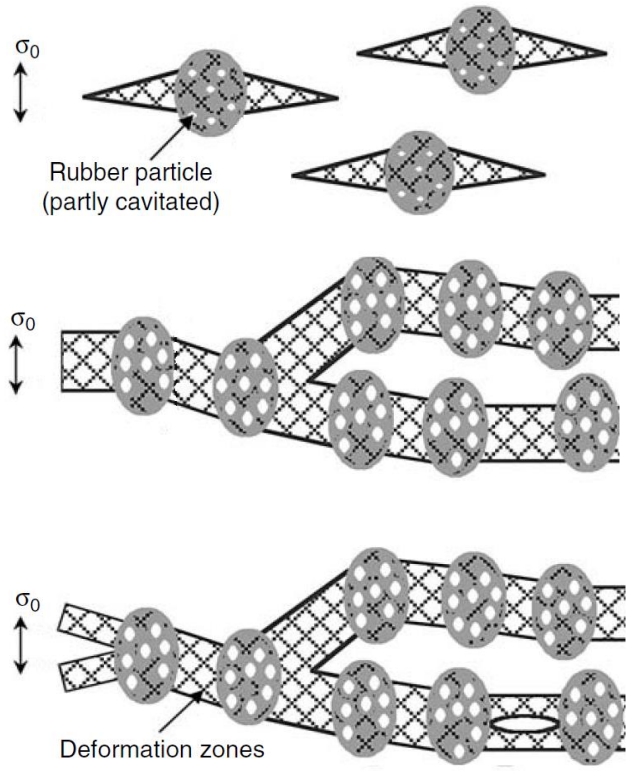

1. Plastic deformation: Generation of stress concentration around the rubber particles and possible cavitation inside the particles

2. Plastic strain softening: Local yielding in the matrix with multiple crazing and extensive shear yielding

3. Strain hardening of the yield zone:
Stretching of the rubber particles to high strains. In samples containing notches or cracks, the rubber particles stop the cracks, preventing further propagation and fracture

Figure 6. Schematic representation of the three-stage mechanism of rubber particle toughening. After [20].
σ_0: Main stress component.

The effectiveness in the increase of material toughness depends on the particles structure and on the deformation process in the host polymer. One of the challenges met in the addition of rubber particles in a stiff matrix is the compatibility between the phases. It was deduced that the surface of the particles must be grafted to the matrix in order to increase compatibility between the phases [16]. In materials such as HIPS, the grafted material covers the outside layer of the particle like a shell. The grafted material improves the adhesion between the rubber particle and the PS, avoiding the debonding of the rubber particle from the matrix.

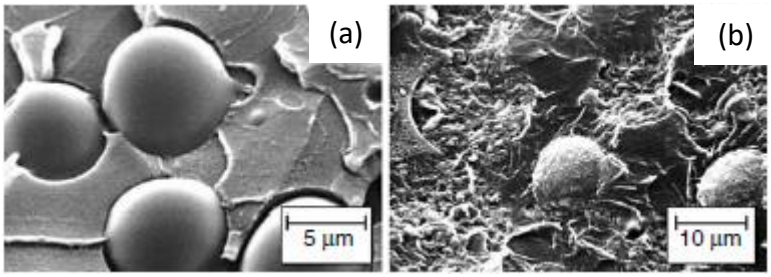

Figure 7. Fracture surface of rubber modified PS in (a) ungrafted PB rubber and (b) PB grafted with PS. After [20].

To demonstrate this principle, Figure 7 compares the fracture cross-section of two types of rubber-modified PS. In Figure 7 (a), PB particles are blended in a PS matrix and Figure 7 (b) is HIPS copolymer. The difference between the two materials fracture behavior is evident. In case of ungrafted PS/PB blend, the particles are highly visible indicating strong crack propagation around them. This is a direct consequence to the fact that there is no bonding between the particles and the matrix. On the contrary, in case of HIPS copolymer (Figure 7 (b)), the rubber particles are grafted to the PS matrix by the shell and the cracks propagate straight through the rubber particles. The advantage of this grafting is confirmed by the values of impact strength of these two materials. The non-compatibilized blend has a notched impact strength of 14 $kJ.m^{-2}$ against 50 $kJ.m^{-2}$ for the HIPS copolymer. This confirms that strong adherence between particles and matrix is essential in crazing material such as HIPS.

4.2.2. Thin layer yielding

To further enhance the toughness of PS and to reach new properties, block copolymers have been developed [16]. This type of copolymer allows control over the structure on a nanometer scale and enables the combination of high mechanical stability with other properties such as transparency or UV resistance. Due to the immiscibility of most polymers, block copolymers tend to segregate into domains, and form ordered structures called microphase-separated structures. These structures are highly dependent on the ratio between the two polymer phases, the global architecture of the block copolymer as well as the processing method and conditions.

As previously presented, PS forms crazes under uniaxial deformation. In a craze, the material is plastically deformed to a high degree. Fibrils are stretched between micro-voids along the direction of stress and interconnected by cross-tie fibrils. It was determined that the thickness of the fibrils is around 10-20 nm and that the maximum strain at break of the craze fibrils is around 200-300 % [21]. The dichotomy between the elongation at break of bulk PS and the one of fibrils, which can be

considered thin layered PS, has been extensively studied. Michler et al. studied different types of styrene/butadiene copolymer with high PS content (74 wt.%) and lamellar morphology [22]. The thickness of the PS layer in these copolymers was in the range of 20 nm and allowed high deformation behavior. The ductile deformation of PS in this type of material is called thin layer yielding. By addition of pure PS to the copolymer, the PS lamellar size were increased above 30 nm and the deformation behavior changed from homogeneous yielding to the formation of numerous small crazes. The addition also leads to an increase of microhardness of about 80 %, more than predicted by additivity law. This confirms a rigidification of the lamellae with the increased width.

With further increase of the PS lamellar size, the number of crazes was reduced to few large crazes, similar to bulk PS. This increase in the lamellar thickness is correlated to the decrease in elongation at break of the material as depicted in Figure 8.

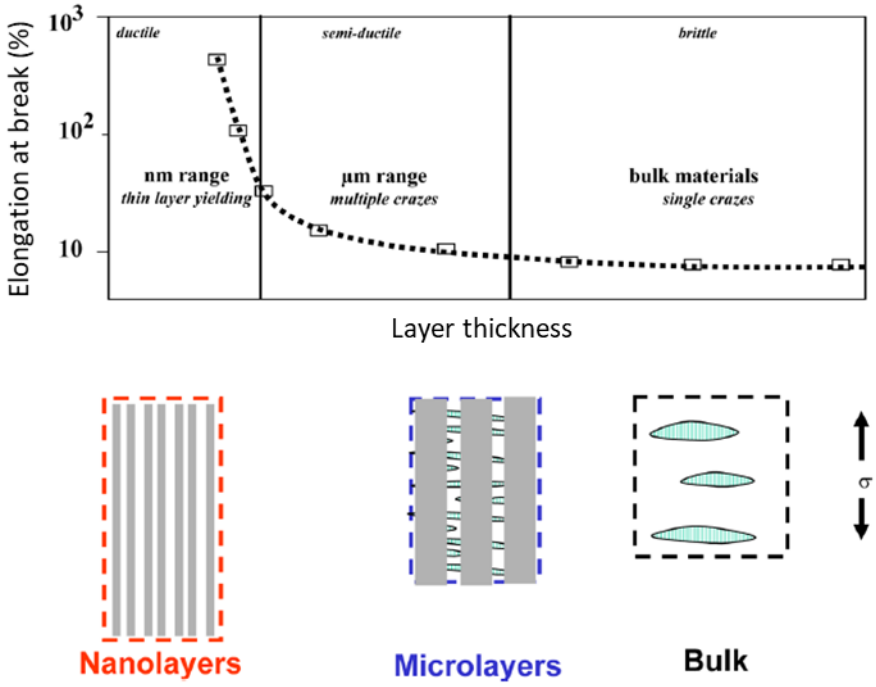

Figure 8. Transition of micromechanical deformation behavior with decreasing PS layer thickness. After [21]

The thin layer yielding is obtained not only in block copolymer but also in blends of PS with another polymer. Van der Sanden et al. have produced multilayered tapes of PS and PE by co-extrusion [23, 24]. They varied the thickness of the PS layer by varying the PS to PE ratio. It was demonstrated that the elongation at break of PS was increased from around 3 % for PS to about 30 % for multilayered PS/PE material with a PS thickness below 1 µm.

The different cases previously presented show significant differences in the arrangement of the layers and nature of the surface: free surfaces surrounding craze fibrils and chemically bounded PB in SBS copolymers. However, a common upper thickness limit to thin layer yielding appears around 20 nm.

The existence of the limit for both types of layer arrangement indicates that thin layer yielding is not a thermal effect resulting in the decrease of glass transition temperature (T_g). Indeed, it was studied that T_g of thin, free films of PS and PMMA was reduced compared to their bulk structure [25, 26]. However, investigation on the SBS block copolymers revealed no decrease of T_g in the PS phase compared to bulk PS [22]. The reduction of T_g in a thin, free film is explained by the presence of more free chain ends leading to an increase in the free volume and larger molecular mobility. In block copolymer such as SBS, the PS chains are not free and are connected to PB chains. Therefore, no reduction of T_g can be observed.

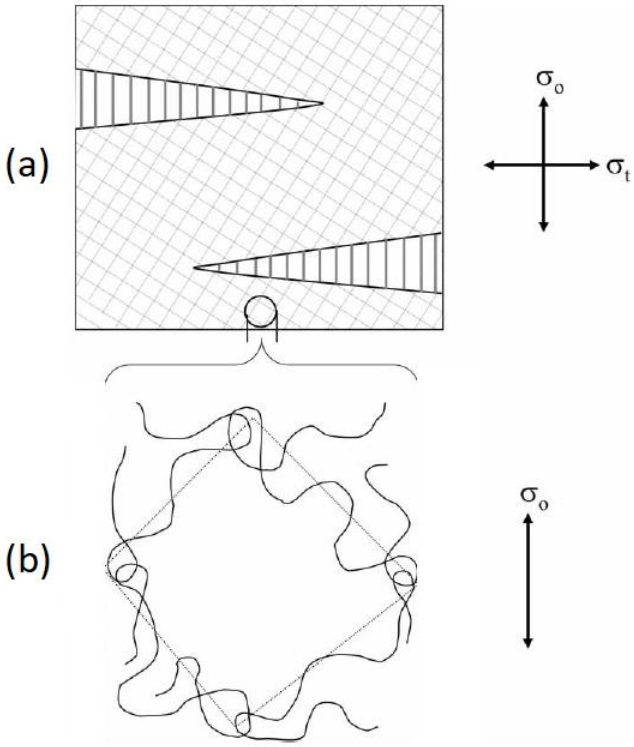

Figure 9. Entanglement networks and state of stress in a (a) bulk polymer and (b) 20 nm thick layer. After [21].

The geometry of a polymer under deformation is best analyzed with the entanglement network model of crazing in a bulk sample as represented in Figure 9 (a). When the sample is exposed to stress, the meshes stretches and dilate. In case lateral constraints are present, voids are forming, and the network elongates in a narrow zone, resulting in the formation of craze. However, if the thickness of the sample

is reduced to about 10 μm, only shorter crazes can form which are less likely to transform into cracks [27]. This means that more crazes can be formed in such a layer. A large number of crazes forming means a larger volume of the polymer which is plastically deformed as described in Figure 8. The reduction of the thickness to about 20 nm is comparable to the mesh size of the entanglement network in PS. In this situation, the stress is transmitted only in the direction of stress as depicted in Figure 9 (b). In such an arrangement, lateral constraints are absent and it is clear that the macromolecules can be stretched to their maximum extension ratio without the formation of crazes or cracks. It is determined that the maximum extension ratio in PS lies about λ_e=4 which corresponds to 200-300 % in elongation at break. If the thickness of the layer is about two times the mesh size, same entanglement will be present in the lateral direction. As a consequence, the stress in the lateral direction σ_t is increased and the main stress component σ_o is reduced by a factor $2\nu\sigma_t$ with ν the Poisson´s constant. As showed in Figure 10, σ_1 and σ_t vary with the layer thickness d. σ_1 decreases while σ_t increases around 2 times the entanglement mesh size. Above these values, the two stress components are stabilizing in value.

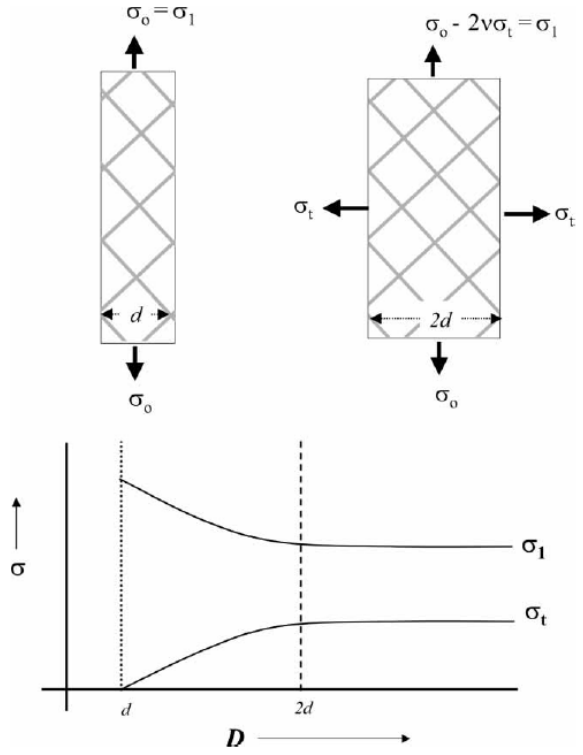

Figure 10. Change of stress in an entanglement network with increasing layer thickness. σ_o applied load, σ_1 stress component in direction of load and σ_t stress component in transverse direction. After [21].

The described consideration can also be extended to other brittle material such as PMMA or SAN. As an example, PMMA has a Me of about 9.1 kg/mol in comparison to PS M_e at 17.5 kg/mol [21]. This means that the entanglement mesh of PMMA has a higher density and the value of d showed in Figure 10 is about 10 nm compared to about 20 nm in case of PS. Consequently, the thin layer yielding effect is smaller for PMMA than for PS.

2.1. Phase separation in copolymers

The nanostructure formed by block copolymers (di, triblock or graft copolymer) in the solid state is of practical interest. Indeed, the control over the morphology is fundamental in achieving application-relevant mechanical and optical properties. The phase behavior of an AB block copolymer is determined by three experimentally controllable factors [28-32]:

1. The overall degree of polymerization N;
2. Architectural constraint (diblock, triblock, star or graft) and composition (ratio between the two phases);
3. The A-B segment-segment interaction parameter χ.

The two first factors are determined by the polymerization conditions and stoichiometry whereas the magnitude of χ is determined by the selection of A-B monomer pairs and has a temperature dependency which is given by:

$$\chi = \frac{\alpha}{T} + \beta \qquad (1)$$

Where α and β are constant depending on composition and architectural constraint of the copolymer.

The decrease of temperature leads to an increase of the interaction parameter χ and favors a reduction in A-B segment contacts. If the value of N is sufficiently large, it is accomplished with loss of translational and configurational entropy by local composition ordering [31]. This type of segregation is called microphase separation in the block copolymer. On the contrary, if χ or N is decreased, the parameter χ decreases and lead to a compositionally disordered phase. It was determined that the product χN, called reduced interaction parameter, is dictating the block copolymer phase state [28, 29, 32].

Two regimes are mainly described depending on the value of χN: weak segregation limit and strong segregation limit. The weak segregation limit corresponds to low values of χN, for example in the

copolymer melt (high temperature) and is characterized by wide interface due to enhanced phase mixing. With increased value of χN, strong segregation appears where A and B domains are formed. The interface between the constituent domains is narrow (about 1 nm) and the system minimizes the total area of such an interface by decreasing the energetically unfavorable contacts.

Microphase separation is a process in which two competing effects are at stake. Antagonist blocks prefer to segregate due to chemical incompatibility. However, the spatial extent of the phase separation is limited by the connectivity of the blocks imposed by the molecule architecture. Therefore, the ratio between the two phases is one of the most important factors determining the phase morphology of block copolymers. The shape of the polymer/polymer interface varies with chain length of each component polymer represented by their volume fraction Φ [31, 33-35].

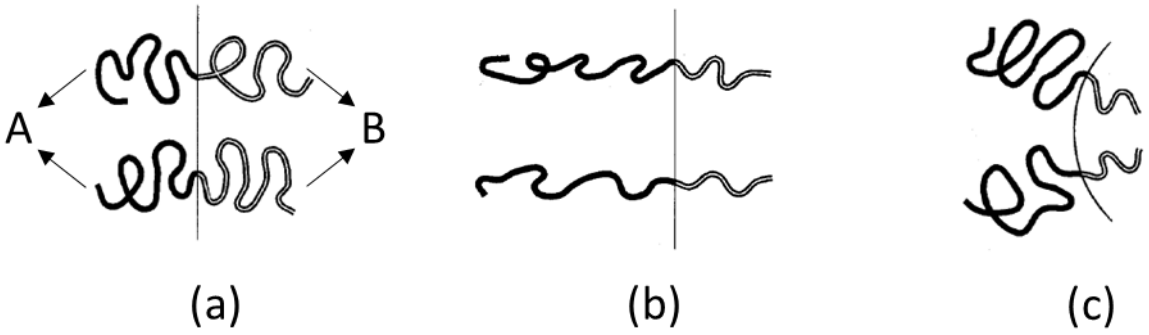

Figure 11. Schematics of chain conformation at the microphase-separated state (a): stable flat interface from a symmetric AB block copolymer where $\Phi_A=\Phi_B$; (b) an unstable flat interface in the case $\Phi_A>>\Phi_B$ and (c): Curved interface where $\Phi_A>>\Phi_B$. After [32].

In a compositionally symmetric AB diblock copolymer (when $\Phi_A=\Phi_B$), the interface formed is linear as depicted in Figure 11 (a). When the volume fraction of A relative to that of B increases, it is more likely that the interface formed will be curved. The A chains would have to stretch significantly to form an instable flat interface as depicted in Figure 11 (b). In this case, the conformational entropy loss of the component A is too high. To gain the conformational entropy, the A chains tend to expend along the direction parallel to the interface. Consequently, the interface becomes convex towards the minor component B as in Figure 11 (c). The effect of interface curvature becomes more and more pronounced as the composition of the block copolymer becomes further asymmetric. The morphological variations observed in a diblock copolymer are shown in Figure 12 [36, 37].

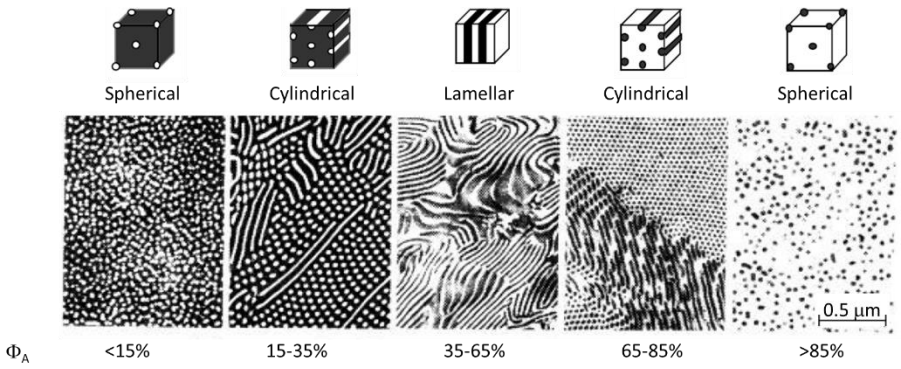

Figure 12. TEM images showing classical morphology of diblock copolymers depending on the ratio of the two phases. After [38].

The most asymmetric block copolymer (where Φ_A <15%) exhibits spherical morphology, with body centered cubic spheres of the minor component A dispersed in a matrix of the major component B. When Φ_A increases to 15-35 %, cylindrical morphology is formed with hexagonal packed cylinders of minor component A in a matrix of the major component B. Symmetric block copolymer (where $\Phi_A=\Phi_B$) exhibits lamellar morphology consisting of alternating layers of each component. With further increase of the component A, the morphology appears in reverse order (hexagonal B cylinders in A matrix and B spheres in A matrix) [32].

The morphologies discussed above and shown in Figure 12 are classical and verified by different studies in styrene/diene systems [39, 40]. However, different types of non-classical bicontinuous morphologies have also been described in diblock or star block copolymers [41, 42]. Some of the morphologies are considered transient when others, such as the gyroid type has been identified as stable. With ABC triblock copolymer, another number of unconventional morphologies have been described [43-49]. The presence of a third block in the copolymer structure leads to new interactions and the morphological features are therefore complex to study.

The development of living polymerization techniques has enabled scientist to design elaborated architectures of block copolymers. The block copolymers can nowadays range from two-component linear macromolecules to multi-component radial and branched chains such as star, miktoarm star or graft copolymers. The modified molecular architecture of block copolymers may significantly alter their phase behavior [22, 37, 50-53]. Consequently, the restriction of changing composition (e.g., in AB diblock copolymer) to achieve the desired morphology can be overcome. Different types of block and graft copolymers have been studied by Hadjichristidis et al. and showed a significant change in phase

behavior between those systems compared to diblock copolymer at similar composition [52, 54, 55]. As an example, lamellar morphology was observed with a miktoarm star copolymer in a composition range in which a cylindrical morphology would be expected for a diblock analogue. As the symmetry of a copolymer has proven to have major influence on its morphology, theoretical studies on the impact of molecular architecture have emerged. Milner calculated the phase diagram of asymmetric miktoarm and demonstrated that the stability window for a particular morphology highly depends on the copolymer architecture. His study successfully predicts the phase behavior of miktoarm star and graft copolymers [50].

The development of A_1BA_2 diblock copolymers (where A_1/A_2 and B are glassy and rubbery blocks, respectively, and $M_{A1}/M_{A2} \neq 1$ where M represent the molecular weight) accentuated the change in phase behavior compared to analogue diblock copolymers. Matsen et al. examined the phase behavior of such copolymers and observed a drastic shift in morphology behavior in comparison to symmetrical ABA triblock copolymers [51]. In this study, an asymmetry factor τ is introduced, whose magnitude lies between 0 for AB diblock and 0.5 for symmetric ABA triblock copolymer. Figure 13 represents the calculated phase diagram of a triblock copolymer depending on τ in function of Φ_A.

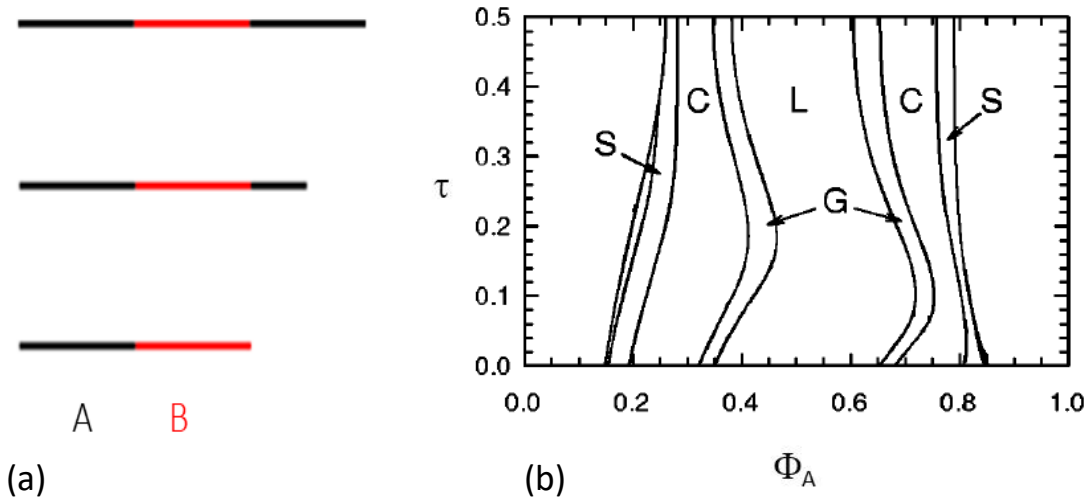

Figure 13. (a) Evolution of ABA triblock copolymer structure with τ and (b) phase diagram of an asymmetric triblock copolymer. S: Spherical C: cylindrical, L Lamellar, G: Gyroid. After [51].

An increase of τ represents an increase in the outer A chain length as described in Figure 13, left. When increasing τ, the transition lines are shifted towards higher overall Φ_A. For example, this theory predicts lamellar morphology for an A_1BA_2 triblock copolymer with an asymmetry factor of 0.1 and a Φ_A of 0.7.

It can be observed that with a similar composition, a diblock copolymer (τ = 0) and a symmetrical triblock copolymer (τ = 0.5) would show a cylindrical morphology. A τ value of 0.1 represents a A_1BA_2 triblock copolymer with short A_2 chain. In this type of configuration, the shorter glassy chain can interact and blend with the rubbery block. As a consequence, the presence of the short A_2 chain does not influences the morphology in comparison to a AB diblock copolymer with Φ_A = 0.65 but the overall amount of PS is increased [16, 51].

Most of the block copolymer made of rubbery and glassy blocks are used with other polymers or additives. In particular, block copolymers are used in combination with homopolymers identical with the constituent blocks of the block copolymer [56-60]. The main application is in blends of PS/PB copolymer with PS [56, 58]. The behavior of the material is influenced by the introduction of homopolymer in the system and can be correlated with a change in phase separation. The main factor influencing the morphology of a copolymer/homopolymer is the length of the homopolymer chain compared to that of block copolymer. The composition of the binary blend determines the type of phase separation: microphase or macrophase separation. Hashimoto et al. studied homopolymers having different interactions in blends with styrene/diene copolymers (AB diblock and ABA triblock) [35, 61-65]. In the case of h-PS in blends with styrene/diene copolymers, three regimes have been identified, depending on the degree of polymerization of the h-PS ($N_{h\text{-}PS}$) compared to that of the PS block in the copolymer ($N_{PS\text{-}block}$):

- If $N_{h\text{-}PS} < N_{PS\text{-}block}$: the h-PS chains are solubilized selectively in the PS domains of the phase separated copolymer and are weakly segregated towards the domain center. It leads to an increase in interfacial area per block, causing swelling of the PS blocks and possibly inducing a change in morphology;
- If $N_{h\text{-}PS} \approx N_{PS\text{-}block}$: the h-PS is still solubilized selectively in the PS domains of the phase separated block copolymer. The h-PS chains tend to be localized in the middle of the PS domains. Therefore, the interfacial area is not affected significantly. In this regime, PS block chains are not substantially swelled;
- If $N_{h\text{-}PS} > N_{PS\text{-}block}$: macrophase separation takes place, leading to the formation of h-PS particles in the microphase separated copolymer matrix or vice-versa. The composition of the blend determines which component form the matrix.

In the first two cases, blending of the h-PS in the PS blocks affects the morphology of the copolymer. For example, in a pure lamellar polyisoprene/PS (PI/PS) diblock copolymer, the molecular volume of the two blocks is identical and the interface between the two phases is flat (see Figure 14 (a)). When a lower average molecular mass (M_n) h-PS compared to the PS block is introduced in the mixture, the added h-PS chains are solubilized in the PS phase and the PI phase is unaffected (see Figure 14 (b)). In this situation, the PS block chains should stretch or the PI chains should be compressed in order to keep a constant segmental volume in each phase. Since the first process is entropically favored, a curved interface is formed in order to maintain a uniform packing density (see Figure 14 (c)) [35]. As the volume fraction of added PS increases, the interface changes to convex curvature toward the dominating PS phase.

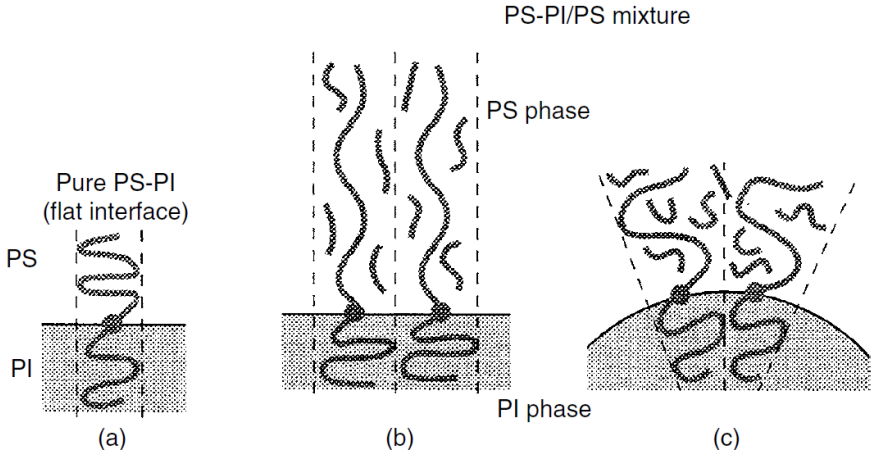

Figure 14. Schematic representation of the morphology transition in h-PS-PI/PS blends with $N_{PS\text{-}block} > N_{h\text{-}PS}$. After [35].

The understanding of this change of morphology is essential when the copolymer is used as an impact modifier in a matrix. A correlation between the change of morphology and the change of physical properties due to the addition of h-PS in PS/PB copolymer has been studied extensively [66-68].

4.3. Deformation behavior of styrenic block copolymers

In the early 1960s, domain theory was proposed to explain the mechanical deformation of SBS thermoplastic elastomers [58, 59]. It postulates that these materials are made of glassy domains dispersed in rubbery matrix, holding the elastomer network together by means of physical cross-links. The development of electron microscopy confirmed this theory, which is currently accepted as a basic model in explaining the mechanical properties of block copolymers. This knowledge pointed out

in which application the control of the nanostructure is essential and determines the strength and ductility of the product.

PS/PB copolymers provide a model for the structure/properties relationship study of phase separated copolymer. As depicted in Figure 15, the stress-strain curve of SBS triblock copolymers is dependent on the amount of PS, hence on its phase morphology. The behavior of such copolymers can be divided in three groups:

1. Rubber-elastic behavior: At low PS content, PB forms the matrix. The copolymer behaves as an elastomer and deforms homogeneously under tension;
2. Ductile behavior: When the copolymer reaches symmetrical composition, alternating layers of PS and PB are formed. The macroscopic drawing and neck-formation prevails during deformation;
3. Brittle behavior: With an increase of PS content, the PB becomes the dispersed phase. Consequently, the tensile strength increases and the elongation at break decreases. The copolymer breaks in a brittle manner due to the localized deformation with development of crazes (see Figure 8).

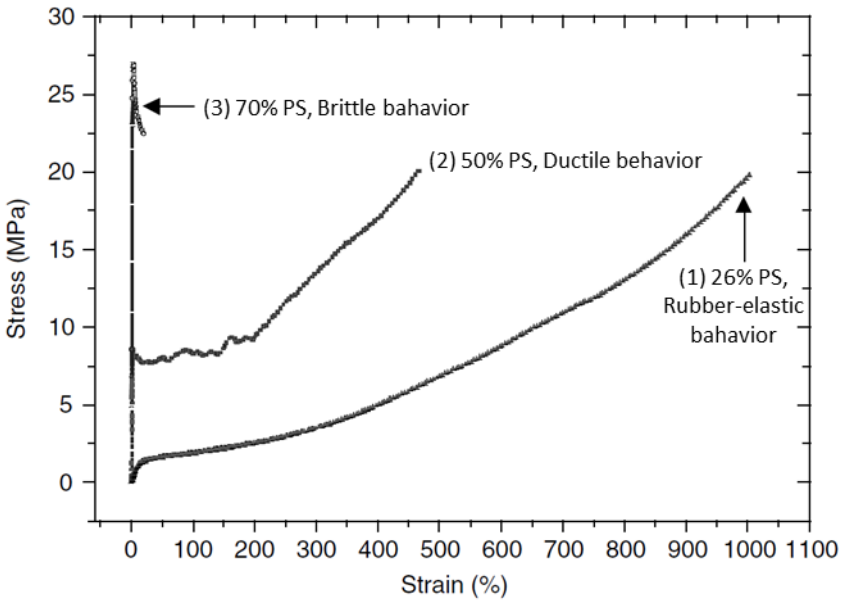

Figure 15. Stress-strain curves of solvent-cast SBS triblock copolymers. Three different compositions are represented. After [36].

The deformation and fracture processes are influenced by the nanostructure of the material and have been extensively studied in copolymers with lamellar morphology [69-72]. Fujimura et al. investigated

the deformation of SBS copolymer with unoriented lamellar structure. Stretching the material beyond the yield point resulted in chevron-like morphology having four-point small angle scattering pattern.

Cohen et al. studied the deformation of lamellar SBS triblock copolymer by applying the deformation to the sample in parallel, perpendicular and diagonal direction to the lamellar orientation [73]. Perpendicular stress led to the formation of chevron-like morphology as depicted in Figure 16 (b).

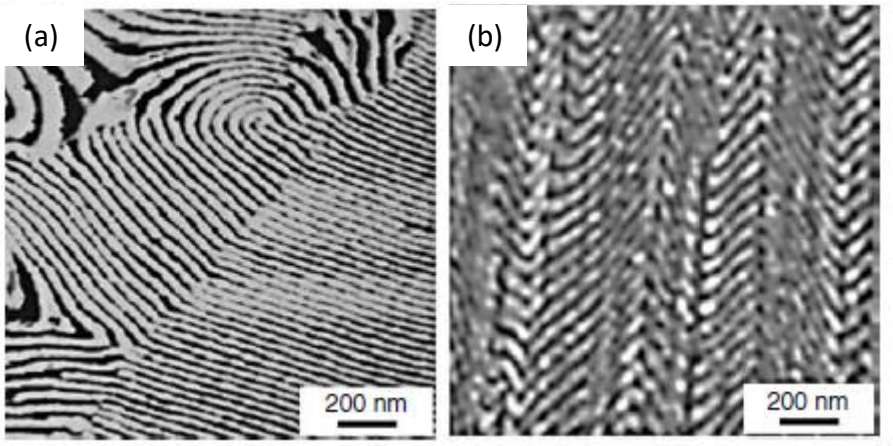

Figure 16. AFM pictures of lamellar SBS triblock copolymer (a) before deformation and (b) after deformation in the direction perpendicular to the lamellar arrangement. After [74].

It was shown that a perfectly aligned lamellar block copolymer exhibits a critical undulation instability under exposure to perpendicular deformation. Deformation occurs by shearing of the rubbery layer between the glassy layers. In order to maintain the parallel arrangement of the layers, the wavelength of the undulations is not large. It was suggested that the nucleation of the chevron-like deformation appears at the region of local defects. The layers located near these defects are slightly misaligned and respond first to the applied stress by rotating away from the strain direction. The layers rotate in opposite directions in the vicinity of defects, causing the nucleation of chevron-like bands also called kink bands. With increasing stress, the kink band propagates parallel to the deformation axis into neighboring layers [73, 75].

The deformation behavior differs when the stress is applied parallel to the orientation of the lamellae. Figure 17 shows the behavior of SBS star block copolymer before and after deformation along the lamellar orientation. The undeformed sample have PS lamellae thickness and spacing of 20 and 42 nm, respectively (see Figure 17 (a)). Deformation in the lamellae directions leads to plastic drawing of both PS and PB phases as in Figure 17 (b). As a result, the thickness and spacing of PS lamellae are reduced

to half their original values. The material is deformed to high degree without any cavitation or micro-void formation.

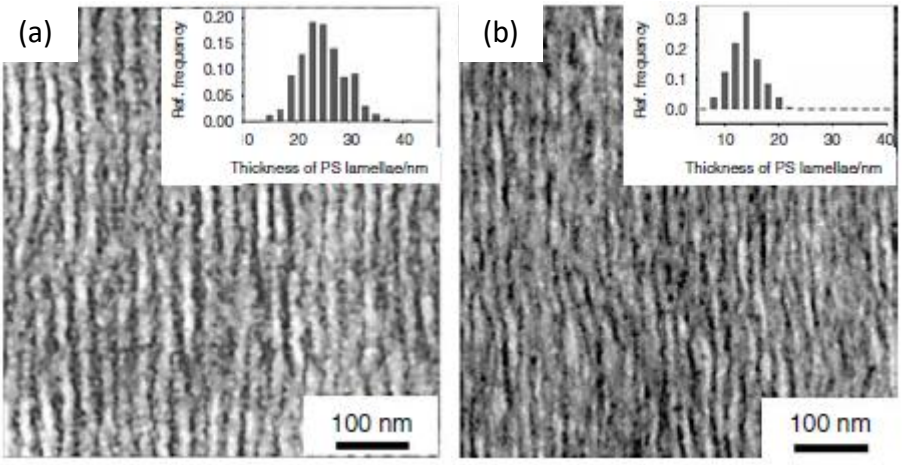

Figure 17. TEM pictures showing the morphology of a lamellar SBS triblock copolymer. Insets show frequency distribution of PS lamellae (a) before and (b) after deformation in parallel direction to lamellae arrangement. After [74].

In the formation of chevron-like morphology, the thickness of PB phase increases, while the PS phase remain unchanged. During the parallel deformation, the thickness reduction of PB layer is more pronounced than in the case of PS. These two observations indicate that the rubbery phase reacts faster to deformation, which is further supported by FTIR (Fourier-transform infrared spectroscopy) spectroscopy results [76].

4.4. Morphology formation in Polyacrylate/PS copolymers

Polyacrylate such as PBA or Poly(2-ethylhexyl acrylate) have similar properties as PB rubber. Both have low T_g and have the advantage of being insensitive to UV degradation compared to PB [77, 78]. However, the development of copolymer based on these acrylates is not possible by anionic polymerization as acrylate are mostly unreactive [10-12].

It is possible to synthesize polymethacrylates such as poly(butyl methacrylate) (PBMA) by anionic polymerization. The synthesis of a range of PS-b-PBMA copolymers was performed by Weidish et al. and gives an indication of the morphology formation in this type of copolymers [79-82].

As already described, the phase separation of copolymer is determined by the phase ratio as well as the segregation factor χN. A series of PS-b-PBMA with Φ_{PS} varying from 17 to 90 % have been synthesized. It was determined that the phase separation of the two blocks appears strong in a range

of Φ_{PS} from 30 to 60 %. Below and above this value, the copolymer has a disordered morphology. This can also be observed by the dependence of T_g of the copolymer as presented in Figure 18.

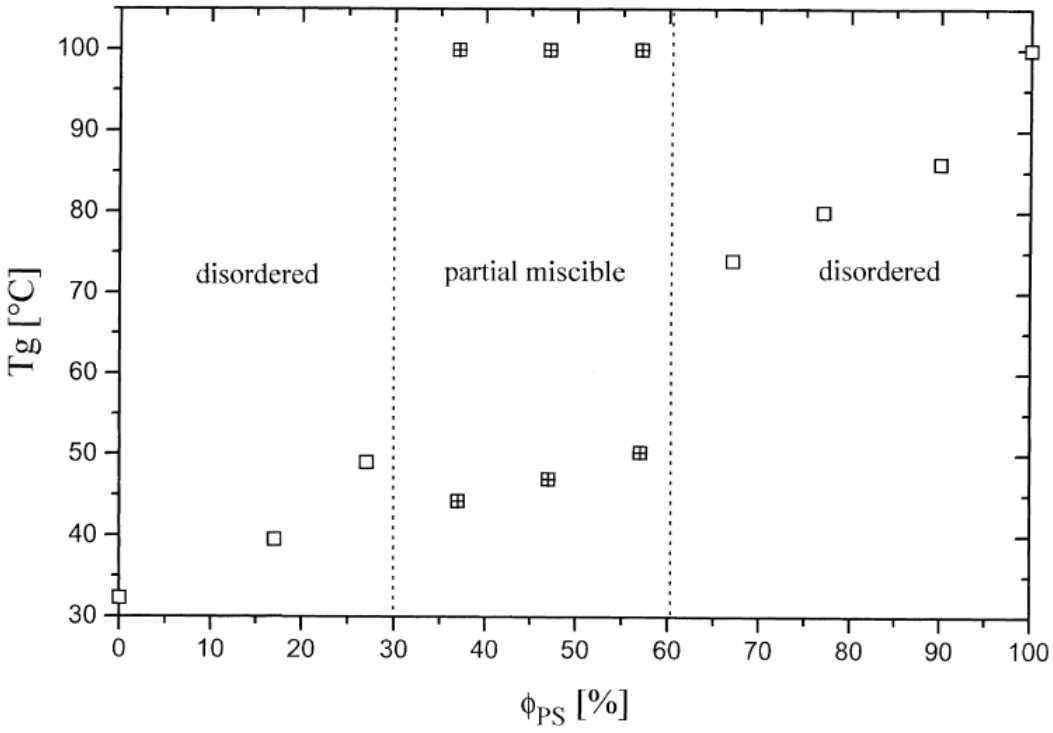

Figure 18. Dependence of the T_g on the Φ_{PS} for $M_n \approx 100$ kg/mol.

It is also observed that below 30 % and above 60 % of PS in the copolymer, the system only has one T_g. It means that mixing between the phases occurs, resulting in distorted morphology. When the Φ_{PS} is between 30 and 60 %, two T_g are measured, one corresponding to the PS phase (around 100°C) and one for the PBMA phase (around 45°C). This shows that the system is separating into domains. It is observed that the T_g corresponding to the PBMA block is varying with the amount of PS in the system while the T_g of PS block is stable at 100°C. This indicates partial mixing between the phases due to a broaden interface. This type of behavior was already reported in case of weakly segregated copolymers.

Another series of PS-b-PBMA with similar Φ_{PS} (around 0.70 %) but with χN varying from 8 to 50 has also been synthesized. This was achieved by varying the molecular weight of the copolymer from 72 to 450 kg/mol. The samples with the lower values of χN show a disordered structure as it could be expected. In the χN range from 10 to 12.5, the sample show weak segregation with large interface as depicted in Figure 19 (a). It was shown that a PBMA-b-PS sample with M_n = 148 kg/mol have an interface of about 9 nm, which is larger than the one observed in PS-b-PI copolymer. With an increase

of M_n to 270 kg/mol with χN of about 30, the structure is intermediately segregated as observed in Figure 19 (b).

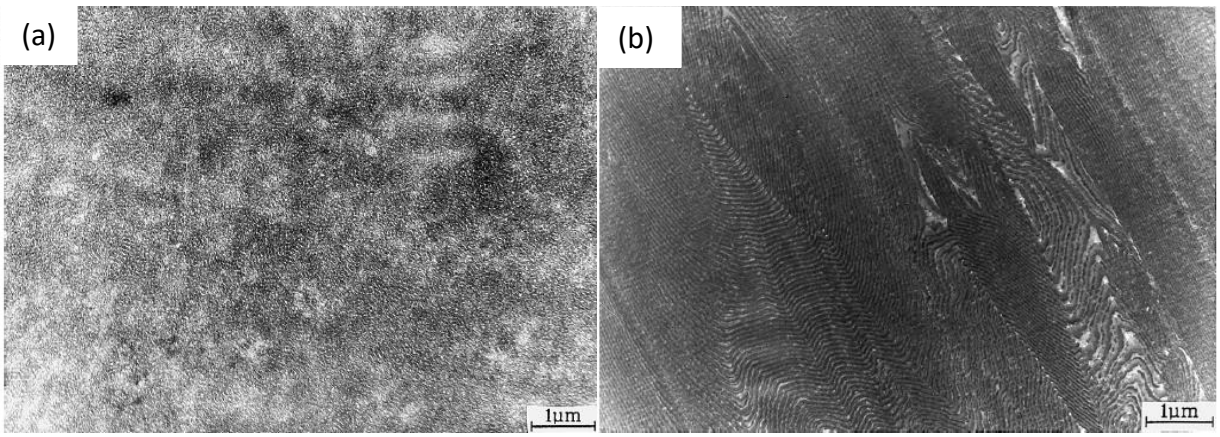

Figure 19. TEM micrograph of PBMA-b-PS with (a) weak segregation (M_n = 130 kg/mol, Φ_{PS} = 70 %) and (b) intermediate segregation (M_n = 270 kg/mol, Φ_{PS} = 70 %). After [80].

In terms of mechanical properties, an increase of Φ_{PS} leads to an increase of tensile strength coupled with a decrease of elongation at break. However, the tensile strength of some of the produced polymers is almost the same compared to h-PS. This is an unexpected result considering that one of the presented samples only has a PS content of only 57 wt.%. The tensile strength of PS-b-PBMA is generally higher compared to PS-b-PB copolymers. This effect can be attributed to the thermoplastic nature of both constituents PBMA and PS. However, the increase of compatibility and interfacial width between the two phases could also contribute to the enhancement of the mechanical properties.

4.5. Kinetic aspect of free-radical polymerization

It is assumed, that the h-PS and the grafted PS, formed during the grafting synthesis, have similar molecular weight and distribution, and are influenced by the same type of synthesis parameters. Therefore, in order to understand the graft copolymerization process, it is essential to study the polymerization of styrene alone.

The free-radical polymerization of styrene proceeds through the following steps including initiation, propagation, and termination.

Initiation

Initiation consists of the homolytic cleavage of an initiator molecule which produces two radicals. It is represented by:

$$I \xrightarrow{k_d} 2R^{\cdot} \quad (2)$$

$$R^{\cdot} + M \xrightarrow{k_i} M_1^{\cdot} \quad (3)$$

where k_d is the rate constant for the initiator dissociation. The equation (3) involves the addition of the radical to the first monomer molecule M to produce the chain initiating radical M_1^*. k_i is the rate constant of the initiation step.

In case of thermal initiator, their decomposition behavior is highly dependent on the temperature of polymerization. The higher the temperature, the more initiator molecules are decomposed into radicals. Initiators have different decomposition rates depending on temperature and the solvent used. This difference in decomposition rates is correlated to the initiator half-life time $t_{1/2}$ which is defined as the time necessary for the initial initiator concentration to be halved. The rate of initiator disappearance (equation (2)) is:

$$-\frac{d[I]}{dt} = k_d[I] \quad (4)$$

which after integration leads to:

$$[I] = [I]_0 e^{-k_d t} \quad (5)$$

where $[I]_0$ is the concentration of initiator at t_0. By setting $[I] = \frac{[I]_0}{2}$, $t_{1/2}$ is defined as:

$$t_{1/2} = \frac{0.693}{k_d} \quad (6)$$

An increase in temperature leads to an increase of the dissociation constant k_d and a decrease of the half-life time.

Propagation

Propagation consists of the growth of monomer by the successive addition of a large number of monomer molecules. Each addition leads to a new radical that has the same identity as the previous one, except that it is larger by one monomer unit. The successive additions may be represented by:

$$M_1^* + M \xrightarrow{k_p} M_2^* \quad (7)$$

$$M_2^* + M \xrightarrow{k_p} M_3^* \quad (8)$$

or in general terms:

$$M_n^* + M \xrightarrow{k_p} M_{n+1}^* \quad (9)$$

where k_p is the rate constant for propagation.

Termination:

The propagation of the chain is stopped by termination reactions. Termination with the annihilation of the radical centers occurs by bimolecular reaction between radicals. Two radicals react with each other by recombination (equation (10)) or by disproportionation (equation (11)), in which a hydrogen radical is transferred to another radical center. The two different modes of termination can be represented in general terms by:

$$M_n^* + M_m^* \xrightarrow{k_{tc}} M_{n+m} \quad (10)$$

$$M_n^* + M_m^* \xrightarrow{k_{td}} M_n + M_m \quad (11)$$

where k_{tc} and k_{td} are the termination rate constant by recombination and by disproportionation, respectively. The termination step can also be expressed by:

$$M_n^* + M_m^* \xrightarrow{k_t} dead\ polymer \quad (12)$$

where the mode of termination is not specified and k_t is defined by:

$$k_t = ak_{tc} + (1 - a)k_{td} \quad (13)$$

where a and (1 - a) are the fraction of termination by coupling and disproportionation, respectively.

The monomers are disappearing by the initiation reaction (equation (3)), as well as by the propagating reaction (equation (9)). The rate of polymerization, or rate of monomer disappearance, is given by:

$$-\frac{d[M]}{dt} = R_i + R_p \tag{14}$$

where R_i and R_p are the rate of initiation and propagation, respectively.

In order to calculate the rate of polymerization, three assumptions are made:

1. The number of monomer reacting in the propagation step is significantly higher than the one reacting in the initiation step; In other terms $R_i << R_p$,
2. The propagation rate is independent of the size of radicals, which means that the constant of propagation k_p is the same for all propagation steps,
3. The concentration of radicals increases initially but almost instantaneously reaches a constant level (steady state value). The rate of change of the radical concentration rapidly becomes and remains equal to zero during the polymerization; In other terms $R_i = R_t$.

With the first assumption, the rate of initiation can be neglected in equation (14) and the polymerization rate is given by:

$$-\frac{d[M]}{dt} = R_p \tag{15}$$

The rate of propagation and, therefore, the rate of polymerization is the sum of many individual propagation steps. Using the second assumptions, the polymerization rate is expressed by:

$$R_p = k_p[M^*][M] \tag{16}$$

where [M] is the monomer concentration and [M*] is the concentration of all chain radicals (by means of all radicals of size M_1^* and larger). The rate of polymerization cannot be directly calculated using this equation as it contains a term [M*], representing a momentary concentration of radicals which is difficult to determine. Therefore, the steady state assumption is made to simplify the case and substitute this term. Using the equation (12) for the termination, R_t is defined by:

$$R_t = 2k_t[M^*]^2 = R_i \tag{17}$$

The use of the factor 2 in the termination rate follows the generally accepted convention for reaction destroying radicals in pairs. Equation (17) can be rearranged to:

$$[M^*] = \sqrt{\frac{R_i}{2k_t}} \tag{18}$$

and substitution in equation (16) yields:

$$R_p = k_p[M]\sqrt{\frac{R_i}{2k_t}} \tag{19}$$

The rate of producing primary radicals by thermal homolysis of an initiator R_d is given by:

$$R_d = 2fk_d[I] \tag{20}$$

where [I] is the concentration of the initiator and f is the initiator efficiency. f is defined as the fraction of the radical produced in the homolysis reaction that initiates polymer chains. The value of f is ususally lower than 1 due to side reactions. The factor of 2 in the equation follows the convention discussed for equation (17).

The initiation reaction is composed of two steps represented by equations (2) and (3). In most polymerizations, the second step of the addition of primary radicals to monomer is much faster that the first one. Therefore, the homolysis of the initiator is the step which defines the rate of the initiation sequence. The rate of initiation is given by:

$$R_i = 2fk_d[I] \tag{21}$$

Substituting equation (21) into equation (19) yields:

$$R_p = k_p[M]\sqrt{\frac{fk_d[I]}{k_t}} \tag{22}$$

The rate of polymerization is proportional to the concentration of monomer and to the square root of the initiator concentration.

The kinetic chain length ν of a radical chain polymerization is defined as the average number of monomer molecules consumed per each radical, which initiate a polymer chain. It is given by the ratio of the polymerization rate to the initiation rate, or the termination rate as the latter two are equal.

$$\nu = \frac{R_p}{R_i} = \frac{R_p}{R_t} \tag{23}$$

The combination of equation (16), (17) and (23) yields:

$$\nu = \frac{k_p[M]}{2k_t[M^*]} \tag{24}$$

Combination between equation (16) and (24) leads to:

$$\nu = \frac{(k_p[M])^2}{2k_t R_p} \tag{25}$$

and by combination with equation (22):

$$\nu = \frac{k_p[M]}{2\sqrt{f k_d k_t [I]}} \tag{26}$$

The degree of polymerization $\bar{X}_n$ is calculated as:

$$\bar{X}_n = \alpha\nu \tag{27}$$

where α is equal to 1 or 2, whether the termination happens by disproportionation or by recombination, respectively.

The chain length is directly correlated to the concentration of monomer and initiator in the following manner:

$$\nu \approx [M]$$

$$\nu \approx \frac{1}{2\sqrt{[I]}}$$

This means that an increase in the monomer concentration leads to a direct increase in the molecular weight while an increase of initiator concentration leads to a moderate decrease in molecular weight.

4.6. Synthesis of graft copolymers

4.6.1. Synthesis method in view of polymerization media

Two main categories of polymerization are usually described in the literature: homogeneous and heterogeneous [83]. This classification is based on the media used for the polymerization indicating whether the reaction mixture is homogeneous or heterogeneous. Mass and solution polymerization are homogeneous processes, whereas suspension and emulsion polymerization are considered heterogeneous.

Mass polymerization is the simplest form of polymerization containing only monomer(s) and initiator in the reaction system. It has the advantage of reducing the amount of contaminants in the polymerization mixture. However, this type of reaction is hard to control, because of the characteristics of radical polymerization. The combination of the exothermic nature and the high probability of gel effect to occur causes issues in the dissipation of heat during the reaction. The viscosity of the reacting mixture increasing during the mass polymerization, accompanied by the exothermic effect may cause formation of local hot spots resulting in degradation and discoloration of the polymer. Therefore, the control of the temperature, as well as the homogeneous stirring are essential. This method is used for the polymerization of styrene as this monomer does not have high tendency to polymerize with gel effect. The heat dissipation problem is resolved by carrying the reaction to low conversion and subsequent recycling of unreacted monomer.

The challenges of mass polymerization can be otherwise addressed by performing the synthesis in a solvent. The solvent aids in the heat dissipation by acting as a diluent and eases the stirring by reduction of the mixture viscosity. However, the incorporation of a solvent presents new considerations, such as the chain transfer to solvent, which reduces the molecular weight of the polymer chains. The purity of the final product may also be affected by the presence of solvent and the difficulty to remove it. The polymer can be isolated from the solvent by precipitation in a non-solvent such as methanol. For industrial use, the polymer is usually isolated by evaporation and recycling of the solvent.

Heterogenous polymerization presents great advantages in terms of heat dissipation and viscosity control. They are three main types of heterogeneous polymerization: precipitation, suspension, and emulsion. Precipitation polymerization starts as homogeneous polymerization, but during the course of the reaction converts into a heterogeneous system, as the formed polymer precipitates in form

of powder. This type of polymerization requires that the used diluting media acts as a solvent for the monomer but does not dissolve the final polymer product. In case of suspension polymerization, the monomer is dispersed in a media (usually water) as droplets (50 - 500 μm in diameter). Suspension stabilizers, which are usually water-soluble polymers, are used to avoid coalescence. The initiator used is soluble in the monomer and not in water, which means that each droplet can be considered as a miniature mass polymerization system. Due to the size of the formed particles, their separation from water is easy to be carried out by filtration.

Similarly to the suspension method, emulsion polymerization is performed with a monomer insoluble in the dispersing media (usually water) [84]. The system is not stabilized with a suspension stabilizer but with an emulsifier. As the emulsifier molecules have both hydrophilic and hydrophobic segments in its structure, it is able to form micelles in the water. Most of the water-insoluble monomer (>95 %) forms large monomer droplets and the rest is present in the micelle formed by the emulsifier. Finally, a very small amount is dissolved in the water as free molecules. It should be noted that the total area of micelles is much larger than the area of monomer droplets, which facilitates the occurrence of the polymerization reaction within the micelle itself. As the initiator is soluble in water, the radicals are formed in the aqueous phase and migrate to the micelles containing the monomer, where the polymerization takes place. As the emulsion polymerization continues, the micelles grow by addition of free monomer molecules from the aqueous solution. These monomers are replaced by dissolution of monomers from the monomer droplets. Due to the small size of polymer particles (100 nm), the formed latex is stable and no segregation of particles or precipitation occurs. Therefore, the polymer cannot be isolated by filtration, but the emulsion must be chemically broken by addition of a salt in an acidic solution.

4.6.2. Graft polymerization methods

Graft copolymers are composed of a linear main chain, the backbone, to which are attached polymeric side chains, the grafts. The two entities are of different chemical nature and the grafts are usually distributed randomly along the backbone [85]. Often, interactions between the backbone and the grafts yield intramolecular phase separation in the bulk copolymer, similarly to linear block copolymers. Independently of the method of synthesis there are three methods used to synthesize graft copolymers as depicted in Scheme 1.

Grafting-onto

Grafting-from

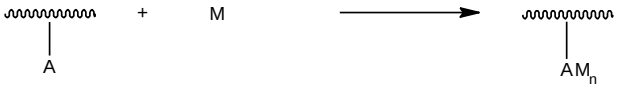

Grafting-through

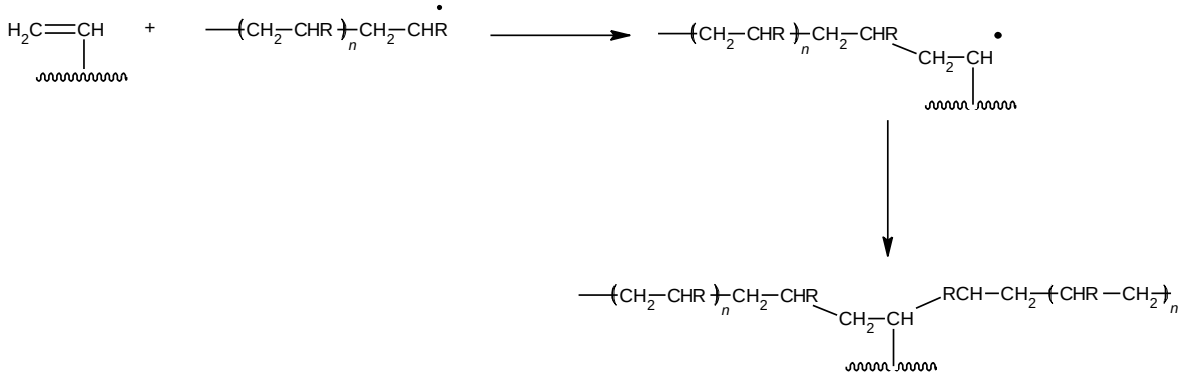

Scheme 1. Methods used for the synthesis of graft copolymers.

In the grafting-onto method, a backbone chain carrying randomly distributed functions reacts with another molecule, or macromolecule carrying functions located selectively at its chain end. The functions are described as A and B in Scheme 1. In this case, no polymerization reaction is needed to perform the grafting, but it implies that access of the functional chain end to the grafting site is permitted. These conditions are not obvious since it is well known that there is some incompatibility between polymers of different chemical nature. The reaction must be carried out in a common solvent for a better homogeneity of the reaction medium. The advantage of this method is the flexibility in the design of both the backbone and the grafts since they are produced separately and can be characterized individually. Knowing the M_n of each component and the overall composition of the graft copolymer, it is possible to calculate the number of grafts per chain and the average distance between two successive grafts along the backbone. However, the presence of non-grafted homopolymer in the mixture is possible. Moreover, the synthesis of a functionalized-terminated polymer requires the use of advanced controlled polymerization techniques. [85]

In the grafting-from process, a polymer chain carries active sites which can be used to initiate the polymerization of a second monomer. The backbone can have initiating sites attached to it or functions able to generate such sites. The type of initiation created by this method can be free-radical, anionic, cationic or Ziegler Natta. Although this method was proven to be efficient, the number of graft is not accessible experimentally and their length can vary greatly within a sample. Moreover, the graft copolymer often contains non-negligible amount of homopolymer.

In the grafting-through method, the polymerization of a monomer is performed in the presence of a backbone carrying pendant unsaturations, which can participate in the process. The grafting process can happen by initiation at the backbone grafting site or a growing polymer can react with the backbone grafting site. As discussed in the next chapter, the second reaction is more likely to happen. This kind of method can involve the formation of cross-linked material if a growing site reacts with another backbone molecule and measures have to be taken if solubility is desired in the product. This kind of polymerization cannot be considered as a way to target specific and tailor-made graft copolymers but is used when specific properties are wanted.

A variation of this method has gained interest as it allows a better tailoring of the architecture. It involves designing a polymer with one unsaturated end chain called macromonomer. In a second step, this macromonomer is copolymerized with a monomer leading to graft copolymer. Since the macromonomer is synthesized separately, it can be tailored and characterized separately. Moreover, cross-linking is impossible in this kind of approach. However, this type of copolymerization requires the use of controlled techniques to prepare the macromonomer. Their synthesis can lead to a mixture of homopolymer, copolymer and backbone in case the copolymerization of the macromolecule with the comonomer is inefficient. Finally, composition drift can appear due to the difference of reactivity between the macromonomer and the comonomer.

The most used plastic synthesized by grafting-through process is HIPS. The specificity of HIPS lies in its morphology induced by the immiscibility of PS and PB. Unlike most particles modified polymers, HIPS have a so-called salami morphology consisting of a PS matrix in which PB particles are dispersed. These particles have themselves occlusions of PS in them as depicted in Figure 20.

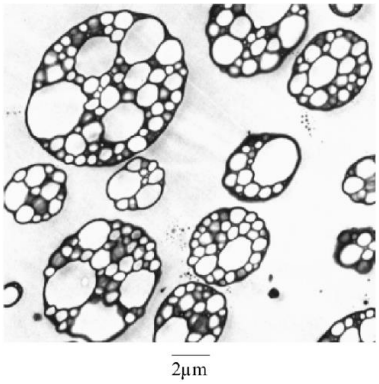

Figure 20. HIPS salami domains of PB particles filled with PS domains in a PS matrix. PB and PS phases appear dark and bright, respectively. After [86].

The grafting is performed by polymerizing styrene in the presence of a partially dissolved PB rubber. Since PB and PS are incompatible polymers, the system phase-separate in the early conversion stage of the reaction. PS forms the continuous phase with the rubber phase existing as discrete particles having themselves occlusions of PS. Due to the non-selectivity of the process, cross-linking of rubber molecules occurs during the reaction. The first factor regulating the mechanical properties of HIPS is the ratio between the gel content (fraction not soluble in solvent) and the rubber content. The second factor is the bounding efficiency between rubber particles and PS chains to ensure transmission of external force between the two phases. As observed in Figure 20, the size of the particles lies around 2 to 6 μm, making the product opaque.

4.6.3. Grafting efficiency of copolymerization

An extensive study of the grafting of styrene onto PB backbone in solution has been carried out by Huang et al. [87-90]. They defined the graft efficiency as the mass of monomer which constitutes the grafted chains divided by the complete mass of monomer incorporated within all chains, both grafted and non-grafted. Therefore, the instant grafting efficiency is expressed as follows:

$$\phi = \frac{rate\ of\ change\ of\ mass\ of\ graft\ chains}{rate\ of\ change\ of\ mass\ of\ all\ chains} \tag{28}$$

Based on the kinetic equation of graft copolymerization, simplified by assumptions, an expression for the instantaneous grafting efficiency can be formulated. Two main parameters determine the expression of this grafting efficiency: the mode of grafting initiation and the mode of termination of PS chains. The grafting can be initiated by primary radicals or by radicals of the growing PS chains and

the termination can happen by recombination or by disproportionation. The ratio between the two modes of termination for PS has been extensively studied and lead to various results [91]. However, it is known that the principal mode of termination is recombination.

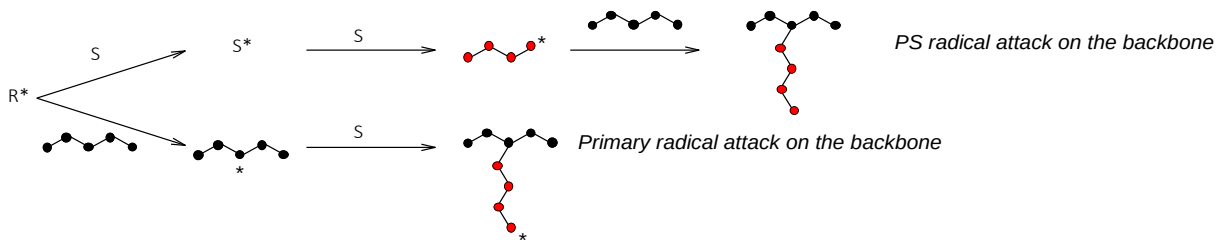

Figure 21. Two types of grafting initiation possible.

It is observed that the dependency of ϕ on the synthesis parameters is determined by the mode of grafting initiation. If the grafting initiation occurs by primary radical attack, the grafting efficiency is influenced by the styrene concentration. On the contrary, if the grafting initiation occurs by PS radicals attack, the grafting efficiency is influenced by the concentration of initiator in the system.

5. Conceptional approach

The typical synthesis of rubber-modified PS leads to the formation of morphology with domains larger than the wavelength of light, making the product opaque. The chemical structure, molecular weight and structural organization of the hard and soft phase determines the optical and mechanical properties of the blend. Reducing the domain size is essential in order to obtain flexible and transparent products. Therefore, in this work, the following had to be considered: design of the backbone size and functionalities, establishment of the graft copolymerization approach, as well as the investigation of the method of polymerization. This chapter describes the principles behind graft copolymerization of styrene onto PBA, needed to narrow down the decisive factors and anticipate possible interactions between the studied parameters.

5.1. Backbone design and synthesis

PBA is a rubbery polymer with a T_g of about -45°C and is used in copolymer products, such as acrylonitrile-styrene-acrylic (ASA). [14]

As previously described, the main advantage of applying this polymer as a precursor for impact-resistant materials in comparison to PB rubber, is its resistance to UV light. Indeed, the C=C double bonds present in PB rubber are prone to oxidation and can initiate cross-linking due to oxygen, UV radiation and heat. [92] This results in deterioration of the rubber with loss of impact strength and discoloration of the material. The PBA rubber is free of C=C double bond which is advantageous in terms of weatherability and resistance against aging. [77, 78]

The C=C double bond present in the PB structure acts as reactive site for the graft copolymerization. Their absence in PBA backbone needs to be overcome in order to create initiation sites for graft chains. For this purpose, two options are feasible. First, BA can be copolymerized with a bifunctional monomer having two double bound functionalities of different reactivity (route A). In this case, the more reactive function of the monomer reacts during the copolymerization with BA while the other function remains unreacted and stays available for the graft copolymerization. Second, BA can be copolymerized with a comonomer having an alkene and another functionality, non-sensitive to radical attack (route B). This second functionality is then converted into radically active sites in the course of a polymer analogous reaction.

In this work, these two options are explored by use of the following routes:

- ***Route A***: Copolymerization of BA with allylmethacrylate (AMA) or dihydrodicyclopentadienyl acrylate (DCPA),
- ***Route B***: Copolymerization of BA with glycidyl acrylate (GA) and glycidyl methacrylate (GMA).

In the route A, BA is copolymerized with two types of comonomer. As depicted in Scheme 2 DCPA is a bifunctional monomer with an acrylate and a cyclic allyl function. AMA is a bifunctional monomer with a methacrylate and an allylic function. Due to the difference of reactivity between the meth-/ acrylate function and the ally function, it is expected that the meth-/ acrylate can polymerize during the synthesis of the backbone, leaving the ally function unreacted and free for further grafting.

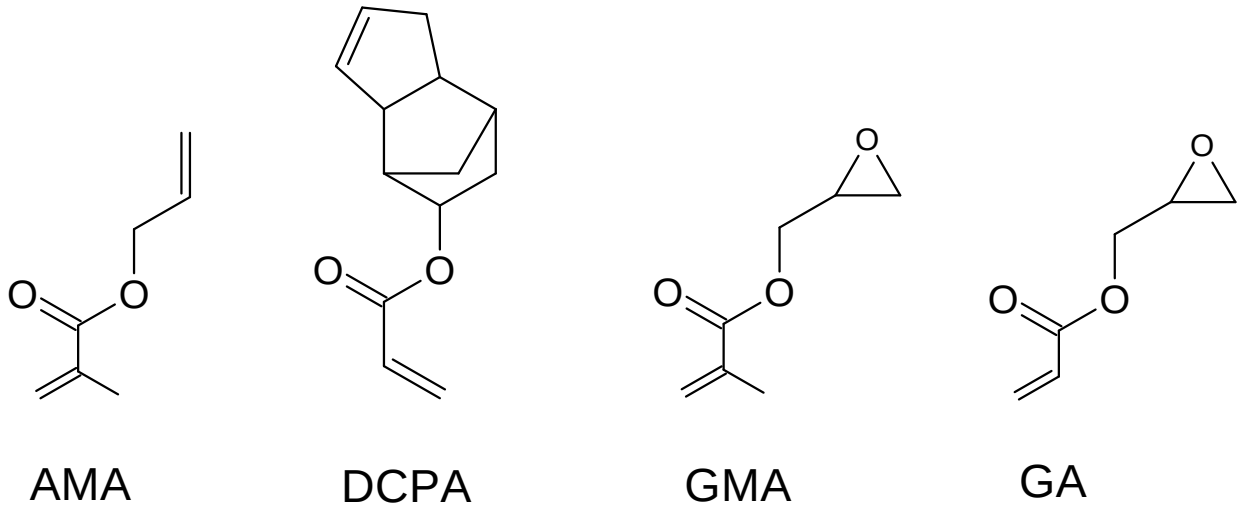

Scheme 2. Chemical structure of AMA, DCPA, GMA and GA monomers.

In the route B, BA is copolymerized with GA and GMA. The use of glycidyl functionalized meth-/ acrylate monomer in the copolymerization with BA represents a good alternative to route A as it allows control over the amount of reactive groups introduced, avoiding the possible cross-linking during the synthesis.

5.2. Method of synthesis: emulsion and solution polymerization

The type of synthesis used for the preparation of the backbone and the subsequent graft copolymerization is crucial, as it determines the architecture of the final product and, therefore, its properties. Four main methods of synthesis are used when performing free-radical polymerization: mass, solution, emulsion, and dispersion polymerization. Mass and dispersion polymerization are excluded in this work, because of their high concentration which would increase the probability of cross-linking and gel effect. Emulsion and solution polymerization are more suitable for the graft

copolymerization of styrene onto PBA and will be the focus of this work. In principle, it is possible to carry out both synthesis routes A and B using the selected polymerization methods. However, route B requires an additional polymer analogous reaction which needs to be carried out in solution in order to reach high conversion of the glycidyl functions.

Table 1. Method of polymerization used for the different steps in route A and B.

Synthesis steps	Synthesis route	
	Route A	Route B
1: Backbone synthesis	Emulsion, solution	Emulsion, solution
2: Backbone analogous reaction	n/a	Solution
3: Graft copolymerization	Emulsion, solution	Solution

Table 1 summarizes the polymerization methods used in the two routes for the needed synthesis steps of the backbone synthesis, its modification and the grafting. Route A studies the synthesis of BA with a bifunctional radically active monomer. It can be performed in 2 steps only, and the influence of the type of synthesis, emulsion or solution, will be studied.

Using route B, the influence of the type of synthesis will be determine for the backbone formation. However, due to the need of carrying the polymer analogous reaction in solution, the graft copolymerization needs to be performed in solution as well.

5.3. Copolymerization of styrene with PBA backbone

5.3.1. Initiation

Two classes of thermal initiator are usually used for free-radical polymerization: azo and peroxides initiators. It was studied and reported that azo-initiators such as AIBN are inefficient toward grafting reaction in presence of PB backbone. [88] This is because AIBN is unable to generate grafting site on the backbone. Therefore, benzoyl peroxide (BPO) and potassium persulfate (KPS) initiators are used in this work. BPO is used in case of the solution polymerization and KPS is used in emulsion polymerization.

In principle, when heat is applied, the initiators decompose into two radicals as depicted in Scheme 3.

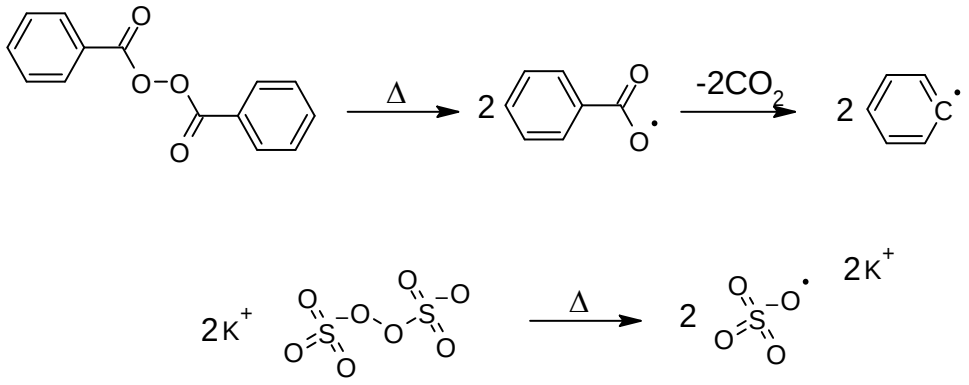

Scheme 3. Thermal decomposition of BPO initiator (top) and KPS (bottom).

In order to moderate the amount of possible cross-linking reaction, as well as to enhance the grafting efficiency, the initiator can be constantly dosed through the reaction course instead of introducing it in one portion at the beginning of the reaction. Using equation (5), it is possible to calculate the concentration of initiator at any time of the reaction, using the decomposition constant k_d. Consequently, it is possible to calculate the amount of initiator which was consumed and need to be replaced in the reaction system.

Figure 22 compares the BPO concentration in the reaction mixture in case the initiator is dosed through the reaction and if it is introduced at once at the beginning of the reaction.

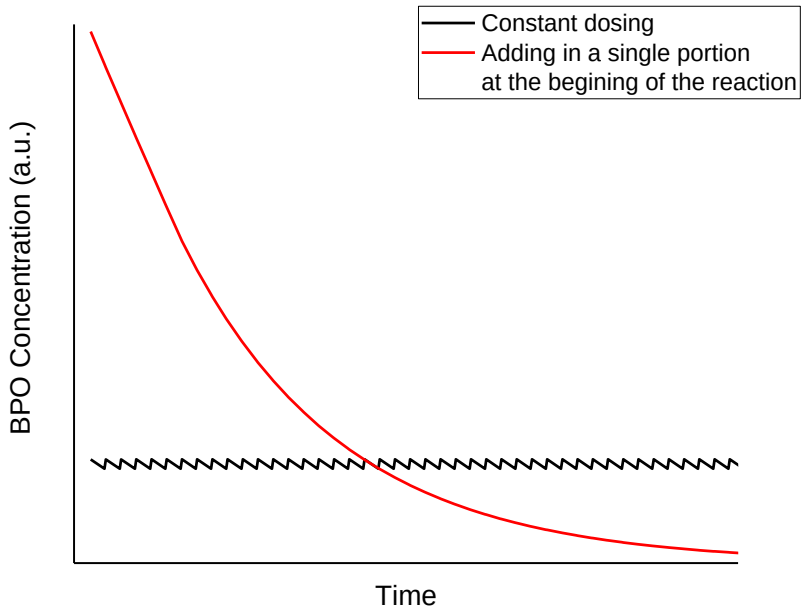

Figure 22. BPO concentration in the reaction mixture when dosed through the reaction course or added in one portion at the beginning of the reaction.

As presented in Figure 22, in the case of the constant dosing method, a part of BPO is introduced at the beginning of the reaction and the following fractions are added by intervals to the mixture. It should be noted, that both options for constant and single portion dosing use the same amount of initiator. However, in the single portion dosing, the amount of initiator in the mixture is varying greatly from the beginning to the end of the reaction, promoting the condition for undesired cross-linking. Therefore, the majority of the experiments reported in this work are using the constant dosing approach.

5.3.2. Process of graft copolymerization

During the graft copolymerization, the backbone is mixed with styrene monomer and a thermal initiator is added. The radicals produced from the initiator (equation (2)) are not selective and can either attack styrene monomers or backbone chains as depicted in Scheme 4.

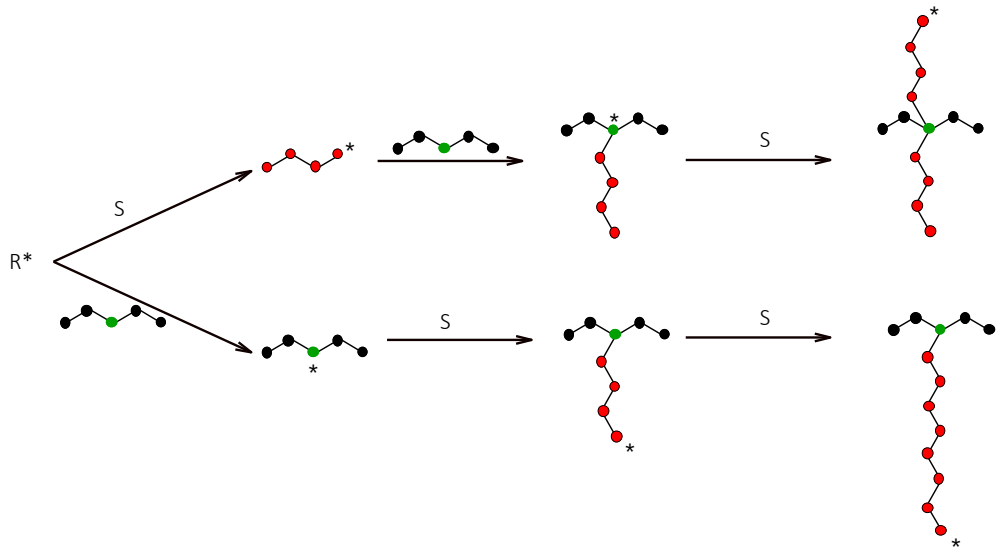

*Scheme 4. Reaction of radical with different entities. Red circles represent styrene units, black circles represent BA units and green circle represent active sites on the backbone. * is indicating the place of the radical.*

The growing PS chain can react with the backbone, forming a graft copolymer chain. Similarly, the radically active backbone can react with styrene monomer to a graft copolymer chain. The difference between the two reactions lies in the location of the active radical after grafting.

In the first case, the radical is located at the reactive site of the backbone. If this reactive site polymerizes further with additional styrene monomer, the backbone has two pendant PS chains. In the second case, the radical is located at the end of the pendant PS chain. If it reacts further with styrene, the graft chain becomes larger. However, the growing side chain can react not only with styrene,

but also with another backbone or graft copolymer molecules, producing various moieties. It can result in the formation of a premise of a network, which can eventually produce cross-linked structures.

Finally, the termination reaction can lead to a variety of outcomes with the formation of h-PS, PBA-g-PS, network structure and possibly unreacted PBA-based backbone. Some of the possible structures arising from the graft copolymerization are showed in Scheme 5.

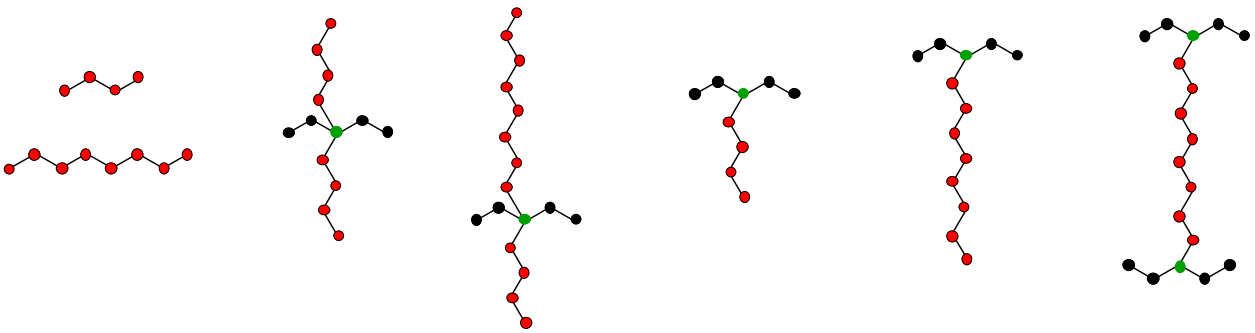

Scheme 5. Possible structures of moieties formed during the graft copolymerization of styrene onto PBA-based backbone.

This is a non-exhausting list which includes the most common structures susceptible to form, such as h-PS and different types of graft copolymer, as well as slightly cross-linked polymers. These structures are prone to react further with other growing moieties and form more complex architectures. Due to the non-selectivity of the radical, it can be observed that the molecular weight of both grafted PS and h-PS is equal.

The main difference in the graft copolymerization reaction of styrene onto PBA-based backbone, in comparison to PB-based systems, is the reactivity of the active sites. The vinyl functions in PB are less reactive compared to the functions in the PBA-based backbone. Cross-linking reactions are more likely to happen if the reactivity of the active sites is higher. Therefore, using the PBA-based backbone instead of a typical PB backbone increases the risk of cross-linking in the graft copolymer product.

The main features of the graft copolymerization can be summarized in the following points:

- Product of the copolymerization of styrene onto PBA-based backbone is a mixture of PBA-g-PS and h-PS with various architectures,
- Both grafted and non-grafted PS chains are growing simultaneously,
- Both grafted and non-grafted PS chains have the same molecular weight distribution,

- Due to the high reactivity of functional groups in the PBA-based backbone, formation of cross-linked structure is possible.

It appears essential to determine the amount of active sites in the backbone, in order to get sufficient grafting efficiency, while aiming to limit the cross-linking reaction.

6. Results and discussion

This chapter presents the results of the experiments performed according to the approach described in chapter 3 and the methodology summarized in chapter 6, together with the discussion of the observed outcomes. As shown in Scheme 6, this work is divided in view of the method used for the polymerization of the backbone: emulsion or solution, as well as the route used for the synthesis of the graft copolymer: Route A and B.

As previously described, PBA alone does not have radically reactive group on its chain and to introduce them, BA must be copolymerized with a comonomer. In the route A, BA is copolymerized with a bifunctional monomer: AMA or DCPA. In this case, the meth-/ acrylic function of the monomer reacts during the copolymerization with BA, while the allyl function does not and stays active for the subsequent graft copolymerization. In the route B, BA is copolymerized with a comonomer having meth-/acrylate functionality and glycidyl functionality, which is unreactive towards radicals. In principle, the methacrylate version is the most commonly produced monomer and therefore cost effective. However, an acrylate version is studied in this work to investigate the influence of the comonomer type on the backbone structure and on the grafting performances. Few studies address the issue of the reactivity ratio between GMA with acrylate and [93-96]. It was shown that a composition drift appears, due to the difference in reactivity of the two monomers. Although no studies have been carried out for the copolymerization of BA with GA monomer, it is expected that the composition drift is reduced due to the similarity of the two comonomers. The modification of PBA-co-GA and PBA-co-GMA backbones using acrylic acid (AA) yield acryloyl groups, as showed in Scheme 6. AA is used as modifier and triphenylphosphine (TPP) as catalyst. It is essential to use an inhibitor to avoid the polymerization and cross-linking reaction with acrylic acid. It is as much important to remove this inhibitor after the modification reaction to proceed with the copolymerization.

In case of both route A and B, a chain transfer agent (tert-dodecanethiol, TDT) is used during the backbone synthesis to modulate M_n and avoid cross-linking reaction. In high concentration, the polymerization of BA (with or without comonomers) leads to branching and cross-linking by hydrogen abstraction. [97, 98]

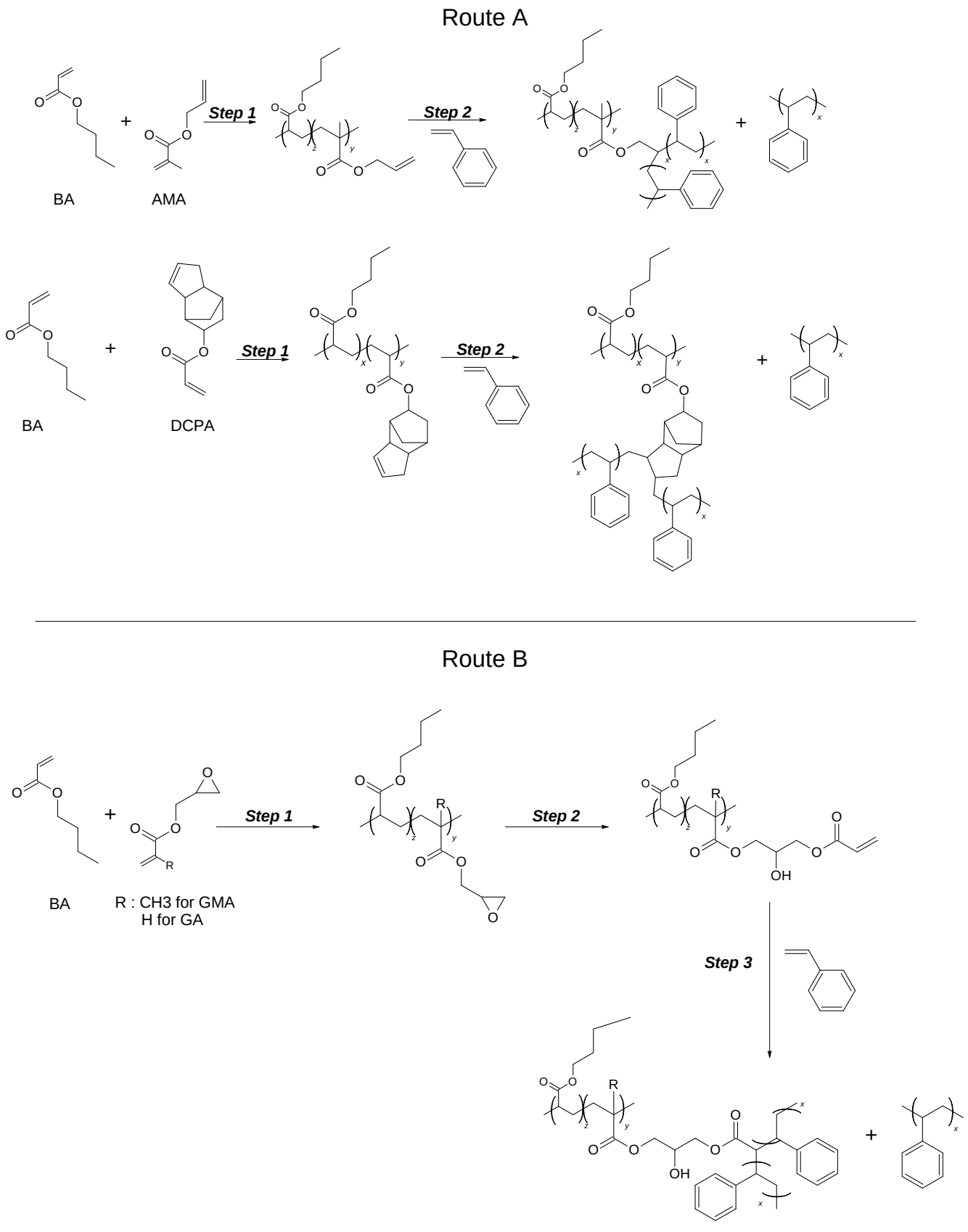

Scheme 6. Synthesis of PBA-g-PS/h-PS blends by route A and B.

Route A requires two steps to synthesize the PBA-g-PS/h-PS blend, whereas route B is performed in three steps due to the necessary modification reaction of PBA-co-GMA or PBA-co-GA.

The nomenclature used for the backbones, modified backbones and the graft copolymers indicates the applied polymerization method, as well as M_n of the backbone and amount of comonomer used.

Firstly, in both route A and B, the names of the backbone are as follows:

$$\mathbf{X\_B_{XX}(M_n\text{-}wt.\%)}$$

where X indicates the type of polymerization method used for the backbone: E for emulsion and S for solution, B_{XX} indicates the type of comonomer used, M_n is the average molecular weight of the backbone in kg/mol, determined from SEC, and wt.% is the experimental weight percentage of the comonomer in the backbone, determined by NMR spectroscopy.

In case of the route A, the graft copolymers are named as follows:

$$\mathbf{G\text{-}X\_B_{XX}(M_n\text{-}wt.\%)}$$

To differentiate copolymers obtained via route A and B, additional information is introduced in the naming of the backbone resulting from the three-step route B. The backbone which underwent the post-modification in the polymer analogous reaction is indicated as follows:

$$\mathbf{X\_B_{XX}(M_n\text{-}N_{Acr})}$$

where N_{Acr} is the number of acryloyl groups per chain of the modified backbone. Therefore, the graft copolymers obtained through route B are named as follows:

$$\mathbf{G\text{-}X\_B_{XX}(M_n\text{-}N_{Acr})}.$$

6.1. Process by emulsion polymerization of the backbone

The method used for the synthesis of the backbone (emulsion or solution polymerization) is expected to influence the properties of both the backbone and the graft copolymer. Emulsion polymerization is advantageous as it does not require the use of organic solvent and avoids any gel effect, due to the cooling capacity of water. In the absence of solvent, the PS chains (grafted or not) can reach high molecular weight. However, the probability of cross-linking is also increased because of the high concentration of backbone and styrene monomer. Both backbone types, from route A and B can be synthesized either by emulsion or solution polymerization. The grafting synthesis, however, can be

performed in emulsion only when route A is used (see Scheme 6). When route B is used, a polymer analogous reaction is required, which needs to be performed in solution to convert the glycidyl functions into acryloyl ones.

6.1.1. Route A: Synthesis of backbone and PBA-g-PS copolymer using emulsion polymerization

The synthesis of graft copolymers using route A is performed in two steps. Firstly, the synthesis of the backbone is carried out using BA and bifunctional comonomers AMA or DCPA. The obtained backbones are used for the subsequent graft copolymerization with styrene.

5.1.1.1. Step 1: Synthesis of PBA-co-AMA and PBA-co-DCPA backbones

The first approach in this work establishes the relationship between the synthesis conditions for pristine PBA and the obtained M_n and dispersity. Without the use of comonomer, only the polymerization parameters of BA in emulsion are evaluated, removing the influence of AMA or DCPA comonomers. The polymers are prepared through emulsion polymerization in presence of a chain transfer agent, TDT. The presence of TDT is essential to regulate the M_n of the backbone and to minimize uncontrolled cross-linking due to hydrogen abstraction [98]. The results of the emulsion polymerizations of BA are presented in Table 2.

Table 2. TDT concentration and molecular weight distribution obtained for the synthesis of PBA in emulsion.

Backbone	TDT	M_n	Đ
	[wt.% rel. M]	[kg/mol]	[-]
E_B_{BA}(51-0)	0.5	51	3.3
E_B_{BA}(31-0)	1	31	4.9
E_B_{BA}(19-0)	1.5	19	4.7
E_B_{BA}(16-0)	2	16	5.7

As expected, the increase of TDT concentration leads to a reduction of M_n of the produced PBA. However, it should be noted, that the dispersity also increases with the amount of TDT used. This effect is due to the formation of higher molecular weight species, which appear as a secondary peak in the SEC in Figure 23. This peak, located at around 2000 kg/mol, is not affected by the addition of TDT in contrary to the lower molecular weight peak.

An amount of 1 wt.% of TDT (relative to BA) as in E_B_{BA}(31-0) appears sufficient to have a M_n around 30 kg/mol and is used for the synthesis of PBA with various comonomers.

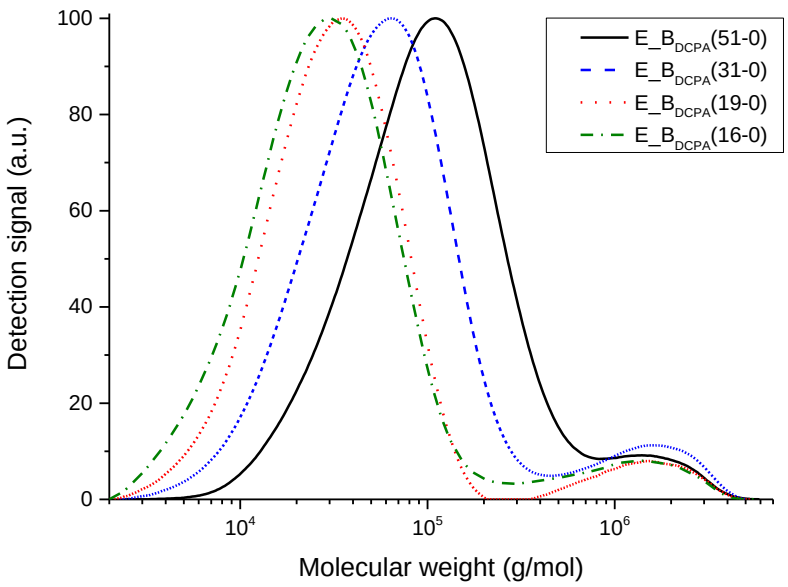

Figure 23. SEC of PBA backbones prepared through emulsion polymerization with various amount of TDT.

A series of PBA-co-AMA and PBA-co-DCPA backbone is synthesized using a TDT concentration of 1 wt.%. The obtained products are characterized for their M_n by SEC and the amount of comonomer in the final graft copolymer is confirmed by NMR. The comparison between the amount of comonomer added in the synthesis ($fw_{DCPA/AMA}$) and the actual amount of these moieties detected in the PBA-co-DCPA and PBA-co-AMA backbones through NMR ($w_{DCPA/AMA}$) is summarized in Table 3. The amount of comonomer used in this study is 10-fold lower than the amount of vinyl-1,2 usually used in PB-g-PS synthesis, radically reactive for grafting reaction. [13] This limits the risk of cross-linking during both the backbone and the copolymer synthesis due to the reactivity of allyl and acryloyl moieties.

Table 3. Synthesis condition and M_n of PBA-co-DCPA and PBA-co-AMA backbones.

Backbone	$fw_{DCPA/AMA}$	M_n	Đ	$w_{DCPA/AMA}$
	[wt.% rel. M]	[kg/mol]	[-]	[wt.% rel. M]
E_B$_{DCPA}$(30-1.0)	1.0	30	2.4	1.02
E_B$_{AMA}$(26-1.4)*	1.0	26	2.0	1.37

* The M_n and Đ are measured only on the polymer peak at about 30 kg/mol

M_n of all produced backbone lies in the range of 30 kg/mol and is comparable to E_B$_{BA}$(31-0), produced without comonomers (Table 2). In case of PBA-co-DCPA, the amount of comonomer detected by NMR

analysis fits well with the feed value. However, a variation is observed for E_B_{AMA}(26-1.4), where the value measured by NMR is higher than the feed one. This phenomenon is likely to arise from the limitation of solubility of E_B_{AMA}(26-1.4) backbone in the NMR solvent, influencing the analysis.

In case of both samples E_B_{DCPA}(30-1.0) and E_B_{AMA}(26-1.4), upon dissolution in THF, a clear difference in the solution quality can be distinguished between the two backbones as depicted in Figure 24. The backbone E_B_{AMA}(26-1.4) prepared with AMA as a comonomer shows cloudiness when dissolved in THF contrary to E_B_{DCPA}(30-1.0), DCPA based backbone.

Figure 24. Dissolved backbone emulsion. Left: E_B_{DCPA}(30-1.0), right: E_B_{AMA}(26-1.4).

As observed in Figure 25, a peak at low molecular weight (1 kg/mol) is detected in sample E_B_{AMA}(26-1.4), which does not appear for sample E_B_{DCPA}(30-1.0).

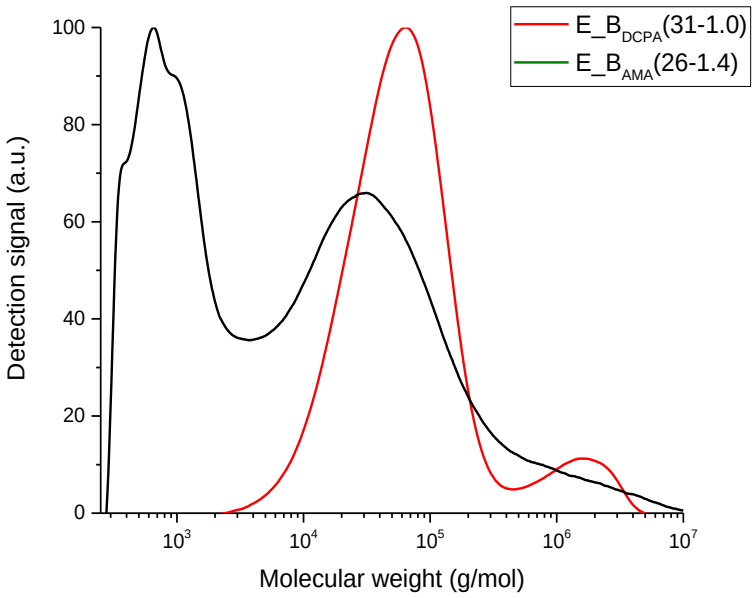

Figure 25. SEC curve comparison between E_B_{DCPA}(30-1.0) and E_B_{AMA}(26-1.4).

Therefore, the cloudiness arising from limited solubility of a certain fraction of the product could cause a potential error in the NMR evaluation, as a portion of the sample remains undetected.

5.1.1.2. Step 2: Grafting reaction of PBA-co-AMA or PBA-co-DCPA with styrene

The produced PBA-co-DCPA and PBA-co-AMA are used for graft reaction using emulsion polymerization. For this purpose, the produced emulsion containing the backbone is diluted with water and emulsifier. The initiator is added in a single portion at the beginning of the reaction. The dosing of styrene, started at the beginning of the reaction, is continued with the first 3 hours of reaction. After the dosing of all components is completed, the reaction is continued for an additional 3 hours.

Table 4 presents a series of four reactions using DCPA- and AMA-based backbones, performed to target hard phase content of 40 and 80 wt.%. The obtained polymers are solvent-casted into films to measure their optical and mechanical properties.

Table 4. Synthesis conditions and physical characteristics of graft copolymerization product from route A in emulsion.

Graft copolymer	PS content	Transmittance	Haze	Clarity
	[wt.%]	[%]	[%]	[%]
G-E_B_{DCPA}(30-1.0)_01	40	74.5 ± 1.9	100 ± 0.7	2.4 ± 0.3
G-E_B_{DCPA}(30-1.0)_02	80	68.1 ± 2.45	100 ± 0.45	2.5 ± 0.2
G-E_B_{AMA}(26-1.4)_01	40	90.4 ± 0.3	25.9 ± 3.0	40.9 ± 5.3
G-E_B_{AMA}(26-1.4)_02	80	68.3 ± 0.4	61.5 ± 1.1	98.6 ± 0.5
Graft copolymer	PS content	E Modulus	Tensile strength	Elongation at break
	[wt.%]	[MPa]	[MPa]	[%]
G-E_B_{DCPA}(30-1.0)_01*	40	-	-	-
G-E_B_{DCPA}(30-1.0)_02	80	1094 ± 176	18.5 ± 1.6	1.4 ± 0.2
G-E_B_{AMA}(26-1.4)_01	40	139 ± 68	9.2 ± 1.1	33.8 ± 8.1
G-E_B_{AMA}(26-1.4)_02	80	1791 ± 47	44.4 ± 2.1	3.5 ± 0.7

*Sample brittleness too high for tensile strength testing.

A major difference appears between grafting products obtained from DCPA-based backbone in comparison to the one from AMA-based backbone. Both G-E_B_{DCPA}(30-1.0)_01 and G-E_B_{DCPA}(30-1.0)_02 have low clarity at around 2.4 % with haze at 100 %, indicating the complete opacity of the film. Their mechanical properties are typical for brittle materials with high E modulus and low elongation at break. The mechanical properties of sample G-E_B_{DCPA}(30_1.0)_01 cannot be measured due to its high brittleness.

In comparison, G-E_B_{AMA}(26-1.4)_01 and G-E_B_{AMA}(26-1.4)_02 have a clarity of 40.9 and 98.6 %, respectively and the film from sample G-E_B_{AMA}(26-1.4)_01 reached Haze as low as 26 %. Moreover, it is observed that the amount of styrene introduced in the system has a direct impact on optical and mechanical performance of the product. With 40 wt.% of PS, the sample G-E_B_{AMA}(26-1.4)_01 has a E modulus of 139 MPa and elongation at break of 34 % and is the most flexible product obtained via this method. The sample G-E_B_{AMA}(26-1.4)_02, with doubled amount of PS hard phase content set at 80 wt.%, is brittle with high E modulus at 1791 MPa and elongation at break of 3.5 %.

The difference between the DCPA- and AMA-based backbones lies in the reactivity of their active site. The pentadiene in DCPA is less reactive in comparison to the allyl in AMA. The double bound present in PBA-co-DCPA backbone does not react during the graft copolymerization and only a blend of PBA-co-DCPA and h-PS is obtained. This leads to a macro-separation between the phases explaining the opacity of the product and the brittle mechanical performance. Nevertheless, the elongation at break of the AMA-based product lies below typical performance of HIPS copolymers (around 30 %).

The difference in the grafting efficiency between the two studied backbones is confirmed by NMR analysis of G-E_B_{DCPA}(30-1.0)_02 and G-E_B_{AMA}(26-1.4)_02 as shown in Figure 26 and Figure 27.

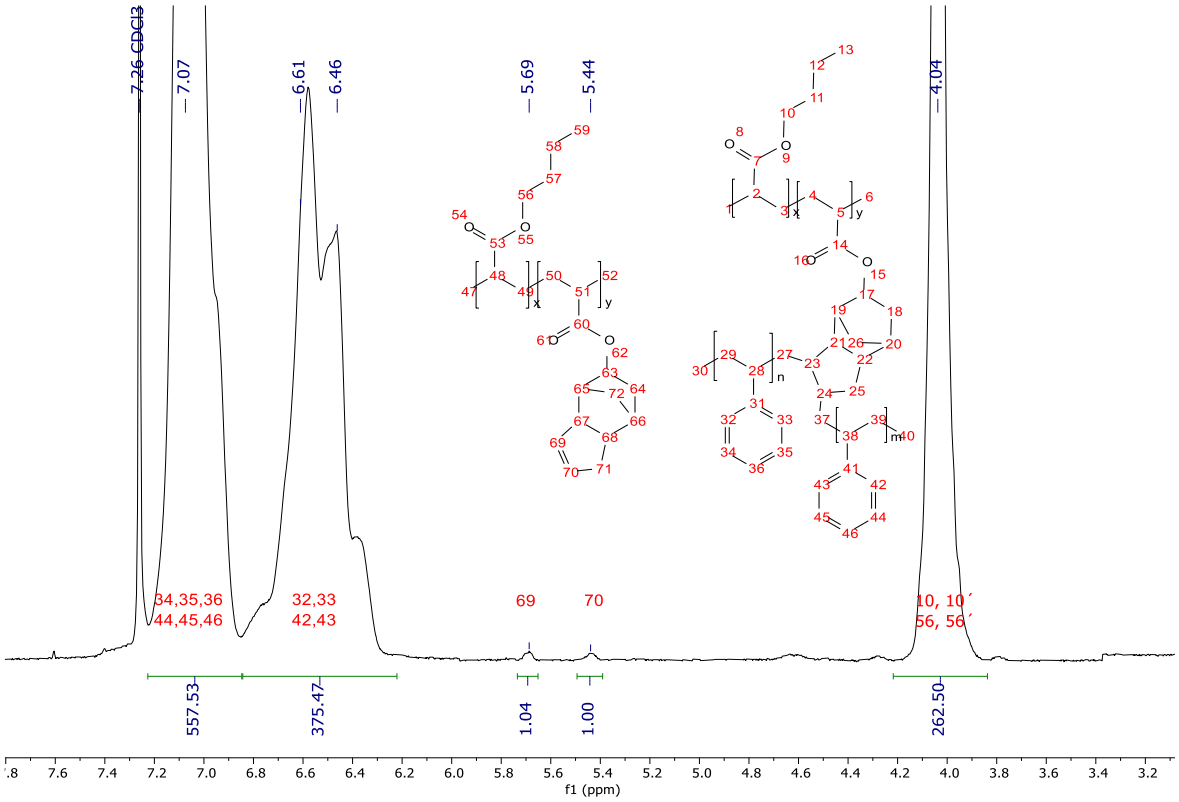

Figure 26. NMR spectrum of G-E_B$_{DCPA}$(30-1.0)_02.

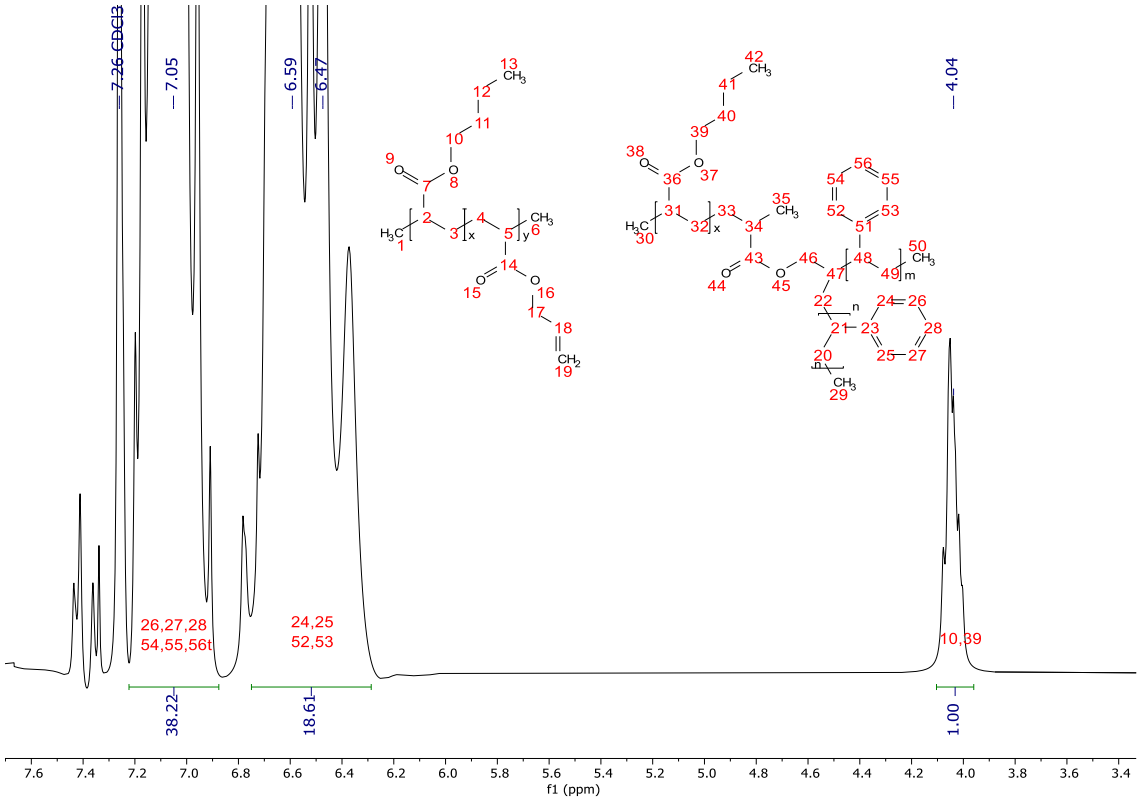

Figure 27. NMR spectrum of G- E_B$_{AMA}$(26-1.4)_02.

The integration of the peaks corresponding to the DCPA comonomer at 5.44 and 5.69 ppm shows that 2 wt.% of DCPA are present in the backbone after grafting reaction. This proves that no grafting of the PS chains has occurred and that DCPA comonomer is not a suitable moiety in a PBA-based backbone for grafting under these conditions.

Another method used to characterize the graft copolymer blends is HPLC. The HPLC chromatogram of h-PS, PBA and graft copolymerization products G-E_B_{DCPA}(30-1.0)_02 and G-E_B_{AMA}(26-1.4)_02 are depicted in Figure 28.

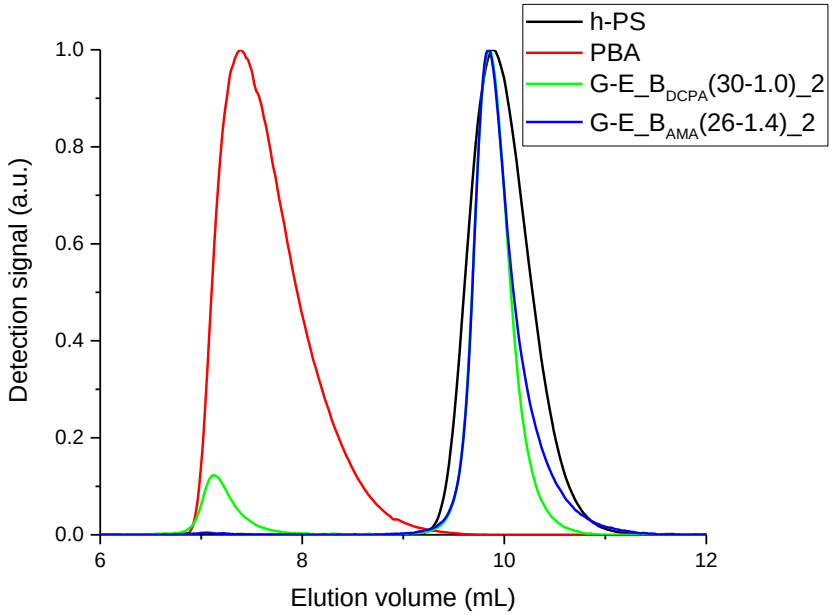

Figure 28. HPLC chromatogram of h-PS, PBA, G-E_B_{DCPA}(30-1.0)_02 and G- E_B_{AMA}(26-1.4)_02.

It is observed that the h-PS is detected at about 10 mL while a reference sample of PBA at about 7 mL. Sample G-E_B_{DCPA}(30-1.0)_02 shows two peaks appearing at PBA and PS elution volume. On the contrary, sample G-E_B_{AMA}(26-1.4)_02 shows a single peak at 10 mL, which corresponds to the elution time of h-PS. The elution time of PBA-g-PS should be similar to h-PS as PS chains are the main constituents of the graft copolymer. This indicates that grafting has happened only in case of G-E_B_{AMA}(26-1.4)_02.

Using route A in emulsion, the graft copolymerization does not occur when PBA-co-DCPA is used as a backbone. Grafting reaction was successfully achieved with PBA-co-AMA backbone, but the resulting

product is brittle and has low transparency. This indicates that there is a strong segregation between soft and hard phases in the obtained blend.

6.1.2. Route B: Synthesis of backbone using emulsion polymerization and PBA-g-PS copolymer using solution polymerization

5.1.2.1. Step 1 and 2: Synthesis of PBA-co-GMA in emulsion and polymer analogous reaction in solution

Route B uses a bifunctional comonomer, GMA, in which the glycidyl function is unreactive to radical polymerization and only the acrylate function in GMA reacts during the backbone polymerization. A polymer analogous reaction is then performed in order to convert glycidyl functions into acryloyl ones, acting as active sites during graft copolymerization.

In order to prepare PBA-co-GMA backbone, BA is copolymerized with GMA with the same conditions as used in the synthesis of E_B_{BA}(31-0) (see 6.1.1) and a series of 3 backbones is prepared (Table 5). The amount of comonomer was chosen to vary the number of reactive sites from 2 to 6 per chain in average.

Table 5. PBA-co-GMA backbones prepared in emulsion.

Backbone	fw_{GMA}	w_{GMA}	N_{GMA}	M_n	Đ
	[wt.%]	[wt.%]	[-]	[kg/mol]	[-]
E_B_{GMA}(28-1.1)	1.15	1.14	2.3	28.3	4.1
E_B_{GMA}(28-2.0)	1.92	1.97	3.9	28.4	4.2
E_B_{GMA}(30-2.7)	2.69	2.65	5.6	30.2	4.6

M_n of all the reaction products lies in the range of 30 kg/mol, comparable to the backbones E_B_{BA}(31-0), obtained through emulsion polymerization in the route A (Table 2). The PBA-co-GMA backbones were fully soluble in THF, showing that no cross-linking occurred during their synthesis.

The amount of GMA detected by NMR, w_{GMA}, in the backbone matches its feed value, fw_{GMA}. This corresponds to the amount of incorporated GMA moieties per chain of backbone N_{GMA} ranging from 2.3 to 5.6. The three backbones exhibit comparable molecular weight distribution with variation in the M_n below 2 kg/mol, as depicted in Figure 29.

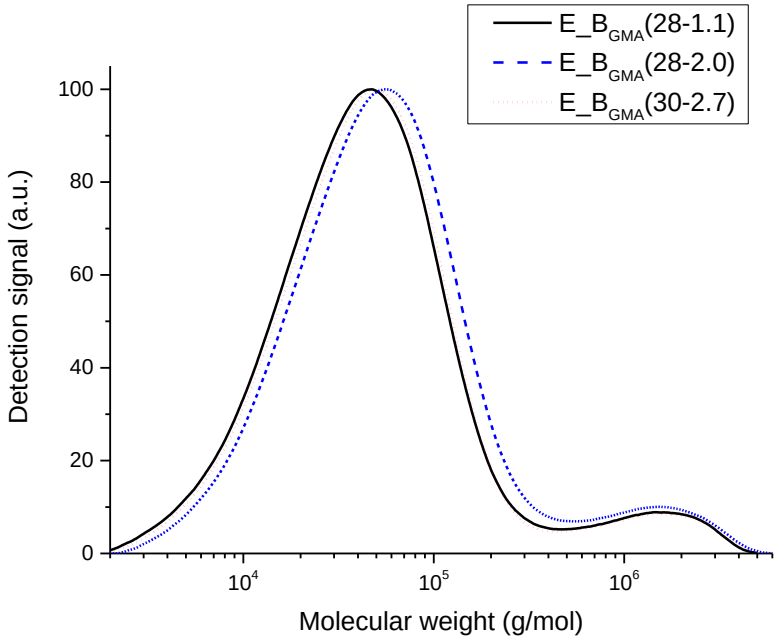

Figure 29. SEC analysis of PBA-co-GMA backbone series.

The main fraction of the polymer appears at a molecular weight of around 30 kg/mol while a smaller fraction of the polymer chains is detected at about 2 000 kg/mol. This bimodal distribution of the backbone explains the high dispersity of 4 to 5, which arises from the emulsion polymerization method and is independent of the presence of a comonomer in the system (as explained in 5.1.1.1.).

The glycidyl functions in the backbone are converted into acryloyl functions through polymer analogous reaction. For this purpose, the polymer is precipitated from the emulsion and the following modification via the polymer analogous reaction is carried out in solution. The modification of PBA-co-GMA is made using acrylic acid (AA) and triphenylphosphine (TPP) or triethylamine (TEA) as catalyst. It is expected that the following conditions have a major impact on the modification yield of the glycidyl functions: the ratio between the components, type of solvent and catalyst, duration, and temperature of the reaction. To determine the synthesis conditions allowing to reach high conversion, the study of these parameters is carried out with use of E_B$_{GMA}$(28-2.0) backbone as presented in Table 6.

Table 6. Polymer analogous reaction conditions of E_B_{GMA}(28-2.0) backbone.

Modification reaction	Backbone	TEA	TPP	AA	MEHQ	Solvent	Solvent	Temperature	Time
	[wt.%]						[type]	[°C]	[h]
#1	11.8	0.2	-	2.2	-	85.8	THF	25	24
#2	11.7	-	0.2	2.3	-	85.7		25	24
#3	11.7	-	0.2	1.6	0.01	86.4	DMF	120	8
#4	26.4	-	1.8	26.4	1.41	44.0	THF	Reflux	16
#5	25.6	1.8	-	25.56	1.46	45.6			16
#6	39.3	-	3.0	18.1	0.18	39.3			16
#7	45.0	-	0.9	9.0	0.09	45.0			60
#8	45.0	-	0.9	9.0	0.09	45.0	Toluene	Reflux	60

When the reaction is performed at boiling point of the solvent, MEHQ is used as inhibitor in order to avoid polymerization of AA and cross-linking between the backbone molecules. The ratio between the components is varied, from an equimolar ratio between the glycidyl functions and AA to a large excess of AA. Similarly, the ratio between backbone and solvent is varied from a diluted system to a concentrated one. Table 7 shows the results in terms of yield of modification in the backbone and the corresponding acryloyl concentration.

Table 7. Acryloyl concentration, yield of modification in E_B_{GMA}(28-2.0) depending on the reaction conditions.

Modification reaction	Acryloyl concentration	Yield of modification
	[wt.%]	[%]
#1	-	0
#2	-	0
#3	0.4	12
#4	2.3	78
#5	1.2	41
#6	1.1	74
#7	1.5	50
#8	1.9	96

All the post-modified backbones showed full solubility in THF, indicating that no undesired cross-linking reaction occurred. It is observed that AA does not react with glycidyl functions at room temperature with either TPP or TEA as catalyst. It appears that high concentrations of AA and backbone

in the solvent, such as in reaction #6, lead to higher acryloyl conversion. The use of TPP is also preferred to TEA as it shows high conversion of the acryloyl moieties (comparison between reactions #4 and #5). Finally, the duration of the reaction around 60 hours, together with the use of a high boiling solvent, such as in the reaction #8, allows to reach a modification yield close to 100%. Figure 30 and Figure 31 shows the ^{1}H NMR spectra of the backbone E_B_{GMA}(28-2.0) and its post-modified polymer with reaction condition from #8. The glycidyl functions in the backbone E_B_{GMA}(28-2.0), appearing between 2.6 and 3.2 ppm, are completely converted into acryloyl functions, appearing between 5.8 and 6.4 ppm in the post-modified backbone. Therefore, the conditions of this reaction are applied for all following modification of the PBA-co-GMA backbones.

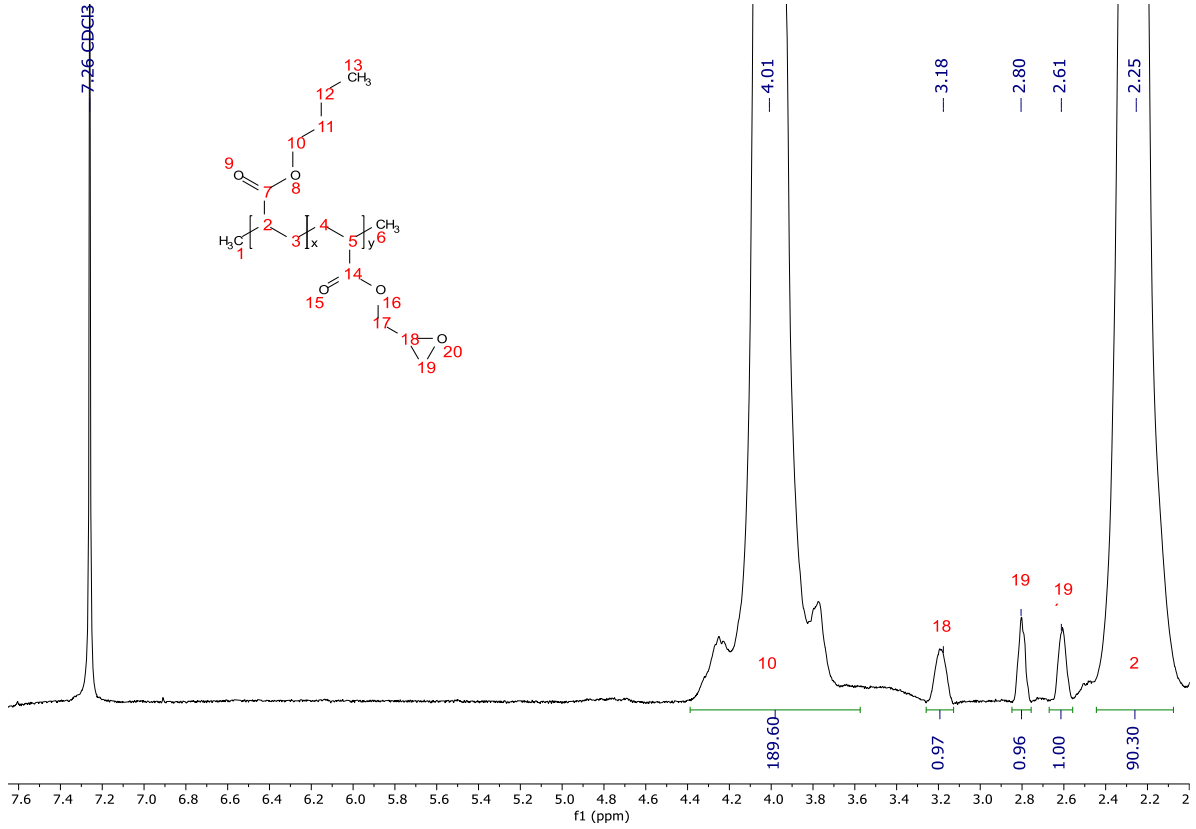

Figure 30. ^{1}H NMR spectra of E_BGMA(28-2.0).

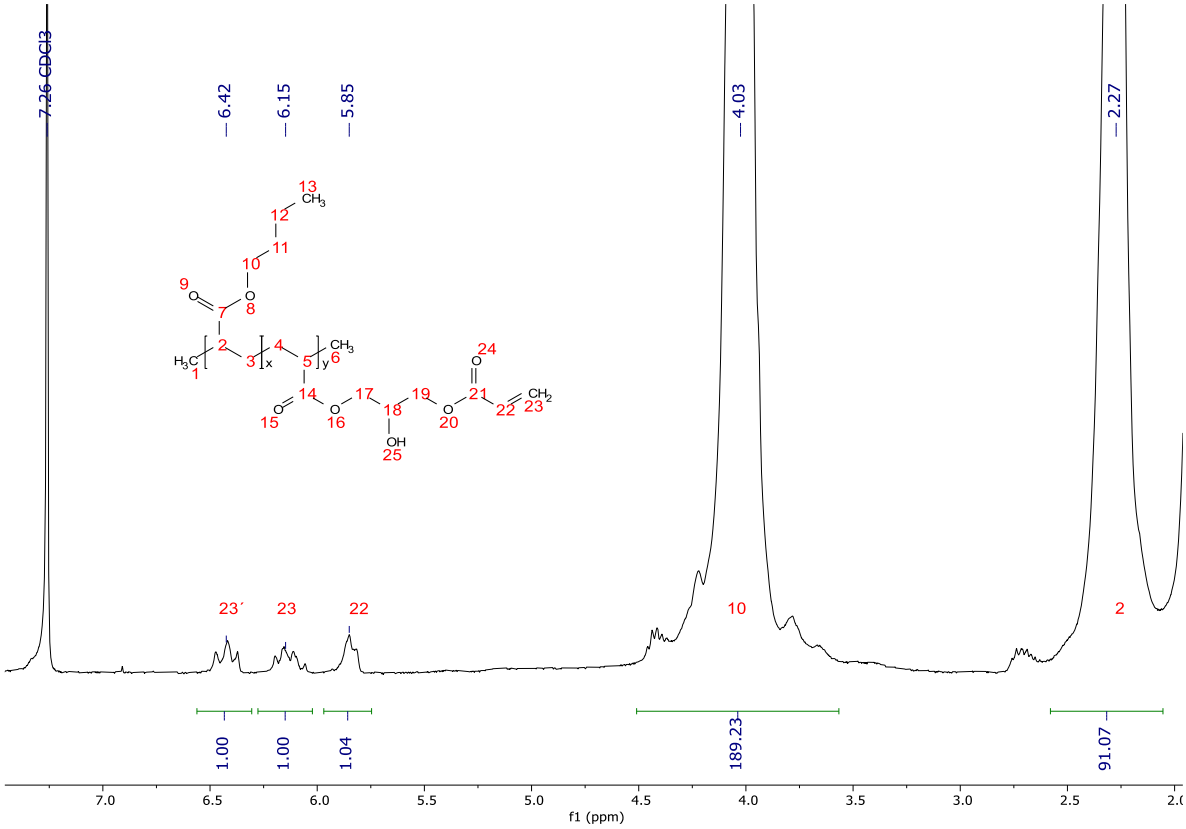

Figure 31. ^{1}H NMR spectra of post-modification version of E_B_{GMA}(28-2.0) with reaction conditions from #8.

The PBA-co-GMA backbones (see Table 5) are used for post-modification via the polymer analogous reaction in solution. The results of the modification in terms of conversion, μ, of the glycidyl groups and the number of the resulting acryloyl moieties per backbone chain (N_{Acr}) are presented in Table 8.

Table 8. Polymer analogous reaction results for PBA-co-GMA series.

Modified backbone	w_{Acr}	N_{Acr}	μ
	[wt.%]	[-]	[%]
E_B_{GMA}(28-2.3)	1.7	2.3	99
E_B_{GMA}(28-3.8)	2.8	3.8	96
E_B_{GMA}(30-5.3)	3.7	5.3	95

The polymers are fully soluble in THF after the reaction, indicating that no cross-linking occurred. The conversion of the glycidyl functions into acryloyl ones lies in the range 95-99 %. It is observed that the conversion is dependent on the starting amount of the reactive groups needed to be modified. The backbones containing lower amount of glycidyl functionalities reach higher conversion. The N_{Acr}, proportional to the content of acryloyl present in the backbone based on the NMR analysis, w_{Acr}, ranges

between 2.3 and 5.3. It should be noted that the ratio between backbone and other components is kept constant independently on the backbone used, as AA and TPP are used in large excess. This can explain the slight decrease in conversion of the glycidyl functions conversion between E_B_{GMA}(28-3.8) and E_B_{GMA}(30-5.3). The yield is, nevertheless, considered sufficient to use the backbones for graft copolymerization with styrene.

5.1.2.2. Step 3: Graft copolymerization of post-modified PBA-co-GMA with styrene in solution

The modified backbones, obtained through the polymer analogous reaction (Table 8), are used in the subsequent step for the graft copolymerization with styrene.

The graft copolymerization reaction is performed in solution using toluene. The initiator and styrene are continuously dosed within the first 10 hours of the reaction. After the dosing of all components is completed, the reaction is continued for additional 14 hours.

Table 9 summarizes the results of the graft copolymerization using the modified PBA-co-GMA backbones: PS content (grafted and non-grafted), conversion (by means of styrene monomer converted into PS) and the fraction of NSF measured by Soxhlet extraction.

Table 9. Graft copolymerization results of modified PBA-co-GMA.

Graft copolymer	w_{Acr}	N_{Acr}	Conversion	PS content	NSF
	[wt.%]	[-]	[%]	[wt.%]	[wt.%]
G-E_B_{GMA}(28-2.3)	1.7	2.3	67.5	70.8	26.8
G-E_B_{GMA}(28-3.8)	2.8	3.8	69.0	75.3	57.7
G-E_B_{GMA}(30-5.3)	3.7	5.3	68.5	78.0	61.1

The most pronounced difference between the samples lies in the NSF, which varies from 27 to 61 wt.%. It is clearly visible that the increase in NSF can be correlated to the increase of N_{Acr}. This means that when the distance between the neighboring acryloyl groups in a single backbone chain increases, the occurrence of cross-linking reactions is reduced.

However, this dependency is not linear. As compared to G-E_B_{GMA}(28-2.3), the value of the NSF is approximately doubled and reaches around 60 wt.% for both samples G-E_B_{GMA}(28-3.8) and G-E_B_{GMA}(30-5.3), although their N_{Acr} is increased. In other words, further increase of N_{Acr} in sample G-E_B_{GMA}(30-5.3) by additional 1.5 related to sample G-E_B_{GMA}(28-3.8) causes only a negligible increase

of NSF, indicating a plateau of this phenomenon. This can be explained by the steric hindrance and saturation on the backbone chains.

The conversion during graft copolymerization was determined gravimetrically, while the PS content was calculated from NMR analysis. It is observed that all these reactions reach a similar conversion of around 68 %. However, a slight increase of 8 % in the PS content is present, which can be explained by the amount of NSF in the samples. The conversion is similar for the three samples and the PS content increases with the NSF. Consequently, a higher portion of the G-E_B_{GMA}(30-5.3) sample is not solubilized in the NMR solvent, as compared to the two others and is therefore not visible in NMR. Only the soluble fraction, richer in PS is quantified, distorting the obtained values of the PS content.

Different moieties are present in the blends after graft copolymerization including h-PS and PBA-g-PS. It is expected that not all of the reactive sites on each backbone will undergo grafting and some unreacted moieties can be present in the end product. The ^{1}H NMR spectrum of the graft copolymer blend G-E_B_{GMA}(28-3.8) is presented in Figure 32.

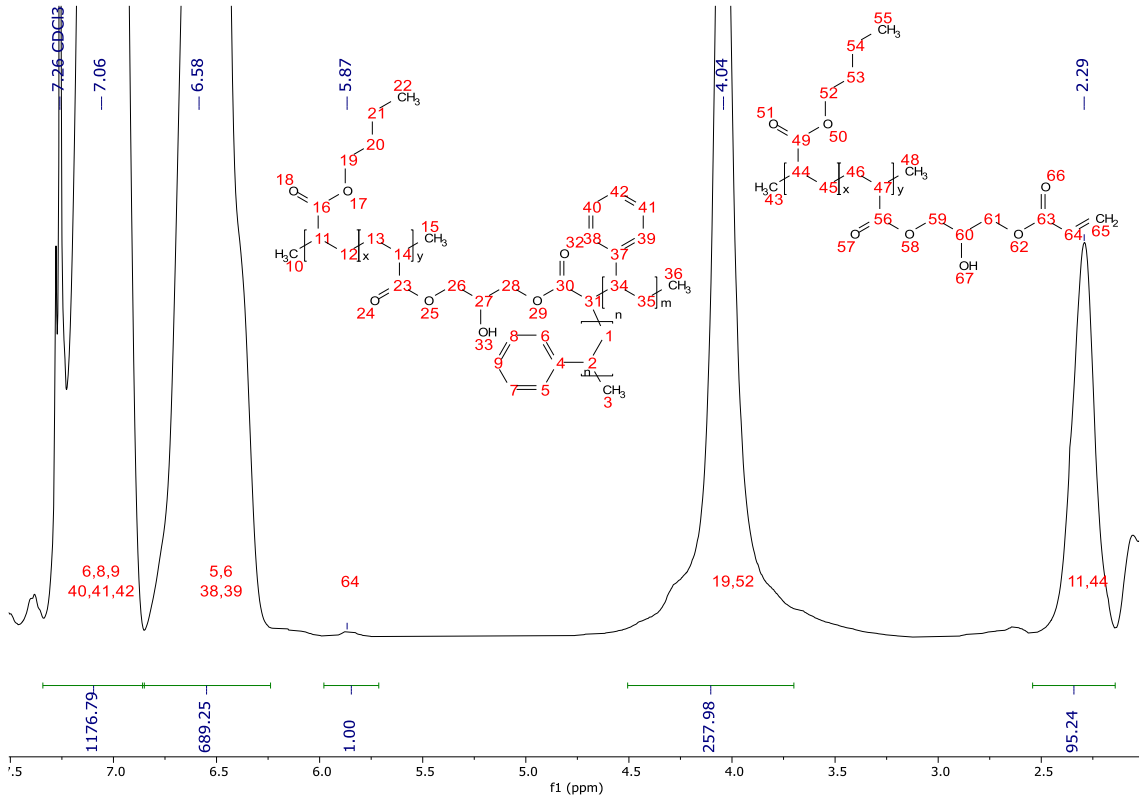

Figure 32. 1H NMR spectrum of G-E_BGMA(28-3.8).

The peaks corresponding to the H nuclei of the PS aromatic ring (H atoms 5,6,7,8,9,38,39,40,41) appear between 6.25 and 7.5 ppm. The acryloyl peak from unreacted groups in the backbone (H atom 64) is detected at 5.87 ppm.

Thin films are prepared by solvent-casting of G-E_B_{GMA}(28-2.3), G-E_B_{GMA}(28-3.8) and G-E_B_{GMA}(30-5.3) in toluene. Due to the high NSF, ranging from 27 to 61 wt.%, the films are too brittle for the mechanical properties to be measured. However, optical properties are reported and listed in Table 10.

Table 10. Optical properties of solvent-casted PBA-g-PS/h-PS samples.

Graft copolymer	N_{Acr}	Transmittance	Haze	Clarity
	[-]	[%]	[%]	[%]
G-E_B_{GMA}(28-2.3)	2.3	91.8 ± 0.2	17.2 ± 2.1	90.9 ± 0.6
G-E_B_{GMA}(28-3.8)	3.8	91.6 ± 0.4	77.5 ± 0.8	11.3 ± 0.5
G-E_B_{GMA}(30-5.3)	5.3	92.4 ± 0.1	40.6 ± 2.1	56.9 ± 4.0

The three samples have high transmittance above 90 %, which proves that most of the light passes through the sample. The scattering of the light, characterized by the values of haze and clarity, is varying greatly between the studied samples. The haze increases significantly with higher N_{Acr} between G-E_B_{GMA}(28-2.3) and G-E_B_{GMA}(28-3.8). However, further increase of N_{Acr} in the sample G-E_B_{GMA}(30-5.3) causes a reduction of haze. A reverse trend is observed for the clarity properties, showing that the sample G-E_B_{GMA}(28-2.3) has the highest transparency. The high variations between the three samples, suspected to originate from the NSF is showing a nonlinear tendency against the backbone structure.

This phenomenon is also observed when measuring the mechanical properties of the sample after extrusion. Contrary to the solvent-casted films, too brittle to be used for mechanical tests, the extruded samples were tested for tensile strength and elongation at break as depicted in Table 11.

Table 11. Mechanical properties of extruded PBA-g-PS/h-PS samples.

Graft copolymer	N_{Acr}	E Modulus	Tensile stress at yield	Elongation at break
	[-]	[MPa]	[MPa]	[%]
G-E_B_{GMA}(28-2.3)	2.3	1293 ± 98	28.7 ± 8.4	2.5 ± 0.9
G-E_B_{GMA}(28-3.8)	3.8	1261 ± 101	32.6 ± 0.7	34.0 ± 9.0
G-E_B_{GMA}(30-5.3)	5.3	1361 ± 55	34.9 ± 1.5	15.0 ± 4.0

All samples have an E modulus and tensile stress in the range of 1300 MPa and 30 MPa, respectively. However, their flexibility varies greatly with values of their elongation at break ranging from 2.5 to 34%.

The elongation at break increases significantly when the N_{Acr} goes from 2.3 to 3.8 and then decreases when the N_{Acr} is further elevated.

Two main conclusions can be drawn from this series of experiments. Firstly, graft copolymerization occurs when route B is used, which is proven by NMR spectroscopy. The step of graft copolymerization is crucial in influencing the presence of the cross-linked fraction in the blend and the transparency and/or flexibility of the samples. The second learning is that the presence of cross-linking reactions during the graft copolymerization, which cannot be avoided in the applied polymerization method without affecting the grafting efficiency and/or the molecular weight of the polymer, influences the physical properties of the samples. A balance between NSF, sufficient grafting efficiency and sufficient molecular weight is necessary to obtain flexible and transparent blend.

5.1.2.3. Statistical analysis of the grafting reaction of styrene onto post-modified PBA-co-GMA in solution

A high number of factors influences the graft copolymerization synthesis, as well as the product properties. A design-of-experiment (DoE) is an efficient tool to determine the influence and interdependence of factors on molecular weight or grafting efficiency. In this method, selected factors are fixed and unchanged through all the experiments, while a limited number of them is varied. Table 12 lists the determining factors relevant for the graft copolymerization synthesis, their influence on the reaction and/or product and their estimated impact, from low to high.

Table 12. Factors of influence and their estimated impact on the synthesis and/or product.

Factor	Influence on	Estimated impact
Solvent type	Choice of polymerization temperature Transfer reaction to the solvent Molecular weight of PS (grafted or not)	Low
Initiator type	Grafting efficiency Molecular weight of PS (grafted or not)	Medium
Temperature	Initiator dissociation constant Styrene propagation constant	Medium

	Molecular weight of PS (grafted or not) Styrene conversion	
Styrene/initiator addition: single portion added at the beginning of the reaction or continuous dosing	Concentration of initiator and styrene vs backbone Molecular weight of PS (grafted or not) Grafting efficiency NSF	High
Structure of the backbone (M_n and N_{Acr})	Grafting efficiency NSF Phase separation behavior of the blend	High
Monomer and initiator continuous dosing duration	Concentration of initiator and styrene versus backbone Molecular weight of PS (grafted or not) Grafting efficiency NSF	Medium
Initiator concentration	Molecular weight of PS (grafted or not) Grafting efficiency NSF Styrene conversion	High
Final polymer concentration	Molecular weight of PS (grafted or not) Grafting efficiency NSF Styrene conversion	High

Two types of initiators, azo and peroxides, are commonly used in solution polymerization, such as AIBN and BPO, respectively. Huang et al. showed that BPO is the best type of initiator in comparison to AIBN to perform graft copolymerization onto PB backbone [88]. BPO has higher half-life time compared to AIBN. This allows working at higher temperature, thus increasing the reactivity rate of styrene.

As previously mentioned, the initiator and/or styrene can be added in a single portion at the beginning of the reaction or dosed continuously through the reaction course. The advantage of the latter is the ability to regulate the concentration between backbone, styrene, and initiator over the complete reaction course. The temperature of the reaction influences the reactivity of styrene and initiator. An increase in temperature increases the dissociation rate of the initiator, as well as the propagation constant of styrene and of the backbone reactive groups.

Three factors, which are expected to influence greatly the outcome of the graft copolymerization synthesis, are selected and varied in the carried DoE. Table 13 lists these factors with their status during the DoE and their chosen values.

Table 13. Status of factors during the DoE and their values.

Factor	Status during DoE	Value
Solvent	Fixed	Toluene
Initiator	Fixed	BPO
Temperature [°C]	Fixed	85
Structure of the backbone (M_n and N_{Acr})	Fixed	Backbone E_B_{GMA}(28-3.8) (M_n=28.4 kg/mol, N_{Acr}=3.8)
Styrene/initiator addition: single portion added at the beginning of the reaction or continuous dosing	Fixed	Continuous dosing
Monomer and initiator continuous dosing duration [h]	Varied	5, 10, 15
Initiator concentration [wt.% (rel. to styrene)]	Varied	0.5, 1, 1.5
Final polymer concentration [wt.%]	Varied	25, 30, 35

The reaction setup is a 250 mL reactor equipped with an anchor stirrer. The temperature of reaction is fixed at 85°C and the solvent is toluene. The backbone used is E_B_{GMA}(28-3.8) as it has medium N_{Acr}, assuring sufficient grafting and lowering the risk of cross-linking reactions. The monomer and initiator are continuously dosed through the reaction, in order to keep the backbone in an excess compared to the styrene/initiator mixture.

The varied factors are: the initiator concentration, the final polymer concentration and the duration of the dosing of the styrene/initiator mixture. Each of these factors is varied on three levels. A full exploration of the system by a DoE using three factors and three levels, requires a minimum of 27 experiments. In order to limit the number of experiments and subsequent analysis required, a fractional design called Box-Behnken design (BBD) is used. The number of experiments is determined using the following equation:

$$N = 2k(k-1) + n_0 \tag{29}$$

where N is the number of experiments, k is the number of factors and n_0 is the number of experiments performed at midpoint. With a choice of 3 factors and 3 repetitions of the midpoint it is necessary to

perform 15 experiments. The list of experiments, as well as the experimental conditions are presented in Table 14.

Table 14. List of DoE synthesis for graft copolymerization and their factors variation based on the BBD.

Graft copolymerization	Initiator concentration	Polymer concentration	Dosing duration
	[wt.% rel. to monomer]	[wt.%]	[h]
#1	1.0	25	5
#2	1.0	25	15
#3	0.5	25	10
#4	1.5	25	10
#5	0.5	30	5
#6	1.5	30	5
#7	0.5	30	15
#8	1.5	30	15
#9	1.0	30	10
#10	1.0	30	10
#11	1.0	30	10
#12	1.0	35	5
#13	1.0	35	15
#14	0.5	35	10
#15	1.5	35	10

In order to evaluate the influence of the factors a list of responses of the system, based on chemical and physical analysis of the product, is determined. The conversion is measured gravimetrically and the E modulus, tensile strength and elongation at break of the blends are evaluated on extruded samples. As the NFS disturbs the casting of films, the optical properties of the blends are not taken into account in the DoE. The list of responses obtained for the 15 DoE experiments is presented in Table 15.

Table 15. List of responses for graft copolymerization product obtained for the DoE experiments.

Graft copolymerization	Conversion	NSF	M_n	E Modulus	Tensile strength	Elongation at break
	[%]	[wt.%]	[kg/mol]	[Mpa]	[Mpa]	[%]
#1	68.8	23.7	18.1	1239 ± 22	26.2 ± 0.5	20.7 ± 21.0
#2	53.4	37.5	18.9	374 ± 34	11.5 ± 0.4	60.5 ± 6.1
#3	55.7	50.2	34.0	745 ± 35	15.6 ± 0.5	42.8 ± 7.5
#4	78.6	29.9	14.7	1104 ± 20	10.0 ± 1.2	0.8 ± 0.4
#5	57.9	51.1	26.8	916 ± 21	19.3 ± 0.8	45.0 ± 5.1
#6	61.2	44.5	13.4	392 ± 18	11.8 ± 0.2	55.9 ± 11.8
#7	61.2	59.0	27.1	40 ± 9	8.5 ± 0.6	67.4 ± 4.1
#8	67.7	46.5	15.9	744 ± 53	17.3 ± 1.0	29.8 ± 11.4
#9	77.4	35.8	15.4	867 ± 33	18.5 ± 0.9	39.2 ± 4.3
#10	64.5	42.6	17.8	1015 ± 27	20.7 ± 2.5	21.5 ± 19.4

#11	69.7	45.0	19.6	1205 ± 24	25.0 ± 0.7	25.3 ± 21.9
#12	86.6	51.6	15.1	457 ± 34	11.2 ± 0.3	50.1 ± 5.3
#13	68.1	46.9	17.8	698 ± 91	15.5 ± 2.8	33.3 ± 14.8
#14	66.8	69.6	24.7	838 ± 44	18.1 ± 0.9	46.8 ± 2.7
#15	89.3	51.9	15.3	1092 ± 90	9.2 ± 2.9	0.7 ± 0.2

The evaluation of the DoE results by statistical analysis allows to determine:

- the influence of each factor on the responses,
- the interaction between factors influencing specific responses,
- the combination of factors needed to reach specific responses targets,
- the repeatability of the graft copolymerization.

Figure 33 represents the factors effects on the responses, estimated by the T-value, which measures the size of the difference relative to the variation in the sample data. The bar chart helps in comparing the relative importance of the effects. A dotted line shows the statistical significance limit above which the effect becomes substantial.

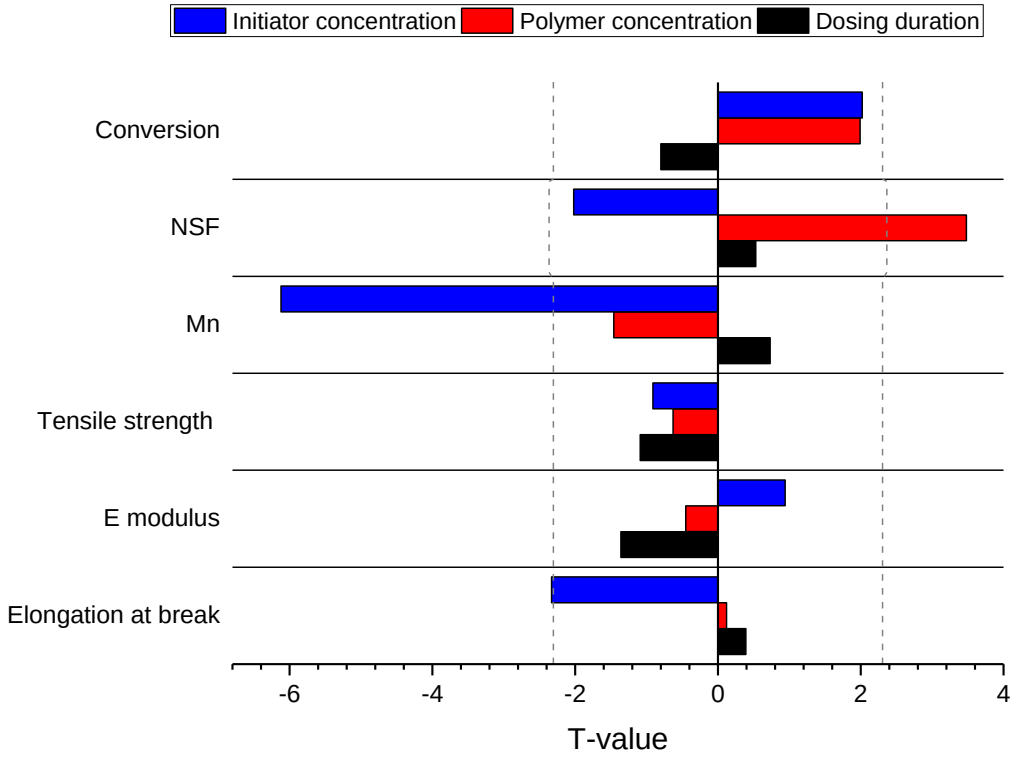

Figure 33. T-values of responses related to the different factors.

It is observed that the mechanical properties of the samples, represented by the tensile strength, the E modulus and the elongation at break are only moderately influenced by the three varied factors. On the contrary, M_n and NSF are greatly influenced by the initiator and the polymer concentration. Between three studied factors, the dosing duration has the smallest influence on the responses, whereas the initiator concentration show the greatest effect.

The main effects of polymer and initiator concentration on the responses are depicted in Figure 34. As already described by the analysis of the T-values, the dosing duration has only limited impact on the responses and its main effect plot is, therefore, not shown.

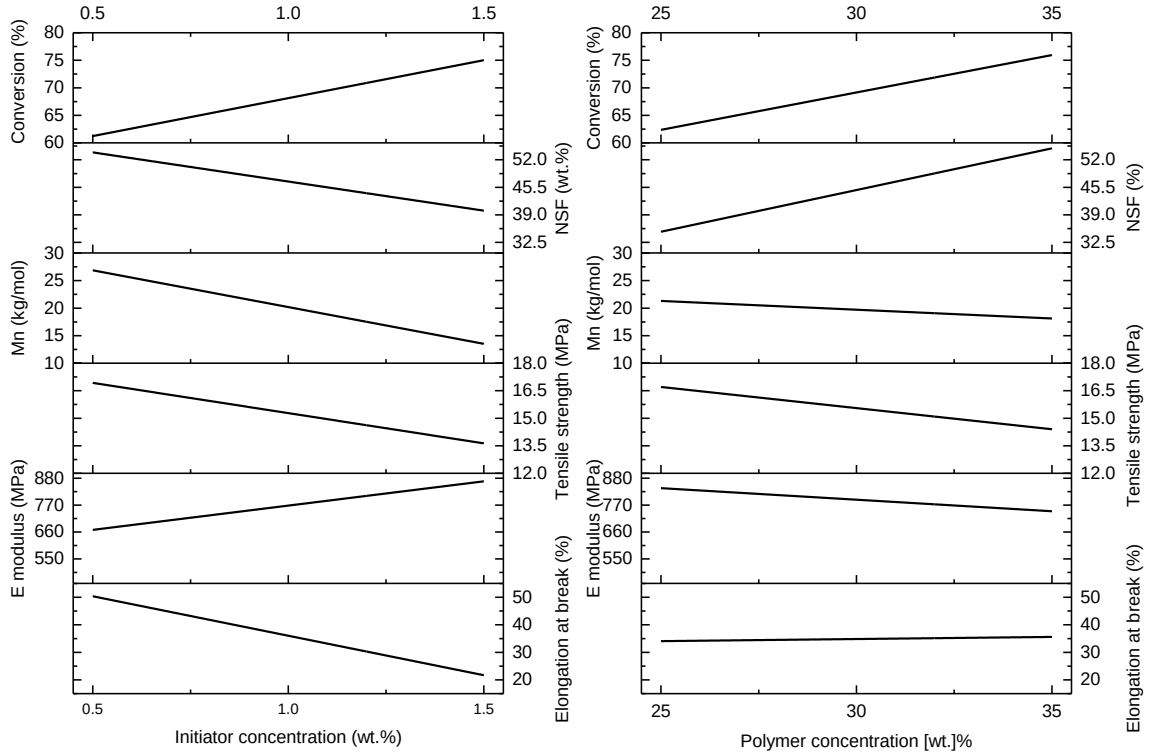

Figure 34. Main effect plot of initiator and polymer concentration.

As it is expected, the increase of initiator and polymer concentration rises the conversion of styrene in the system and decreases M_n of the graft copolymer blend. This is due to a higher concentration of radical and/or styrene in the solvent.

The NSF increases with the initiator concentration. This is correlated to the fact, that a higher number of radicals in the system increases the initiation of styrene. Henceforth, the number of growing chains is higher and the probability for them to create cross-links by attacking multiple backbone chains is

lowered. It is also observed, that an elevation of the polymer concentration leads to higher NSF in the final product. Higher concentrations of backbone and styrene in the solvent increase the probability for a growing PS chain to attack more than one backbone molecule, initiating cross-linking.

No major impact of the factors is observed on the E modulus and tensile strength. However, the elongation at break is more than halved when the initiator concentration increases from 0.5 to 1.5 wt.%. This is explained by the reduction of the M_n with increase of the initiator concentration.

The following outcome of the DoE is the evaluation of interaction between two factors influencing the responses. To evaluate the interaction between the polymer and initiator concentration, interaction plots are used, as shown in Figure 35.

The interaction plot displays the fitted values of the responses on the Y-axis, while the X-axis shows the values of the polymer concentration. Meanwhile, the various lines represent values of the initiator concentration. If the lines representing the different levels of initiator concentration are parallel, it means that no interaction occurs between polymer and initiator concentration. The more unparallel the lines are, the greater the strength of the interaction.

It appears that none or only a slight interaction between the two factors is present for the conversion and the elongation at break. A slight interaction is visible for M_n and NSF.

As anticipated, M_n decreases with an increase of initiator concentration. It is expected that M_n would increase at elevated polymer concentration, due to the lower interaction with the solvent. However, it is observed only when 1.5 wt.% of initiator is used. This can be explained by the fact that the NSF increases with the polymer concentration and that the SEC measurement analyzes only the soluble part of the sample.

Strong interaction between the polymer and initiator concentration appears for the E modulus and tensile strength of the samples. This means that the variation of tensile strength and E modulus with the polymer concentration is different, depending on the initiator concentration used. Indeed, the tensile strength increases with the polymer concentration when 0.5 wt.% of initiator is used, but the tendency is reversed at 1 wt.% of initiator concentration. A similar principle but with an inverse effect is observed with the E modulus.

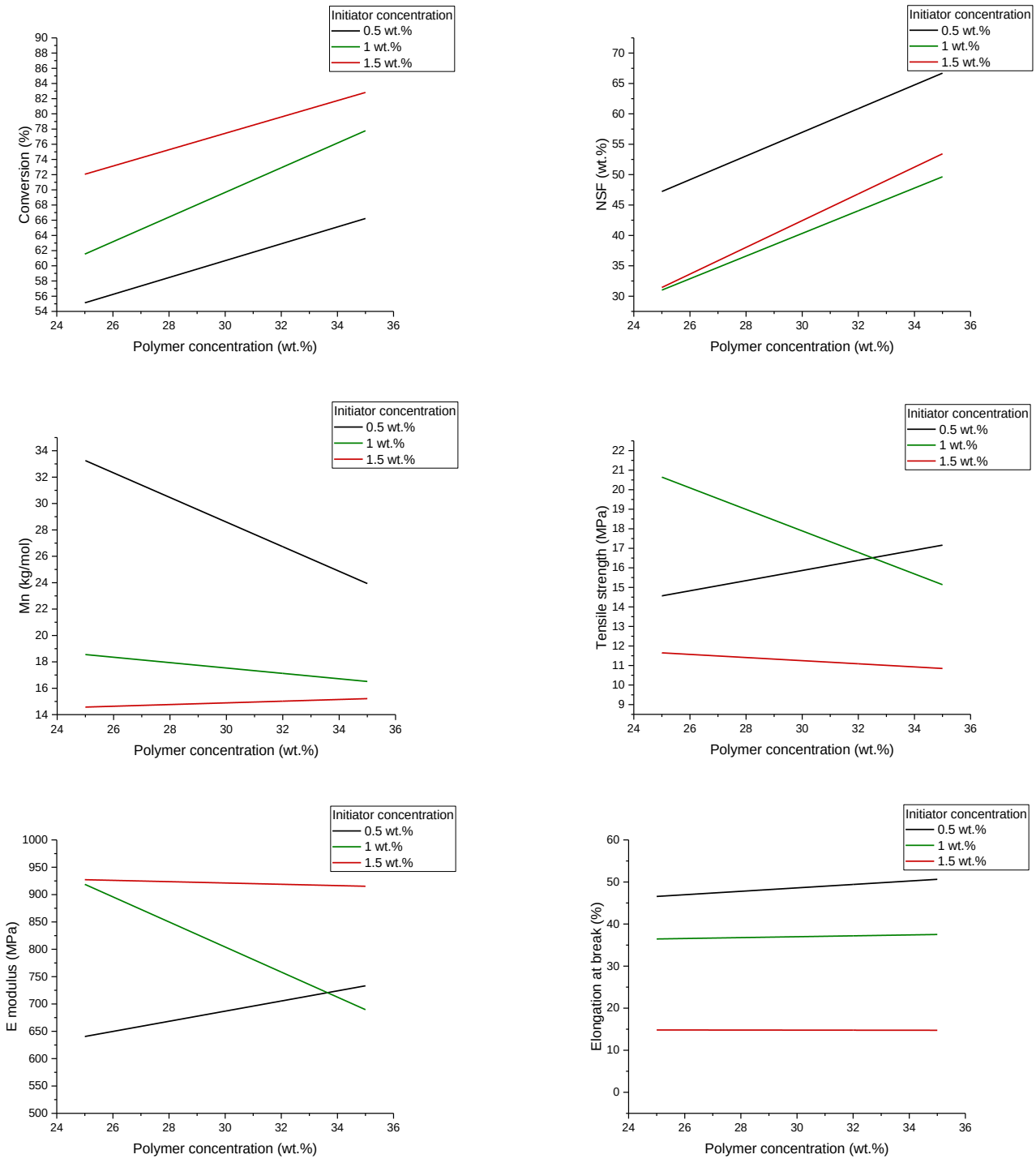

Figure 35. Interaction plot for the polymer and initiator concentration.

Contour plots are used to represent the variation of the response values in function of 2 factors. The contour plots for the 6 responses in function of polymer and initiator concentration are depicted in Figure 36. These plots are used in order to evaluate the effect of factor variation on multiple responses and determine the area of optimal response values.

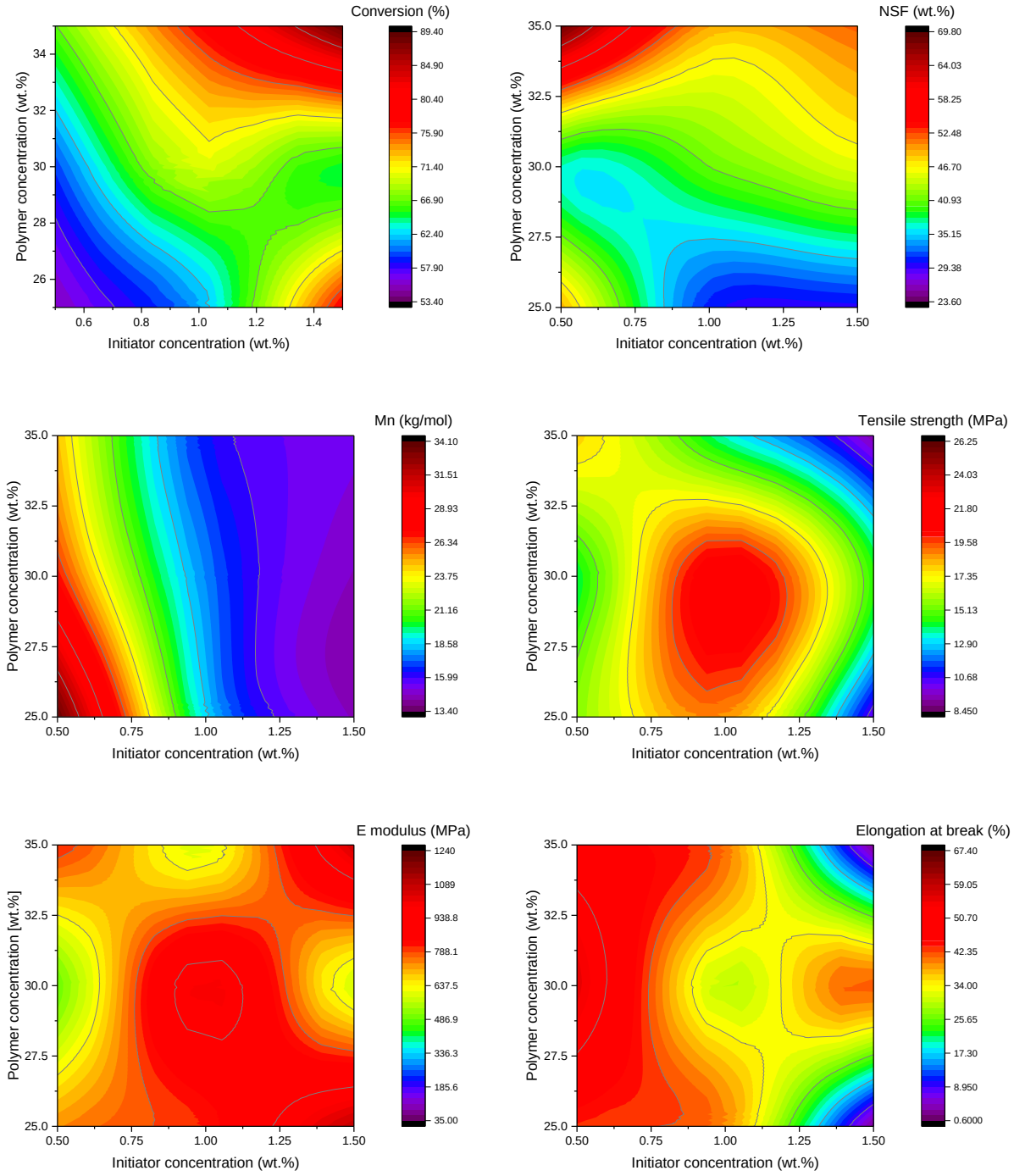

Figure 36. Contour plots of various responses in function of polymer and initiator concentration.

As already mentioned, the initiator concentration is the main factor determining the decrease of M_n. However, this dependency of M_n is not directly correlated to changes in mechanical properties, which are additionally impacted by the polymer concentration. The lack of clear trend in correlation between the M_n and the mechanical properties is expected to arise from the observed variation of NSF and

conversion. The NSF is increasing with the polymer concentration as the amount of backbone in the solvent is higher, that probability to form cross-links is increased. An increase in the initiator concentration reduces the NSF in the sample as the more radical present in the reaction mixture, the more PS chains are formed and the possibility for them to form cross-link between the backbone chains is reduced.

The E modulus and tensile strength are globally evolving in opposite manner to the elongation at break. However, some areas on the contour plots combine moderate E modulus and elongation at break. These areas are used for optimization reaction, which targets at reaching specific values of the responses.

The repeatability of the graft copolymerization is evaluated by comparing the responses of DoE experiments #9, #10 and #11. The three synthesis are performed under the same conditions with an initiator concentration of 1 wt.%, a polymer concentration of 25 wt.% and a dosing duration of 5 h. The average of their measured responses, their standard deviation (SD) and coefficient of variation (CV) are presented in Table 16.

Table 16. Responses values for the 3 center points and their average.

Graft copolymerization	Conversion	NSF	M_n	E Modulus	Tensile strength	Elongation at break
	[%]	[wt.%]	[kg/mol]	[MPa]	[MPa]	[%]
#9	77.4	35.8	15.4	867	18.5	39.2
#10	64.5	42.6	17.8	1015	20.7	21.5
#11	69.7	45.0	19.6	1205	25.0	25.3
Average±SD	70.5 ± 5.3	41.1 ± 3.9	17.6 ± 1.7	1029 ± 139	21.4 ± 2.7	28.7 ± 7.6
CV [%]	7.5	9.5	9.8	13.5	12.6	26.5

The CV of conversion, NSF and M_n, is below 10%. However, the variation of mechanical properties is more pronounced with a CV ranging from 12 to 27 %. The source of theses variations is attributed to the NSF in the samples. The cross-linked particles, formed during the polymerization, increase the viscosity of the mixture by creating a gel. At a high NSF, the reaction mixture segregates between the gel and solution, making it inhomogeneous. This kind of heterogeneity is responsible for high disparity in the local concentration of components, further enhancing the formation of cross-links.

The optimization is performed by fixing desired responses and calculating the levels of the factors which should be used for the synthesis. The validity of the DoE is confirmed when the measured properties correspond to the targeted ones.

In the following study, two optimization reactions are performed aiming at different values of E modulus and elongation at break. Consequently, the required levels of the initiator concentration, polymer concentration and dosing duration are calculated based on the selected target values. The set targets and results of the optimization synthesis are depicted in Table 17.

Table 17. Optimization reaction – Targeted and obtained responses.

	Target			Results		
Graft copolymerization	Conversion [%]	E Modulus [MPa]	Elongation at break [%]	Conversion [%]	E Modulus [MPa]	Elongation at break [%]
#opt1	>60	>700	>20	84.6	769 ± 136	16.1 ± 7.1
#opt2	>60	>500	>50	59.9	439 ± 98	80.2 ± 11.5

It is observed that the target values of mechanical data are achieved. As desired, #opt1 has moderate elongation at break and high E modulus, while #opt2 has high elongation at break and lower E modulus. The elongation at break of #opt1 is, however, slightly lower than the targeted value. Similarly, the E modulus in case of #opt 2 is lower than the targeted value. Thus, these reactions prove the validity of the performed DoE. Based on the carried experiments, it was possible to define the window of mechanical properties reachable in the studied system. It can be concluded that the E modulus of graft copolymer can be as high as 750 MPa, while its elongation at break remains above 15 %.

As mentioned before, the origin of the cross-linking reaction lies in the reactivity of the functional groups of the backbone and in the viscosity of the reaction mixture. Indeed, a high number of reactive sites in the backbone leads to higher probability of cross-linking. Similarly, high viscosity of the reaction mixture reduces the mobility of the chains and increases the probability of local gel effects, which leads to higher reaction speed, increasing the possibility of cross-linking. As already described in 4.1.2.1, the backbone E_B_{GMA}(28-2.0) has a bimodal distribution, with the main peak around 50 kg/mol and an additional high molecular weight peak at around 2 000 kg/mol. Such results of emulsion synthesis with use of a chain transfer agent where the formation of such bimodal distributed polymer has already been described. [101] In the graft copolymer studied in this work, the bimodal distribution of the E_B_{GMA}(28-2.0) backbone is expected to have an influence on the viscosity of the reaction mixture, as

well as on the amount of the reactive groups present in a single backbone chain. In order to investigate the formation of the low and high molecular weight fractions in the backbone, samples are collected during the synthesis of the backbone and analyzed via SEC. The resulting SEC curves are presented in Figure 37 and the evolution of M_n, Đ and calculated N_{GMA} in Table 18.

Table 18. Evolution of M_n and Đ during the synthesis of backbone E_B_{GMA}(28-2.0).

Time	N_{GMA}	M_n	Đ
[h]	[-]	[kg/mol]	[-]
0.5	57.2	423.5	3.3
1.5	7.5	55.3	7.8
3.5	3.9	28.4	4.2

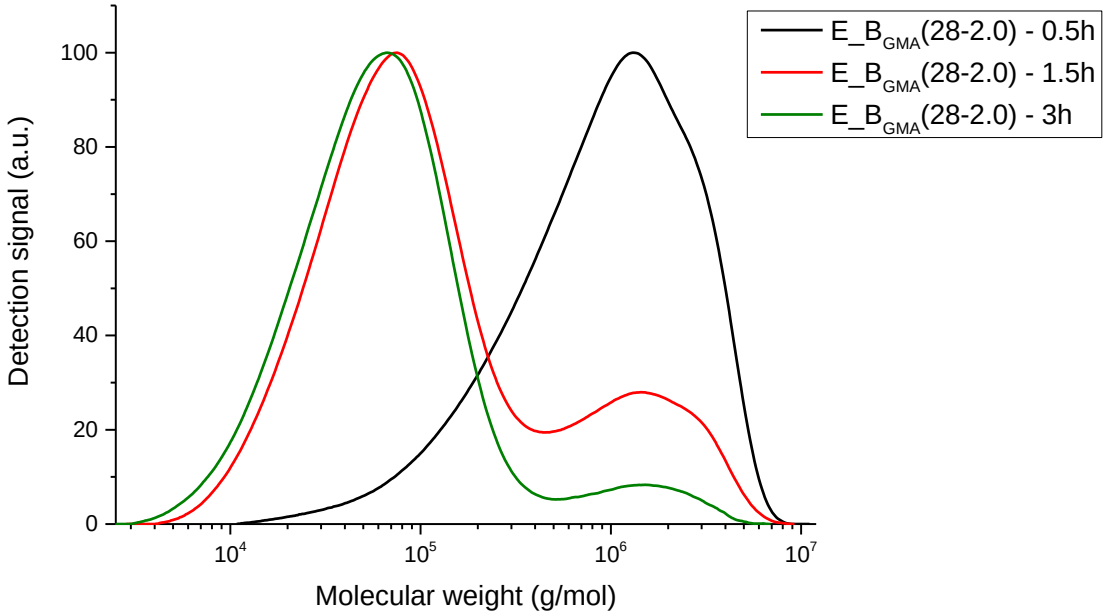

Figure 37. SEC of the backbone E_B_{GMA}(28-2.0) – Evolution with the reaction time.

It appears that high molecular weight chains, with M_n around 424 kg/mol are formed at the early stage of the reaction, while the peak at about 50 kg/mol is formed in the later stage. Consequently, the theoretical amount of GMA moieties per chain of polymer, N_{GMA}, lies at 57.2 in these high M_n chains.

This study shows a great difference between the molecular weight distribution during the reaction course and its final state in the backbone product. The molecular weight distribution of the backbone

influences the number of reactive groups present per backbone chains and consequently the course of the graft copolymerization. Therefore, having a portion of the chains with N_{GMA} up to 57 increases the probability of cross-linking occurrence during the graft copolymerization.

The emulsion polymerization of PBA-co-GMA and the subsequent complete conversion of the glycidyl functions into acryloyl ones was shown. The graft copolymerization of styrene onto the backbone was proven to be successful in comparison to the route A performed in emulsion. The influence of reaction factors such as polymer concentration, initiator concentration and dosing time of initiator/styrene has been studied through a DoE. It showed the importance of the initiator concentration on the course of the reaction, the architecture of the product and its mechanical properties. The DoE also highlighted the presence of NSF in all samples and the impact it represents on the stability and repeatability of the synthesis. The synthesis of the backbone via emulsion polymerization is the source of development of high molecular weight chains over 400 kg/mol, which influences the probability of cross-linking due to high reactive groups concentration and increase of reaction mixture viscosity.

Synthesis of PBA-g-PS/h-PS is achieved using route B where the PBA-co-GMA backbone is synthesized by emulsion, while the post-modification and the graft copolymerization with styrene are performed in solution. This process offers numerous advantages in comparison to route A, especially in term of backbone design. However, the polymerization of the backbone in emulsion leads to the formation of a polymer with a bimodal distribution. Consequently, it increases the probability of cross-linking during the graft copolymerization with styrene, which reduces the repeatability of the process and the processability of the product.

6.2. Process by solution polymerization of the backbone

As described in the previous section, the synthesis of PBA-based backbones by emulsion polymerization leads to the formation of polymer with bimodal distribution. Polymerization of the backbone in solution reduces the chance of cross-linking and allows the formation of polymer with monomodal molecular weight distribution. In this section, route A and B are studied with a polymer backbone synthesized by solution polymerization.

6.2.1. Route A: Synthesis of backbone and PBA-g-PS copolymer using solution polymerization

In the route A, the backbone is synthesized by copolymerization of BA with AMA and subsequently used for graft copolymerization with styrene.

5.2.1.1. Step 1: Synthesis of PBA-co-AMA backbone

Due to the bifunctionality of AMA, the solution polymerization of PBA-co-AMA can easily lead to cross-linking reaction. In order to avoid it, AMA is copolymerized with BA in the presence of TDT as a chain transfer agent. Furthermore, a portion of the monomers and initiator are continuously dosed through the reaction course to avoid the conditions promoting the cross-linking. Such continuous addition of the monomer and initiator mixture allows to carry the reaction in a diluted state. A series of 3 backbones is prepared, varying the final polymer concentration in the solvent and the feed amount of AMA, fw_{AMA}. Table 19 shows the synthesis conditions, as well as M_n and Đ of the synthesized polymers.

Table 19. Synthesis conditions of PBA-co-AMA backbones via solution polymerization (CL means that the product was cross-linked).

Backbone	fw_{AMA}	Polymer concentration	NSF	M_n	Đ
	[wt.%]	[wt.%]	[wt.%]	[kg/mol]	[-]
S_B_{AMA}(CL-4)	4	50	100	-	-
S_B_{AMA}(CL-2)	2	33	100	-	-
S_B_{AMA}(29-2)	2	25	0	29.2	3.2

It is observed, that the polymerization with 2 wt.% of AMA and 25 wt.% of polymer concentration in the solution does not cross-link and produces a backbone with a M_n of about 30 kg/mol. An increase in the polymer concentration and/or in the amount of AMA results in the presence of non-soluble particles in the reaction mixture. Therefore, the materials cannot be characterized via SEC and are omitted in further study. The molecular weight distribution of S_B_{AMA}(29-2) is represented by the SEC curve in Figure 38 and compared to the E_B_{AMA}(26-1.4) presented in part 5.1.1.1.

The backbone S_ B_{AMA}(29-2) has a broad distribution with a Đ of 3.2, higher than the typical distribution of a polymer prepared by free-radical polymerization, which usually have a dispersity between 1.5 and 2. This broad distribution is due to branching of the polymer chains due to the presence of AMA as comonomer.[99] However, by comparison to the equivalent backbone prepared by emulsion polymerization E_B_{AMA}(26-1.4), it shows monomodal distribution of the molecular weight and no fraction of oligomeric chains. The polymerization of PBA-co-AMA was achieved without cross-linking in solution and the backbone can be used for graft copolymerization.

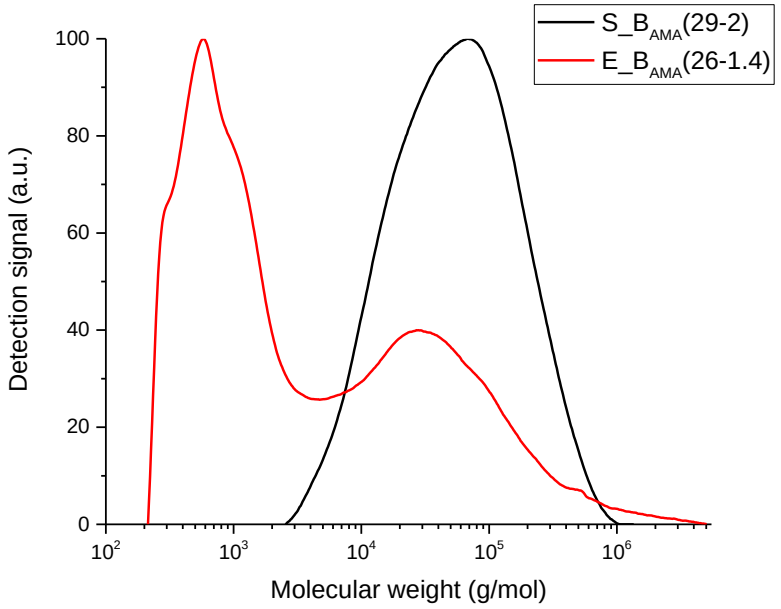

Figure 38. SEC curve of solution vs emulsion polymerization PBA-co-AMA.

5.2.1.2. Step 2: Graft copolymerization of PBA-co-AMA with styrene

The backbone S_B$_{AMA}$(29-2) is used for graft copolymerization with styrene in toluene. The final polymer concentration in the solution is varied to observe its impact on M_n and the tensile properties. The results including the mechanical properties of the product measured on extruded and injection molded samples are presented in Table 20.

Table 20. Graft copolymerization of S_B$_{AMA}$(29-2) with styrene.

Graft copolymer	Polymer concentration	M_n	Đ	NSF	Conversion	E Modulus	Elongation at break
	[wt.%]	[kg/mol]	[-]	[wt.%]	[%]	[MPa]	[%]
G-S_B$_{AMA}$(29-2)_01*	30	14.8	2.8	0	55.5	-	-
G-S_B$_{AMA}$(29-2)_02*	40	18.5	2.6	0	82.7	-	-
G-S_B$_{AMA}$(29-2)_03	50	21.9	2.6	0	98.3	1176	1.7

*Brittleness of the sample is too high to perform tensile strength test.

The increase of polymer concentration causes an increase of the conversion from 55 to 98 % and an increase of M_n from 14 to 22 kg/mol. The copolymerization syntheses do not lead to cross-linking reactions and the products are fully soluble in toluene. The specimen G-S_B$_{AMA}$(29-2)_03 shows high E modulus and low elongation at break. Although the samples G-S_B$_{AMA}$(29-2)_01 and G-S_B$_{AMA}$(29-2)_02 could be processed by extrusion and injection molding, the obtained specimens are too brittle

to be characterized by tensile testing. The analysis of the molecular weight distribution of the backbone and its grafting products is presented in Figure 39.

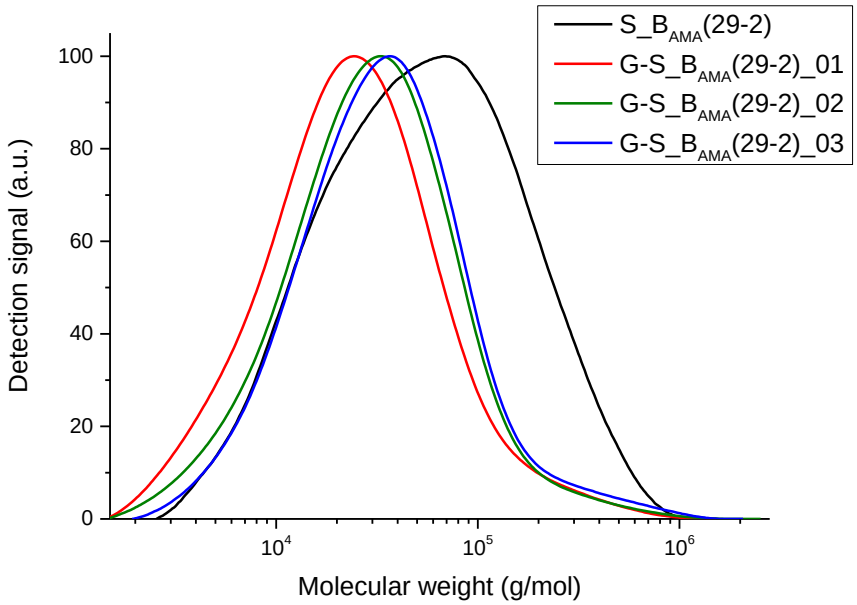

Figure 39. SEC curves of S_B$_{AMA}$(29-2) backbone and its graft copolymerization products.

It is observed that the molecular weight of the graft copolymerization products is lower than the backbone. This suggests that no or low amount of chains are grafted when using PBA-co-AMA as backbone. This is confirmed by NMR analysis, which shows that the amount of unreacted AMA groups is constant in the backbone after the graft copolymerization step.

By comparison to the polymerization of PBA-g-PS using route A in emulsion, the reaction in solution is less effective, yielding low to no grafting. This could be ascribed to the high dilution of the allyl functions in the polymer and in the solution. In principle, use of higher polymer concentration in the solvent or an increase in the number of functional groups on the backbone is expected to promote the grafting efficiency. However, exceeding the applied concentration of the polymer solution is not feasible in the studied system due to the high viscosity of the reaction media, causing difficulties in mixing and monomer diffusion at high reaction conversion. Furthermore, increasing the amount of AMA in the backbone is limited due to the high risk of crosslinking of the backbone.

6.2.2. Route B: Synthesis of PBA-g-PS in solution

As it was demonstrated in 6.1.2, it is possible to carry out the synthesis of graft copolymer blends in three steps. However, it was observed that if the backbone is obtained by emulsion polymerization, it contains a fraction of high molecular weight species. It was determined that these long backbone chains are one of the origin of the formation of cross-links during the graft copolymerization. On the contrary, the use of solution polymerization is expected to narrow down the molecular weight distribution of the backbone and, therefore, reduce the probability for cross-linking during the subsequent graft copolymerization.

5.2.2.1. Step 1 and 2: Synthesis of PBA-co-GMA and PBA-co-GA in solution and polymer analogous reaction in solution

The solution polymerization of BA is studied to determine the relationship between the synthesis parameters and the M_n and Đ of the obtained polymer. TDT is used as a chain-transfer agent during the polymerization of BA in order to regulate M_n of the backbone and to minimize the cross-linking reaction caused by hydrogen abstraction [98]. Toluene and cyclohexane are used as solvents for the syntheses, as they have different boiling point and transfer constant [100]. The obtained M_n and Đ of the synthesized PBA are shown in Table 21.

Table 21. Synthesis conditions and molecular weight distribution of PBA polymers.

Backbone	TDT	BPO	Solvent	Set temperature	M_n	Đ
	[wt.% rel. M]	[wt.% rel. M]	[type]	[°C]	[kg/mol]	[-]
S_B_{BA}(26-0)	1.0	1.0	Toluene	100	26	2.1
S_B_{BA}(15-0)	1.0	0.5	Toluene	100	15	2.3
S_B_{BA}(20-0)	0.5	0.5	Toluene	100	20	2.5
S_B_{BA}(30-0)	1.0	1.0	Cyclohexane	90	30	1.9
S_B_{BA}(31-0)*	1.0	1.0	Cyclohexane	90	31	1.8
S_B_{BA}(38-0)*	0.75	1.0	Cyclohexane	90	38	2.0
S_B_{BA}(45-0)*	0.5	1.0	Cyclohexane	90	45	2.0
S_B_{BA}(50-0)*	0.25	1.0	Cyclohexane	90	50	2.0
S_B_{BA}(98-0)*	0.2	0.1	Cyclohexane	90	98	2.0

* BPO is introduced when the reaction mixture is at 85 °C.

The polymer concentration in the solvent is set at 50 wt.%. At this concentration gel effect occurs, which causes the mixture to heat up. The temperature in the reaction mixture increases until boiling of the solvent/monomer mixture. Due to the high boiling temperature of toluene, the reaction mixture

with a set temperature of 100 °C reaches an exothermic peak up to 120°C. In the cases where cyclohexane is used as solvent, the exothermic peak reaches 92°C for a set temperature of 90°C.

It is expected that when toluene is used as a solvent, the reaction system reaches significantly higher temperatures, and the reactivity of BA is increased. This effect reduces the impact of TDT and BPO action in comparison to reactions with cyclohexane as solvent. This observation can explain the fact that when toluene is used as solvent, no increase of M_n is reached with a reduction of TDT and BPO amounts. This is observed by comparing samples S_B_{BA}(26-0), S_B_{BA}(15-0) and S_B_{BA}(20-0). Furthermore, the use of cyclohexane reduces the transfer constant by a factor of 4 (reported for styrene at 60°C in [100]), which results in higher M_n compared to the synthesis carried out in toluene.

With reduction in the amount of TDT in the mixture, M_n is increased from 31 kg/mol with 1.0 wt.% of TDT to 50 kg/mol with 0.25 wt.% of TDT (see Table 21, S_B_{BA}(31-0) and S_B_{BA}(50-0)). A further decrease of TDT concentration causes a high gel effect and visible cross-linking of the material. In order to obtain M_n higher than 50 kg/mol, the BPO concentration is reduced from 1.0 to 0.1 wt.% relative to styrene. In case of sample S_B_{BA}(98-0) M_n reaches 98 kg/mol without high gel effect and/or cross-linking. Thus, the established synthesis condition of the pristine PBA as in case of S_B_{BA}(38-0), S_B_{BA}(50-0) and S_B_{BA}(98-0) are selected for the following synthesis of PBA-co-GMA and PBA-co-GA backbones.

A series of PBA-co-GMA and PBA-co-GA backbones are synthesized with various amount of comonomer, TDT and BPO. As already described, the type of comonomer is expected to have an influence on the distribution of reactive sites in the backbone and therefore in the graft copolymer blend. The synthesis condition of the backbone, as well as the resulting M_n and Đ in respect to the used amount and type of comonomer in each backbone are described in Table 22. M_n of the produced backbones lies in the range obtained with the pristine PBA (Table 21) under the same conditions. The amount of comonomer measured by NMR corresponds to the feed value, as the polymerization conversion reaches nearly 100 %.

Table 22. Synthesis condition and M_n of PBA-co-GMA and PBA-co-GA backbones.

Backbone	Comonomer	TDT	BPO	M_n	Đ	w_{GMA}	w_{GA}
	[type]	[wt.% rel. M]	[wt.% rel. M]	[kg/mol]	[-]	[wt.%]	[wt.%]
S_B_{GMA}(26-1.9)	GMA	0.75	1.0	26	2.8	1.92	-
S_B_{GMA}(35-9)	GMA	0.75	1.0	35	2.9	9.00	-
S_B_{GMA}(52-1.1)	GMA	0.25	1.0	52	3.0	1.10	-
S_B_{GMA}(50-4.7)	GMA	0.25	1.0	50	2.6	4.73	-
S_B_{GMA}(104-0.6)	GMA	0.20	0.1	104	2.2	0.56	-
S_B_{GA}(55-1.1)	GA	0.25	1.0	55	2.6	-	1.10
S_B_{GA}(98-0.5)	GA	0.20	0.1	98	1.9	-	0.52
S_B_{GA}(98-1.3)	GA	0.20	0.1	98	2.0	-	1.28

The literature states that acrylate and methacrylate have different copolymerization parameters with BA. For example, GMA copolymerizes with BA at a ratio of 2.15/0.12 in a butan-2-one solution [101]. This means that a composition drift appears during copolymerization: GMA-rich chains are formed at the beginning of the reaction, while BA-rich chains are formed toward the end of the reaction. Although no copolymerization parameters are available for GA and BA in the literature, it is reported that 2-hydroxyethyl acrylate copolymerizes with BA at a ratio of 0.94/0.23 [102]. Therefore, it can be assumed that GA copolymerizes with BA with lower composition drift in comparison to GMA.

The composition drift is usually measured by comparing feed value and measured amount of comonomer present in the copolymer at low conversion (e.g. 20 %) [101, 102]. In this work, this composition drift is measured during the synthesis of backbones S_B_{GMA}(52-1.1) and S_B_{GA}(55-1.1) by quantifying the amount of comonomer in the copolymer through the reaction course by NMR analysis. The ratio between the concentration of comonomer measured and the one in the feed is plotted against the reaction conversion and is depicted in Figure 40.

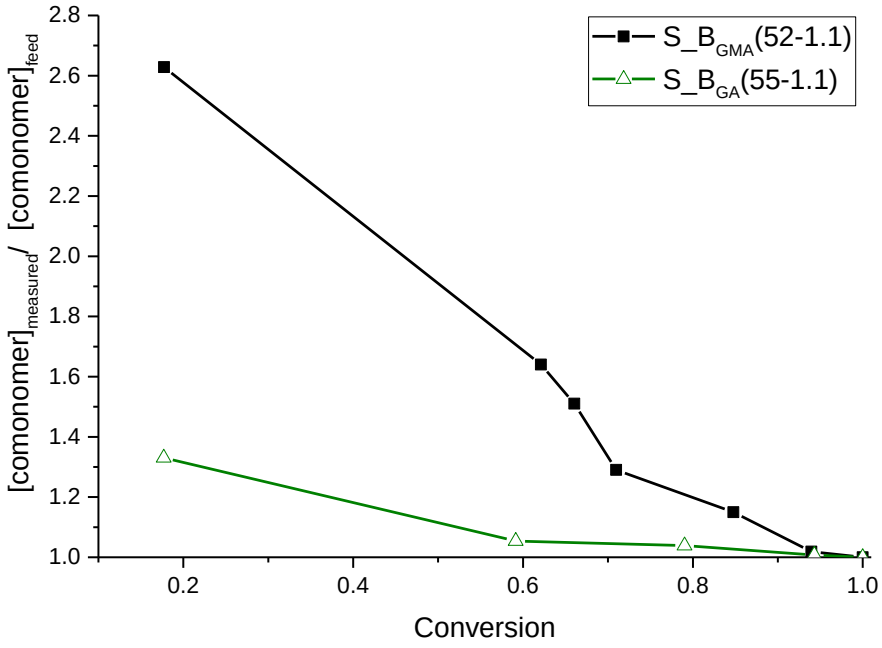

Figure 40. Composition drift through the reaction during synthesis of B_{GMA}(52-1.1) and B_{GA}(55-1.1).

At 20 % of conversion, the GMA content in the polymer is around 2.6 times higher than in the feed value of the reaction mixture. This correspond to a GMA content in the copolymer of about 2.8 wt.%, compared to the feed value of 1.1 wt.% in the mixture prior to the reaction. In other terms, it means that the polymer chains formed at the beginning of the reaction contain up to 9 GMA units per chain. As a consequence, the chains formed at the end of the reaction have lower amount of GMA per chain than the targeted value, which is about 4.1. As expected, the composition drift is reduced when GA is used as comonomer. When the conversion of 20 % is reached, the GA content in the copolymer is around 1.3 times higher than in the feed value of the reaction mixture, yielding an amount of GA per chain around 6, while the targeted value was 4.7.

The backbones are post-modified by polymer analogous reactions as already described in Foto - 1798540944: .1.2.1.

All the produced backbones show full conversion of the glycidyl functions to the acryloyl ones. Furthermore, all these polymers are fully soluble in toluene, indicating that no cross-linking reaction occurred during the backbone polymerization step or its modification. The theoretical number of BA

moieties distance between two adjacent reactive groups are represented by the value N_m. M_n, N_{Acr} and N_m are listed in Table 23.

Table 23. M_n, N_{Acr} and Nm of the post-modified PBA-co-GA and PBA-co-GMA backbones.

Backbone	M_n	N_{Acr}	N_m
	[kg/mol]	[-]	[-]
S_B_{GMA}(26-3.5)	26	3.5	58
S_B_{GMA}(35-22)	35	22.0	12
S_B_{GMA}(52-4)	52	4.0	101
S_B_{GMA}(50-16.7)	50	16.7	24
S_B_{GMA}(104-4.1)	104	4.1	198
S_B_{GA}(55-4.7)	55	4.7	91
S_B_{GA}(98-4)	98	4.0	192
S_B_{GA}(98-9.8)	98	9.8	78

5.2.2.2. Step 3: Graft copolymerization of post-modified PBA-co-GA or PBA-co-GMA with styrene in solution

The modified backbones, obtained through the polymer analogous reaction in solution (Table 23), are used for the graft polymerization step with styrene. The influence of the backbone synthesis method and structure on the properties and morphology of the graft copolymer blend is investigated.

5.2.2.2.1. Influence of the backbone synthesis method on the graft copolymer blends properties.

In order to determine the influence of the backbone synthesis method and its effect on the graft copolymerization process, the modified backbone S_B_{GMA}(26-3.5) (Table 23) is copolymerized with styrene. The mechanical properties of the product G-S_B_{GMA}(26-3.5) are compared to G-E_B_{GMA}(28-3.8) (see 5.1.2.2., Table 9) which differs only by the method of backbone synthesis. The synthesis of G-S_B_{GMA}(26-3.5) is performed twice as the repeatability of the grafting procedure is a key factors in the process (see 5.1.2.3.). The results are shown in Table 24.

Table 24. Graft copolymerization products of backbone G-E_B_{GMA}(26-3.8) and G-S_B_{GMA}(26-3.5).

Synthesis	Conversion	M_n	NSF	E Modulus	Tensile strength	Elongation at break
	[%]	[kg/mol]	[wt.%]	[MPa]	[MPa]	[%]
G-E_B_{GMA}(28-3.8)	69.0	15.4	57.7	1261 ± 101	32.6 ± 0.7	34.0 ± 9.0
G-S_B_{GMA}(26-3.5)_01	66.1	23.2	0	1386 ± 9	9.6 ± 1.3	0.6 ± 0.1
G-S_B_{GMA}(26-3.5)_02	66.0	26.6	0	1319 ± 37	13.4 ± 2.7	0.9 ± 0.2

When the backbone is synthesized in solution, the NSF of the graft copolymer is eliminated as compared to the graft copolymer obtained from the emulsion synthesized backbone. While G-E_B_{GMA}(28-3.8) shows 58 wt.% of NSF, no insoluble fraction is extracted in samples G-S_B_{GMA}(26-3.5)_01 and G-S_B_{GMA}(26-3.5)_02. The mechanical properties of the extruded samples are also affected when the solution-based backbone is used instead of the emulsion-based backbone. For the samples G-S_B_{GMA}(26-3.5)_01 and G-S_B_{GMA}(26-3.5)_02, elongation at break and tensile strength are lower, while the E modulus is in a comparable range with G-E_B_{GMA}(28-3.8). It is important to mention that although the experiment was repeated only 2 times, the variation in the resulting physical properties is low. This correlates with the hypothesis that cross-linking during the synthesis, as observed in see 5.1.2.3. reduces the repeatability of the results.

The type of synthesis of the backbone influences its molecular weight distribution as well as the synthesis course of the graft copolymerization. The solution polymerization of the backbone opens new possibilities as its monomodal distribution allows a higher number of reactive sites as well as higher concentration of polymer in the solvent during the graft copolymerization.

5.2.2.2.2. Influence of the backbone structure on the synthesis process

This section will focus on the influence of grafting site density and molecular weight distribution of the backbone on specific properties, such as the NSF and mechanical and optical behavior of the solvent-cast films.

A series of post-modified PBA-co-GMA backbones with varying amount of active sites and M_n is used as starting material for graft copolymerization. M_n of backbones varies between 26 and 104 kg/mol, the N_{Acr} between 3.5 and 22 and N_m from 12 to 198. All the grafting reactions are performed under the same conditions. The results are presented in Table 25.

Table 25. Graft copolymerization results of modified PBA-co-GMA backbones.

Graft copolymer	Backbone			Graft copolymer			
	M_n	N_{Acr}	N_m	NSF	M_n	Đ	PS content
	[kg/mol]	[-]	[-]	[wt.%]	[kg/mol]	[-]	[wt.%]
G-S_B_{GMA}(26-3.5)	26	3.5	58	50	47	4.2	54.0
G-S_B_{GMA}(35-22)*	35	22.0	12	93	-	-	-
G-S_B_{GMA}(52-4)	52	4.0	101	17	48	5.0	59.5
G-S_B_{GMA}(50-16.7)	50	16.7	24	73	-	-	-
G-S_B_{GMA}(104-4.1)	104	4.1	198	0	52	5.2	62.1

*The reaction is stopped after 3h due to high cross-linking.

The evident conclusion arising from the results presented in Table 25 is that the cross-linking behavior is directly related to N_m in the backbone. This effect is visible when NSF is plotted in function of N_m as depicted in Figure 41.

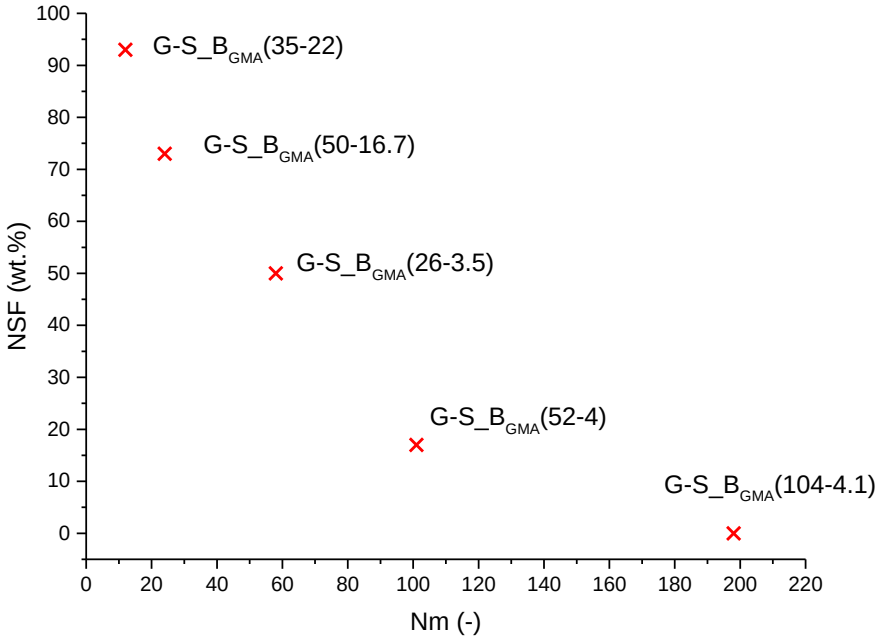

Figure 41. Plot of NSF in function of N_m.

It is logically observed that the amount of cross-linking in the graft copolymerization product decreases with the increase of space between two reactive groups. The NSF decreases from nearly 100 wt.% with a distance of only 20 units between 2 reactive groups to 0 wt.% when the distance is increased to 200.

A decrease of NSF can be achieved by doubling M_n of the backbone while keeping the number of acryloyl group per chain constant. For example, the NSF decreases from 50 to 17 and finally to 0 wt.% with an increase of M_n in samples G-S_B_{GMA}(26-3.5), G-S_B_{GMA}(52-4) and G-S_B_{GMA}(104-4.1) as observed in Figure 41. This effect can also be achieved by keeping M_n constant while reducing the amount of acryloyl per chain as observed between G-S_B_{GMA}(35-22) and G-S_B_{GMA}(26-3.5), as well as between G-S_B_{GMA}(50-16.7) and G-S_B_{GMA}(52-4).

During the copolymerization, the torque of the overhead stirrer is measured. Due to the formation of PS chains, whether they are grafted or not, the viscosity of the mixture increases, which could have an influence on the measured torque. The torque could be influenced by the disturbance and

heterogeneity in the mixture due to the cross-linking reaction. Figure 42 shows the evolution of torque with the reaction time for the copolymerization reactions presented in Table 25.

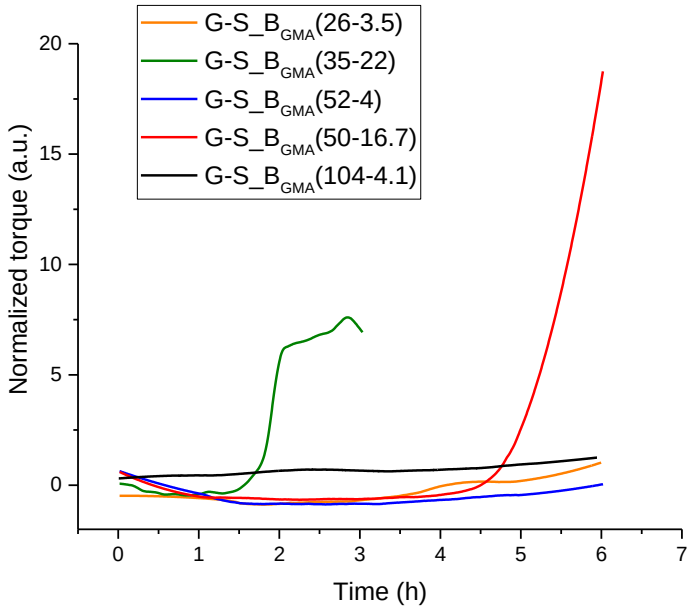

Figure 42. Torque evolution during synthesis of graft copolymers.

It is observed that the torque increases strongly during the synthesis of G-S_B_{GMA}(35-22) and G-S_B_{GMA}(50-16.7), while it stays constant for the other samples. These two samples have the highest amount of measured NSF at the end of the reaction. This means that the formation of PS, grafted or not, is not responsible for the increase of torque but the cross-linking reaction is. In case of G-S_B_{GMA}(35-22), the torque is increasing after only 1 h of reaction, whereas it increases after 4 h for G-S_B_{GMA}(50-16.7). This is correlated to N_m of the two samples, as the probability to form a cross-linked network is higher for sample G-S_B_{GMA}(35-22) with the reactive groups closer to each other compared to G-S_B_{GMA}(50-16.7). It should be noted that due to the high increase of torque and heterogeneity of the reaction mixture, the reaction of G-S_B_{GMA}(35-22) was stopped after 3 hours.

As observed in Table 25, M_n of the different graft copolymers is around 50 kg/mol, independently of the backbone used for the synthesis. As an example, the SEC RI-elugram of G-S_B_{GMA}(104-4.1) and a comparison to its backbone S_B_{GMA}(104-4.1) is depicted in Figure 43.

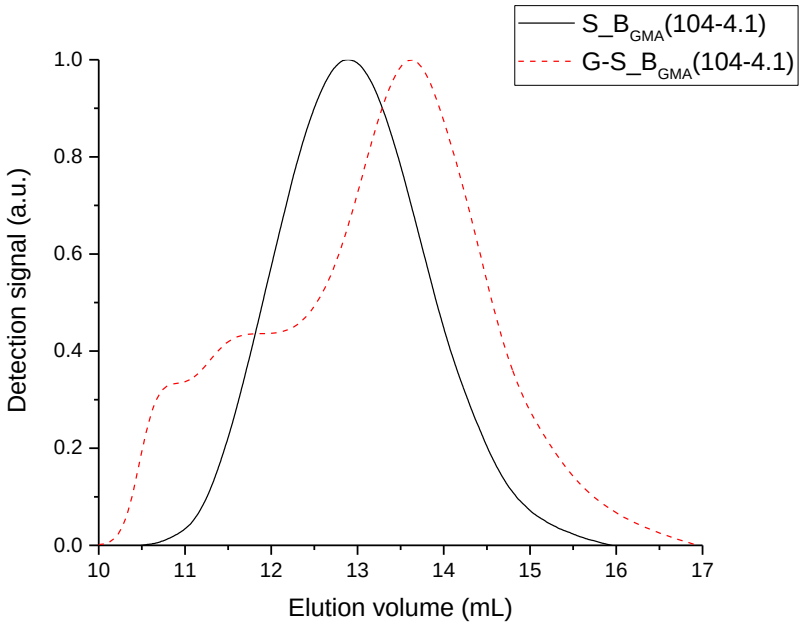

Figure 43. RI-elugram of S_B$_{GMA}$(104-4.1) and G-S_B$_{GMA}$(104-4.1).

The SEC curve of the graft copolymer shows two distinct areas: one area at low elution volume from 10 to 12.5 mL, corresponding to high molecular weight, and another one at high elution volume from 12.5 to 17 mL, corresponding to lower molecular weight chains. The lower molecular weight fraction corresponds to h-PS formed during the synthesis and the higher molecular weight fraction is attributed to the graft copolymer. This explains why M_n of the G-S_B$_{GMA}$(104-4.1) blend is lower than the one of its backbone S_B$_{GMA}$(104-4.1). Furthermore, the dispersity of the blend lies between 4.2 and 5.2 in comparison to 1.9-3.0 for the backbone. This value of dispersity above 4.0 is due to the broad peak consisting of h-PS and copolymer, as observed in Figure 43, in comparison to a dispersity of the backbone between 2 and 3.

As summarized in Table 25, the amount of PS in the blend, grafted or not, varies from 54 to 62 wt.% for the samples with NSF below 50 wt.%. The amount of PS in the samples with a higher NSF (G-S_B$_{GMA}$(35-22) and G-S_B$_{GMA}$(50-16.7)) is not measured, as the samples are poorly soluble in NMR solvent and, therefore, not detected. The differences in the amount of PS measured in the samples G-S_B$_{GMA}$(26-3.5), G-S_B$_{GMA}$(52-4) and G-S_B$_{GMA}$(104-4.1) can be explained by their difference in NSF. The amount of PS incorporated into the NSF is not analyzed by NMR due to their insolubility in the NMR solvent. Therefore, it can be observed that the decrease of NSF is related to an increase of measured PS content.

This series of experiment proved the feasibility of the graft copolymerization reaction and its limits in terms of backbone structure to balance between low cross-linking and high PS content in the graft copolymer blend.

5.2.2.2.3. Influence of the backbone comonomer type on the grafting synthesis

As previously explained, there is a difference in reactivity between acrylates and methacrylates, causing higher composition drift with GMA-based backbones compared to GA-based ones. The goal of this section is to evaluate the influence of the comonomer type in the backbone on the NSF and M_n of the graft copolymer. A comparison between copolymer blends based on backbones having similar amount of grafting sites but varying by the type of comonomer is presented in Table 26.

Table 26. Comparison of NSF and M_n of copolymer blends made from GA- and GMA-based backbones.

Graft copolymer	Backbone			Graft copolymer		
	M_n	N_{Acr}	N_m	NSF	M_n	PS content
	[kg/mol]	[-]	[-]	[wt.%]	[kg/mol]	[wt.%]
G-S_B_{GMA}(52-4)	52	4.0	101	17	48	59.5
G-S_B_{GA}(55-4.7)	55	4.7	91	0	54	64.2
G-S_B_{GMA}(104-4.1)	104	4.1	198	0	52	62.1
G-S_B_{GA}(98-4)	98	4.0	192	0	49	65.3

A comparison between G-S_B_{GMA}(52-4) and G-S_B_{GA}(55-4.7) shows a decrease of NSF of 17 wt.% when using GA-based backbone compared to the GMA-based one. When GMA is used as the comonomer, GMA-rich chain segments are formed at the beginning of the backbone polymerization, while BA-rich chains are formed at a later stage. After post-modification of the GMA-based backbone and during its graft copolymerization procedure, the acryloyl-rich chain segments have higher probability for cross-linking. This effect is reduced when GA is used as the comonomer as the composition of the PBA-co-GA chains is more homogeneous.

Samples G-S_B_{GMA}(104-4.1) and G-S_B_{GA}(98-4), which have similar N_m around 195, have 0 wt.% of NSF. This means that both the comonomer used for the synthesis of the backbone as well as the N_m play a role in the NSF.

The M_n of the graft copolymers varies between 48 and 54 kg/mol, independently from the molecular weight of the backbone. As previously explained, the M_n of the blend around 50 kg/mol is due to a mixture of high molecular weight graft and low molecular weight h-PS, as observed in Figure 44.

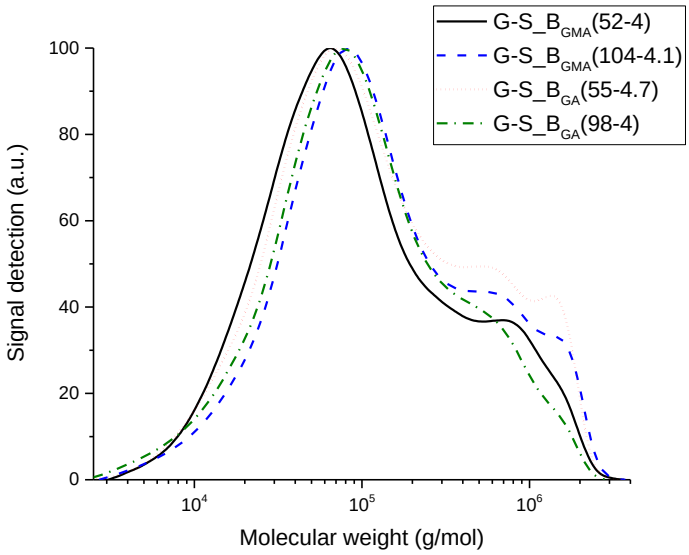

Figure 44. Molecular weight distribution of graft copolymer with GMA- and GA-based backbones.

Although the general shape of the SEC curve is the same for all samples, the height of the different peaks and shoulder differs, indicating a variation in the ratio between graft copolymer and h-PS. This aspect will be developed in details in the next section.

5.2.2.2.4. Influence of the backbone structure

It is expected that the structure of the backbones does not only play a role during the graft copolymerization process, but also in the mechanical and optical properties of the solvent-cast films. GA- and GMA-based backbone with various N_{Acr} and M_n are used in the synthesis of graft copolymer. Mechanical and optical properties are measured on solvent-cast films and presented in Table 27.

Table 27. Mechanical and optical properties of the solvent-cast films.

Graft copolymer	Backbone			Graft copolymer				
	M_n	N_{Acr}	N_m	Haze	Clarity	E Modulus	Tensile strength	Elongation at break
	[kg/mol]	[-]	[-]	[%]	[%]	[MPa]	[MPa]	[%]
G-S_B_{GMA}(52-4)	52	4.0	101	23.0 ± 3.9	91.5 ± 3.8	1010 ± 58	16.5 ± 1.2	3.4 ± 0.9
G-S_B_{GMA}(104-4.1)	104	4.1	198	42.1 ± 0.6	38.9 ± 1.1	660 ± 153	19.7 ± 1.7	3.6 ± 0.3
G-S_B_{GA}(55-4.7)	55	4.7	91	13.6 ± 1.8	99.3 ± 0.1	1172 ± 147	21.9 ± 4.9	3.0 ± 0.6
G-S_B_{GA}(98-4)*	98	4.0	192	69.1 ± 2.4	16.5 ± 2.1	-	-	-
G-S_B_{GA}(98-9.8)	98	9.8	78	59.9 ± 3.8	7.9 ± 0.4	1034 ± 189	16.1 ± 3.0	1.3 ± 0.4

*Brittleness of the sample is too high to perform tensile strength test.

G-S_B_{GMA}(52-4) and G-S_B_{GMA}(104-4.1) both have 4 acryloyl groups per chain but M_n varying from 50 to around 100 kg/mol. Therefore, their N_m varies from 100 to 198. It appears that this increase of spacing between reactive groups decreases the transparency of the produced films with an increase of haze from 23 to 42 % and a reduction of clarity from 92 to 39 %. In terms of mechanical properties, the tensile strength and elongation at break are similar, whereas the E modulus is slightly reduced with increase of N_m. The effect is amplified when comparing the samples G-S_B_{GA}(55-4.7) and G-S_B_{GA}(98-4). The increase of N_m from 90 to 192 leads to a strong reduction of transparency, which is shown by an increase of haze from 14 to 69 % and a drop of clarity from 99 to 17 %.

By comparing samples G-S_B_{GMA}(52-4) and G-S_B_{GA}(55-4.7), it is observed that the blend prepared with the GA-based backbone has a significantly higher transparency with haze at 14 %, compared to 23 % with the GMA-based backbone. E modulus and tensile strength are also increased when GA-based backbone is used. Elongation at break of both samples lies in the same range, at 3.4 and 3.0 %.However, the tendency is different when comparing the blends prepared with GMA and GA-based backbones with a M_n at around 100 kg/mol. Indeed, G-S_B_{GMA}(104-4.1) has higher transparency with haze at 42 %, compared to that of G-S_B_{GA}(98-4) at 70 %. In terms of mechanical properties, the sample G-S_B_{GMA}(104-4.1) has elongation at break at 3.6 %, while G-S_B_{GA}(98-4) is too brittle for tensile testing. This phenomenon can be further correlated to the difference of morphology in the studied blends which is addressed in section 0.

Doubling the N_{Acr} and keeping the M_n constant in case of sample G-S_B_{GA}(98-9.8) compared to G-S_B_{GA}(98-4) has a negligible impact on the transparency. Although haze decreases from 70 to 60 %, the clarity is also reduced from 17 to 8 %. Moreover, elongation at the break remains low at 1.3 %, while E modulus and tensile strength are in the same range as for the GMA derived samples.

Highly transparent PBA-g-PS/h-PS samples were synthesized successfully and a clear trend between backbone molecular weight and transparency can be established. However, the elongation at break of the solvent casted samples remains low.

5.2.2.2.5. Evolution of properties of the graft copolymer blends during graft copolymerization reaction

The h-PS and PBA-g-PS formed simultaneously during the synthesis (see Table 27) can be distinguished as they appear as two shoulders on the SEC curve. Therefore, to study the formation of PS in grafted and non-grafted form through the reaction course, samples were taken out from the reacting mixture

at selected time intervals and characterized. The obtained SEC curves as presented in Figure 44 show a distinct presence of the shoulders coming from h-PS and PBA-g-PS. A deconvolution method is used to separate the shoulders into separate peaks (for further details on the method, see 8.5). The area under the deconvoluted peaks is proportional to the amount of each component in the blend. Therefore, the amount of graft copolymer and h-PS can be determined and the grafting efficiency of the reaction is calculated along the reaction course. The evolution of grafting efficiency observed during copolymerization reaction of samples presented in Table 27 is depicted in Figure 45.

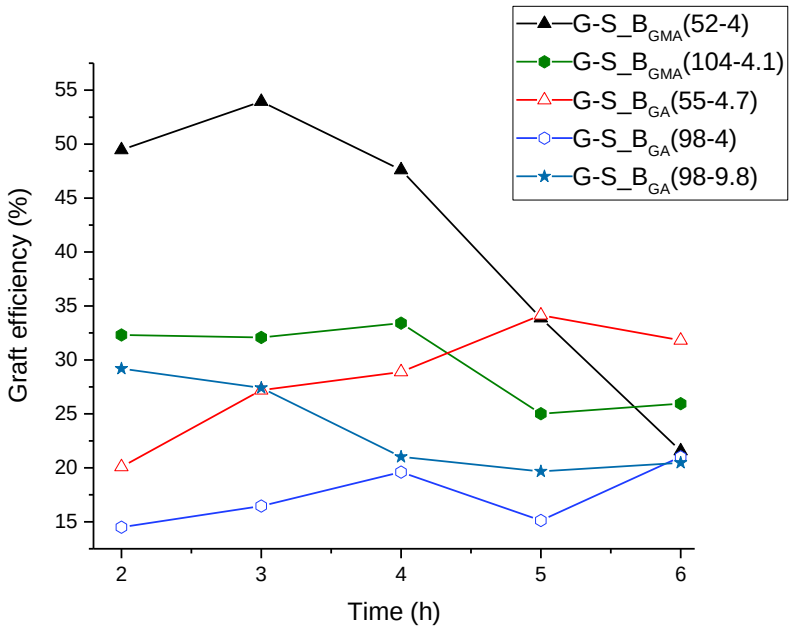

Figure 45. Evolution of grafting efficiency through the reaction course of graft copolymerization.

In this series, the sample G-S_B_{GMA}(52-4) after 6 h of reaction time is the only one that is not fully soluble in toluene and has a NSF of 17 wt.%. Therefore, the grafting efficiency for this copolymer blend after 6 h is evaluated only in the soluble fraction. All the other samples are completely soluble and the grafting efficiency is representative of the entire sample.

The blend G-S_B_{GMA}(52-4) shows a moderately increasing grafting efficiency up to 3 h, followed by a decrease from 3 to 6 h from about 45 to 20 %. The intense reduction of the grafting efficiency from 3 to 6 h is partially attributed to the increasing cross-linking fraction of the sample. However, a similar trend is observed with G-S_B_{GMA}(104-4.1), although no cross-linking reaction occurred. This indicates that the grafting of PS onto PBA backbone chains occurs mostly within the first 3 h of reaction.

In comparison, the samples G-S_B_{GA}(55-4.7) and G-S_B_{GA}(98-4), prepared with GA-based backbones show a slow increase in grafting efficiency through the complete graft copolymerization course. Moreover, it is observed that the grafting efficiency at 2 h is lower in the case of the GA-based backbone compared to the GMA-based one. However, during the polymerization, the grafting efficiency decreases with the GMA-based backbone and increases with the GA-based backbone and the curves cross or converge after 6 h of reaction. This is the case between G-S_B_{GMA}(52-4) and G-S_B_{GA}(55-4.7) and between G-S_B_{GMA}(104-4.1) and G-S_B_{GA}(98-4).

An assumption is that this difference in the grafting behavior between the GMA- and GA-based backbones is related to the distribution of reactive groups along the backbone chain. As previously mentioned, the reactivity ratio for the copolymerization of BA with GMA induces a composition drift. Therefore, the backbones based on GMA have a fraction of chains with a high density of reactive sites.

Although the reactive sites undergo grafting from the beginning of the reaction in case of both backbone types, the grafting reaction is promoted over the formation of h-PS in case of GMA-based backbones. Once the reactive sites are consumed, mainly h-PS is formed. For the GA-based backbones, the formation of both grafted and h-PS, is more constant along the course of the reaction.

A different trend is observed for sample G-S_B_{GA}(98-9.8), which contains double amount of reactive site per chain as compared to the rest of the studied series, showing a steady decrease of grafting efficiency through the reaction course. Due to its high grafting site density, this sample have higher grafting efficiency after 2 h of reaction compared to the sample G-S_B_{GA}(98-4). However, in the further course of reaction, the grafting efficiency decreases and reaches similar value as sample G-S_B_{GA}(98-4). The reason for the decrease of grafting efficiency, as well as the limitation of its value to a maximum of around 30 % can be ascribed to the steric hindrance of the grafting sites at a later reaction stage. [103]

5.2.2.2.6. Relation between the copolymer structure and its morphology

It was observed that the type of backbone influences the mechanical and optical properties of the solvent-cast films. This is due to a change in the structure of the copolymer, which arises from a variation in the density of grafts per chain. It is also known, that the mechanical and/or optical properties of such blends are correlated to the type of their morphology at a nanoscale and the size of the hard phase domains. This part focusses on the morphology of the solvent-cast films and its influence on the physical properties of the blends.

Figure 46 shows TEM images with magnification at 40 000 from solvent-cast films of the blends described in Table 27. In the obtained TEM images PS phase appears dark, while the bright areas are representing the PBA phase. The strongly dark areas on the images correspond to breaks or thick parts of the films. Clear differences in terms of morphology can be observed between the studied samples. Indeed, samples G-S_B_{GMA}(104-4.1) and G-S_B_{GA}(98-9.8) in Figure 46 (b) and (e) show lamellar morphology, which is distinguished by an alternation of PS and PBA phase with a thickness of about 10 nm.

On the other hand, the interpenetrating areas of PBA and PS on the samples G-S_B_{GMA}(52-4), G-S_B_{GA}(55-4.7) and G-S_B_{GA}(98-4) in Figure 46 (a), (c) and (d) indicates that they have co-continuous morphology.

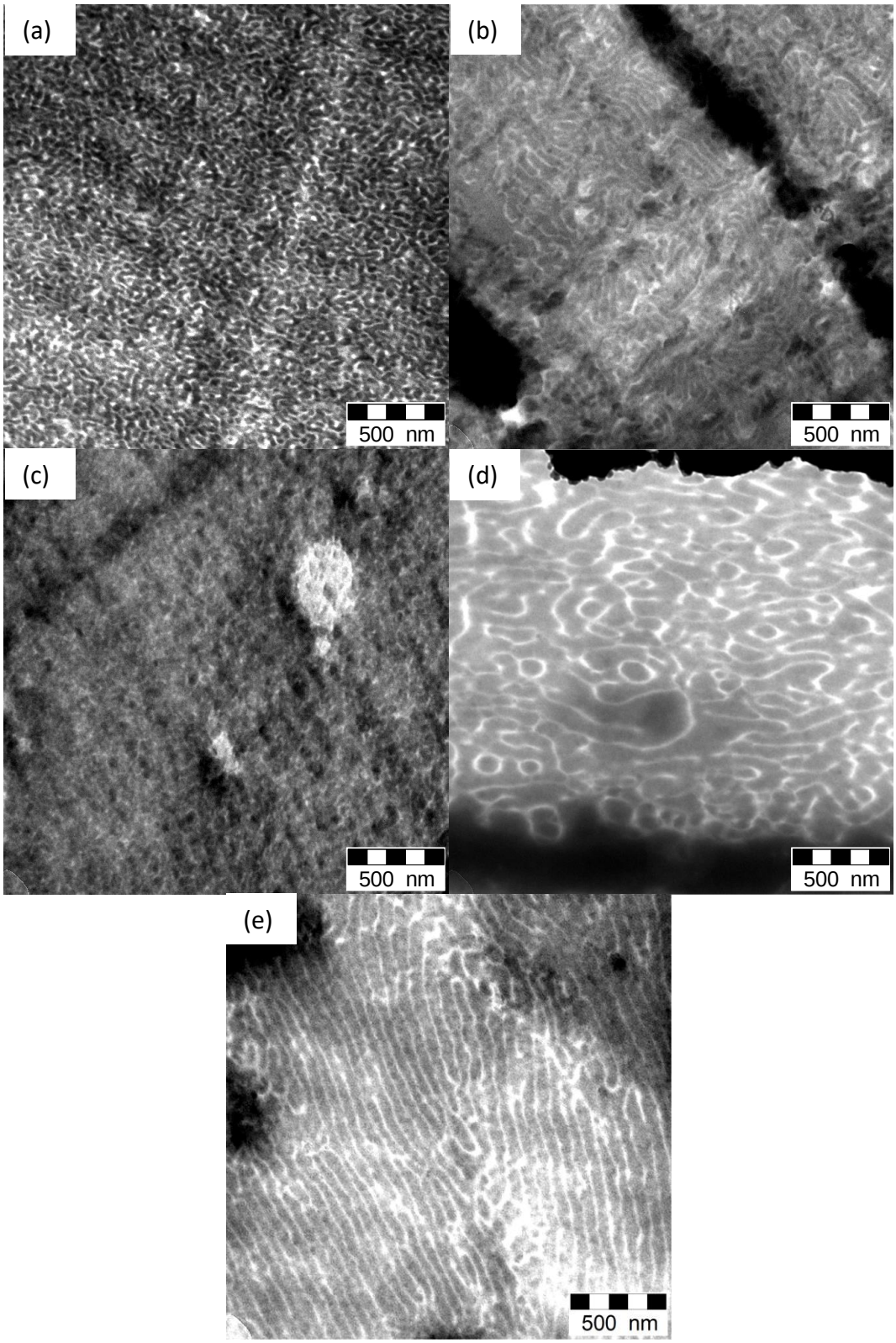

Figure 46. TEM images of copolymer at magnification 40 000. (a) G-S_B_{GMA}(52-4); (b) G-S_B_{GMA}(104-4.1); (c) G-S_B_{GA}(55-4.7); (d) G-S_B_{GA}(98-4); (e) G-S_B_{GA}(98-9.8). PS phase appears dark.

The amount of PS in the samples is varying between 59.5 and 65.3 wt.%. However, no correlation between the amount of PS and the morphology can be observed based on the TEM images. This means that the morphology is influenced mainly by the type of backbone used for the graft copolymerization. Furthermore, one of the most important factors when analyzing the morphology of copolymers is the size of the PS domains, as it can be correlated to their optical and mechanical behavior. It is observed that all the samples, having lamellar or co-continuous morphology, show microphase separation and their PS domain thickness is lower than 200 nm. Moreover, there is an evident difference in the size of PS domains between the samples. G-S_B_{GMA}(52-4), G-S_B_{GMA}(104-4.1) and G-S_B_{GA}(55-4.7) have PS domains below 50 nm, while G-S_B_{GA}(98-4) and G-S_B_{GA}(98-9.8) have larger PS domains, up to about 200 nm. The reduced domain size in G-S_B_{GMA}(52-4), G-S_B_{GMA}(104-4.1) and G-S_B_{GA}(55-4.7) correlates well with the mechanical characteristics of the films. They show larger elongation at break in comparison to G-S_B_{GA}(98-4) and G-S_B_{GA}(98-9.8).

It is known from literature, that the thickness of PS domains should be below a critical value of 20 nm to allow elongation up to few hundred percent [13, 20]. In case of the obtained blends, depicted in Figure 46, the PS domains size ranges from 200 to 50 nm, approaching the critical value in sample G-S_B_{GMA}(52-4), G-S_B_{GMA}(104-4.1) and G-S_B_{GA}(55-4.7). This explains the fact that the elongation at break of the studied blends lies in the range of 0-4 % only.

No clear correlation appear between the optical characteristics and the difference of domain size in the blends. As the size of the PS domains below 200 nm is smaller than the wavelength of the visible light, their variation does not substantially affect the transparency.

To correlate the optical properties to the morphology, it is essential to study larger scale of the TEM pictures. Therefore, following TEM images of the investigated series of blends (Table 27) with magnification at 10 000 are shown in Figure 47.

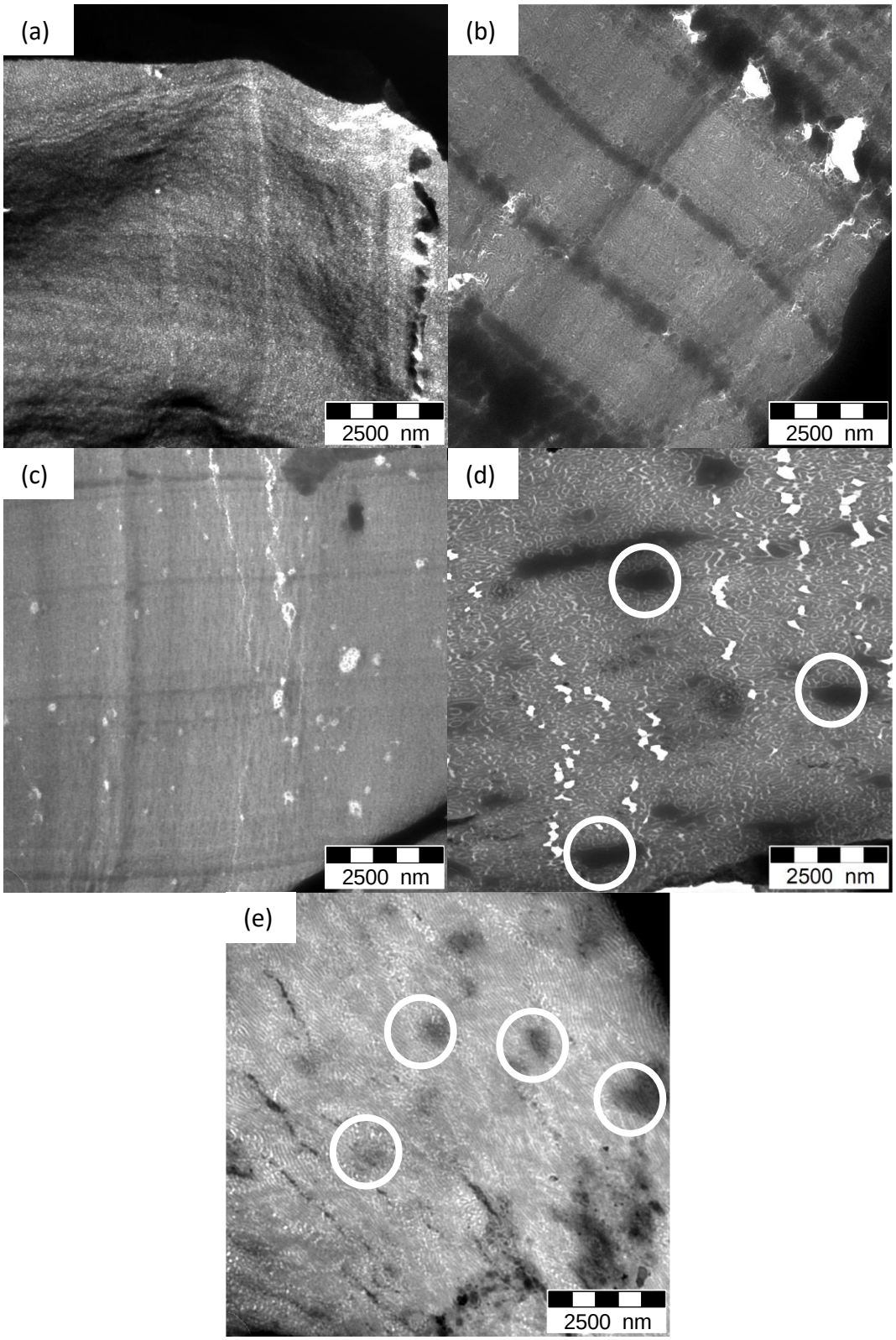

Figure 47. TEM images at magnification 10 000. (a) G-S_B_{GMA}(52-4); (b) G-S_B_{GMA}(104-4.1); (c) G-S_B_{GA}(55-4.7); (d) G-S_B_{GA}(98-4); (e) G-S_B_{GA}(98-9.8). PS phase appears dark.

At lower magnification, it is possible to observe larger areas of the sample and detect heterogeneities in the system. It is visible in Figure 47 that micrographs (a), (b) and (c) have dark lines or zones corresponding to thick areas of the film due to cutting, while image (d) shows white area due to breaking of the film during cutting. The micrographs of G-S_B_{GA}(98-4) and G-S_B_{GA}(98-9.8) in Figure 47 (d) and (e), reveal dark areas (circled on the image) that represent larger domains of PS. The size of these PS domains are in the range of 0.5 to 2 μm. This explains the haze above 60 % and clarity below 20 % since light is diffracted and scattered. In contrast, there are no large dark regions visible in the micrographs of the samples G-S_B_{GMA}(52-4) and G-S_B_{GA}(55-4.7) correlating well with the haze below 25 % and clarity above 90 %.

As depicted in Figure 47, (b), the sample G-S_B_{GMA}(104-4.1) have higher haze and lower clarity compared to G-S_B_{GMA}(52-4) and G-S_B_{GA}(55-4.7), however, the TEM images does not indicate the presence of large PS domains in this blend. This can be explained by the morphology of this blend observed in Figure 46 (b). For G-S_B_{GMA}(104-4.1) some PS domains are large and the continuity of the morphology is less evident compared to the samples G-S_B_{GMA}(52-4) and G-S_B_{GA}(55-4.7) with higher transparency (Figure 46 (a) and (c)). Therefore, it can be concluded that an increase of M_n of the backbone affects the mixing between soft and hard phase, increasing the domain thickness of both phases.

It has been described that the structure and architecture of the blocks in di- or triblock copolymer influences the mobility of the constituent chains. As a result, the microphase separation behavior was found to be reflected in a shift of their phase behavior. The molecular mobility of the chains can be well characterized by the T_g of the components. [37]

As shown in Table 28, two distinct T_g are observed in the blend: one at low temperature, corresponding to the PBA block ($T_{g\text{-}PBA}$) and one at high temperature, corresponding to the PS block ($T_{g\text{-}PS}$). The T_g of the backbone alone, S_B_{GMA}(52-4), is measured at -54.9°C and the T_g of pure PS with M_n of 20 kg/mol was taken from the literature. [104]

Table 28. T_g values of blends and reference materials.

Polymers	$T_{g\text{-}PBA}$ [°C]	$T_{g\text{-}PS}$ [°C]
S_B_{GMA}(52-4)	-54.9	-
G-S_B_{GMA}(52-4)	-42.4	91.7
G-S_B_{GMA}(104-4.1)	-45.4	102.8
G-S_B_{GA}(55-4.7)	-39.2	98.2
G-S_B_{GA}(98-4)	-46.0	98.4
G-S_B_{GA}(98-9.8)	-42.6	98.4
PS_M_n 20kg/mol	-	97.1

It is well established, that the factors influencing the T_g value are: thermal history of the sample, system pressure, diluent type and concentration, polymer structure, M_n and Đ [105]. As all the samples are prepared under the same conditions (film casting and drying of the blend), it is expected that only the three latter factors have an impact on the T_g in the studied system. A direct comparison between the backbone S_B_{GMA}(52-4) and the graft copolymer blend prepared with this backbone G-B_{GMA}(52-4) shows an increase of $T_{g\text{-}PBA}$ from -54.9 to -42.4°C. This tendency is observed for all graft copolymer blends with an increase of $T_{g\text{-}PBA}$ from 8.9 to 15.7 °C compared to the backbone. Since the structure of the backbone in the graft copolymer blend is not different from ungrafted backbone, the shift in T_g results essentially from mixing of PS chains in PBA segments. Due to the low M_n of h-PS of around 20 kg/mol their migration and mixing into the soft phase is facilitated. The comparison of samples G-S_B_{GA}(55-4.7) and G-S_B_{GA}(98-4) is relevant as it shows a relationship between morphology and shift of $T_{g\text{-}PBA}$. The sample G-S_B_{GA}(55-4.7) does not have strong phase separation as showed in Figure 46 (c) in comparison to G-S_B_{GA}(98-4) in Figure 46 (d). This change in morphology correlates with a difference in $T_{g\text{-}PBA}$ shift, which arises from doubling the M_n of the backbone between samples G-S_B_{GA}(55-4.7) and G-S_B_{GA}(98-4). Sample G-S_B_{GA}(98-4) shows an increase of its $T_{g\text{-}PBA}$ of about 8.9°C compared to the ungrafted backbone, whereas sample G-S_B_{GA}(55-4.7) has $T_{g\text{-}PBA}$ 15.7°C higher compared to the ungrafted backbone. This means that the mixing of PS chains with PBA is facilitated in case of the blend G-S_B_{GA}(55-4.7) prepared from a shorter backbone relative to G-S_B_{GA}(98-4).

5.2.2.3. Processing by extrusion and its influence on the blend´s properties

It is well known, that the method of processing has great influence on the morphology of copolymers [16]. The film solvent-casting method leads to a thermodynamically stable and most relaxed nanostructure. Melt processing followed by rapid cooling, on the other hand, does not allow

the phases in the copolymer to organize themselves slowly and can lead to different morphologies when compared to solvent-casting ones. Therefore, the variation in morphology between the solvent-cast films compared to the samples processed by extrusion and injection molding can be correlated to a change in physical properties such as mechanical strength and transparency. All the samples prepared from the selected series of backbones are processed by solvent-casting, as well as by extrusion/injection molding. The stress-strain behavior of both sets of samples have been measured and are presented in Table 29.

Table 29. Comparison of mechanical properties between solvent-cast film and extruded/injected samples.

Graft copolymer	Solvent-cast films			Extruded/injection molded specimens		
	E Modulus	Tensile strength	Elongation at break	E Modulus	Tensile strength	Elongation at break
	[MPa]	[MPa]	[%]	[MPa]	[MPa]	[%]
G-S_B_{GMA}(52-4)	1010 ± 58	16.5 ± 1.2	3.4 ± 0.9	452 ± 83	17.8 ± 1.3	45.4 ± 2.1
G-S_B_{GMA}(104-4.1)	660 ± 153	19.7 ± 1.7	3.6 ± 0.3	1033 ± 121	30.9 ± 1.0	33.1 ± 6.8
G-S_B_{GA}(55-4.7)	1172 ± 147	21.9 ± 4.9	3.0 ± 0.6	1096 ± 150	30.0 ± 2.5	52.6 ± 4.5
G-S_B_{GA}(98-4)*	-	-	-	1170 ± 74	32.0 ± 1.0	18.9 ± 5.0
G-S_B_{GA}(98-9.8)	1034 ± 189	16.1 ± 3.0	1.3 ± 0.4	1098 ± 157	30.3 ± 2.3	35.4 ± 5.5

*Brittleness of the sample is too high to perform tensile strength test.

As expected, major differences appear between the specimens obtained from solvent-cast films and the melt-processed samples. For all the tested samples, the flexibility increases when processed by extrusion. The samples after melt processing have elongation at break between 9 and 30 times higher than their solvent-cast equivalents. However, the general tendency is similar with the tensile strength. It is often observed, that an increase of elongation at break occurs simultaneously with a reduction of the tensile strength. Yet, in case of the studied blends, both values are increasing when the material is processed by extrusion and injection molding. Moreover, the flexibility and tensile strength of the melt-processed samples are comparable to HIPS copolymers. Such enhancement of the mechanical properties can originate either from a chemical modification of the copolymer, such as cross-linking during extrusion and/or a change in the morphology organization. Figure 48 and Figure 49 depict the morphology of selected blends prepared by solvent casting (left) and extrusion (right) at a magnification of 10 000 and 40 000.

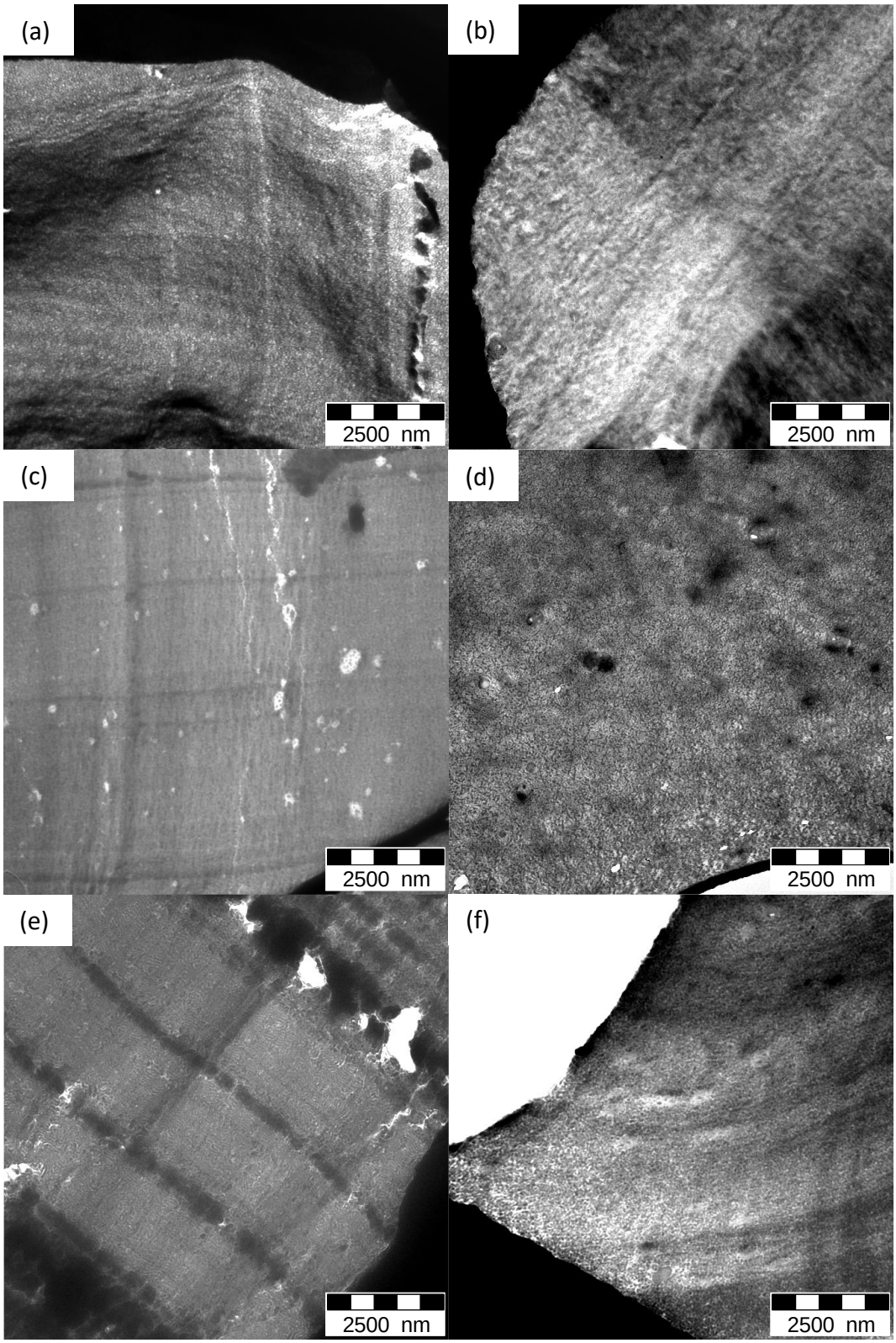

Figure 48. TEM images of solvent-cast films and extruded samples at magnification 10 000. (a) G-S_B_{GMA}(52-4) film; (b) G-S_B_{GMA}(52-4) extruded; (c) G-S_B_{GA}(55-4.7) film; (d) G-S_B_{GA}(55-4.7) extruded; (e) G-S_B_{GMA}(104-4.1) film; (f) G-S_B_{GMA}(104-4.1) extruded. PS phase appears dark.

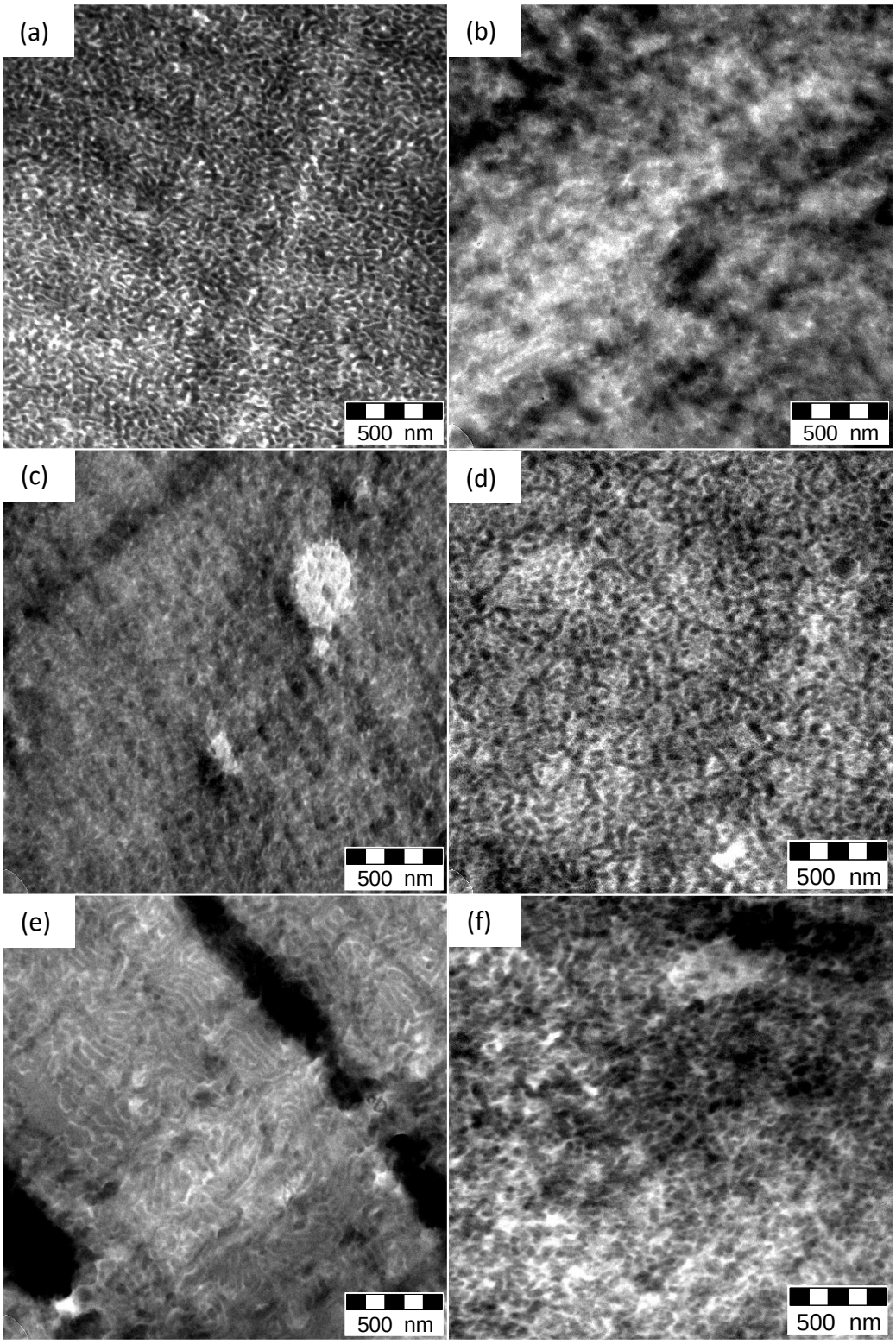

Figure 49. TEM images of solvent-cast films and extruded samples at magnification 40 000. (a) G-S_B$_{GMA}$(52-4) film; (b) G-S_B$_{GMA}$(52-4) extruded; (c) G-S_B$_{GA}$(55-4.7) film; (d) G-S_B$_{GA}$(55-4.7) extruded; (e) G-S_B$_{GMA}$(104-4.1) film; (f) G-S_B$_{GMA}$(104-4.1) extruded. PS phase appears dark.

The TEM images with magnification of 10 000 do not show major differences between solvent-cast films and melt-processed samples. However, it can be observed that the extruded sample is opaque in comparison to the solvent-cast film as shown in Figure 50. In case of the melt-processed samples, it is possible to distinguish particularly large PS domains, reaching up to 400 nm as in the example of the sample G-S_B_{GA}(55-4.7). This observation explains the altering of the optical properties in the injection molded specimens.

Figure 50. Pictures of (left) solvent-cast films and (right) extruded samples.

The variation in the morphology between the samples obtained via extrusion in comparison to the solvent-casted material can be observed in the TEM images at a magnification of 40 000 as presented in Figure 49. A reorganization of the morphology is visible, especially for sample G-S_B_{GMA}(104-4.1), where the lamellar morphology is present in the solvent-cast film, but is no longer detected in the material which underwent melt processing. Instead, the morphology of the injection molded specimens appears to be co-continuous with an interconnected network of PS and PBA domains.

However, no major differences in the size of domains are visible on the extruded samples in comparison to the solvent-cast ones. The PS domains in the melt-processed samples have a size of about 40 to 60 nm, which is in the same range as their solvent-cast counterparts. It is concluded, that a chemical modification of the blend happens during the extrusion processing. As observed on the NMR spectrum of product G-S_B_{GMA}(52-4) before extrusion in Figure 51, not all of the acryloyl groups present in the backbone are reacting with styrene during the graft copolymerization.

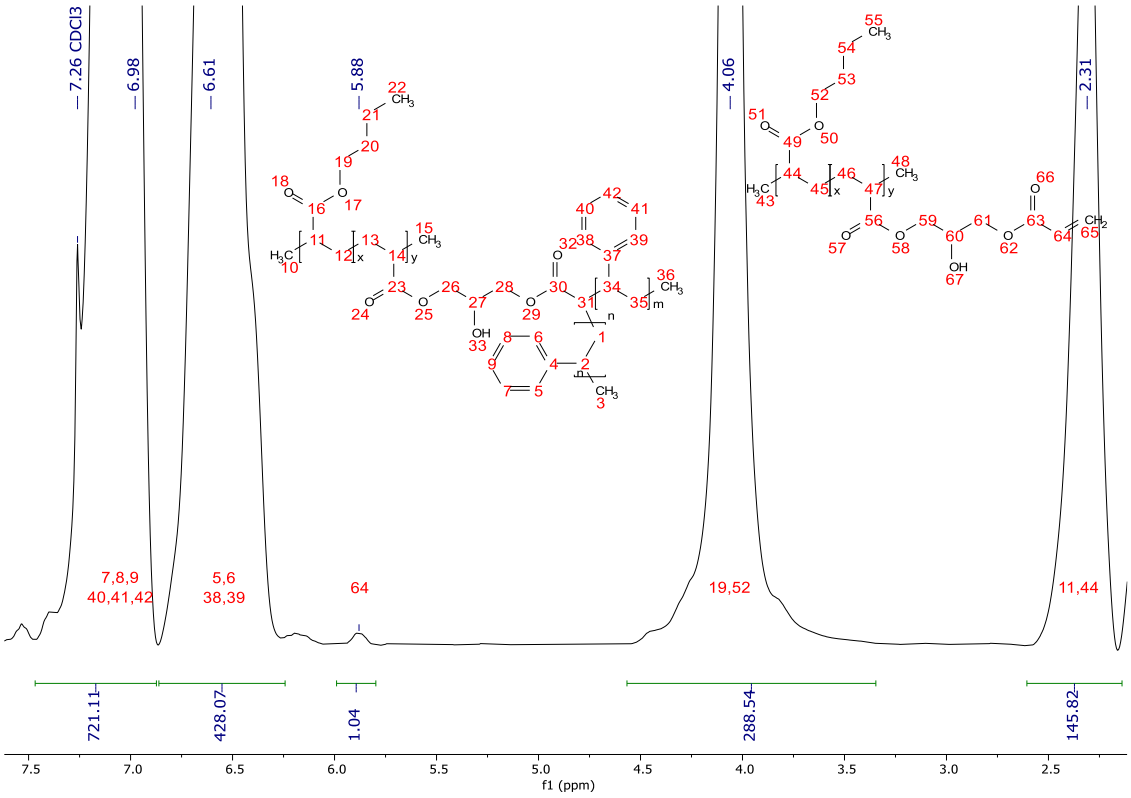

Figure 51. NMR spectrum of G-S_B$_{GMA}$(52-4)

The double bound corresponding to the acryloyl moiety, appearing at 5.88 ppm, is detected. These insaturations can then react during the extrusion of the material and form cross-links between the copolymer molecules. To study this phenomenon, the NSF was measured on samples G-S_B$_{GMA}$(52-4) and G-S_B$_{GA}$(55-4.7) before and after melt processing. The results are presented in Table 30.

Table 30. NSF of G-S_B$_{GMA}$(52-4) and G-S_B$_{GA}$(55-4.7) before and after melt processing.

Graft copolymer	NSF before extrusion	NSF after extrusion
	[wt.%]	
G-S_B$_{GMA}$(52-4)	16.9	59.4
G-S_B$_{GA}$(55-4.7)	0.0	18.8

It is observed that the NSF of both sample increases after melt processing at 200 °C. This increase is, however, not uniform and more pronounced in case of G-S_B$_{GMA}$(52-4) compared to G-S_B$_{GA}$(55-4.7). The difference in the NSF between the two samples does not appear neither on their TEM pictures nor on their mechanical behavior, as both samples have elongation at break above 45 %. The reaction

happening during the extrusion reinforces the polymer and increases its elongation at break and tensile strength.

The processing method used for PBA-g-PS/h-PS samples plays an essential role in evaluating their physical proprieties. Whereas solvent casted films showed low elongation at break and high transparency, extruded samples showed elongation at break reaching 55% but poor visible transparency. The evaluation of their morphology showed large difference, which explains the change in physical properties. Chemical modification due to the reaction of the remaining olefinic bounds during processing of the sample are to account for this morphological change.

4.2.2.4. Blending of graft copolymer product and high molecular weight PS

As already described, the addition of homopolymer to a matrix of graft copolymer results in a shift in morphology and, therefore, a change in the mechanical properties of the blend. The influence of the addition of h-PS (Styrolution PS 124N™, referred as PS 124N) to the synthesized copolymer blends (Table 27) is studied. For this purpose, the synthesized copolymer/h-PS blends are further blended with h-PS during the extrusion and the tensile strength and elongation at break of the final products are tested. Figure 52 display the tensile strength and elongation at break of the synthesized copolymer blends before and after addition of the PS 124N.

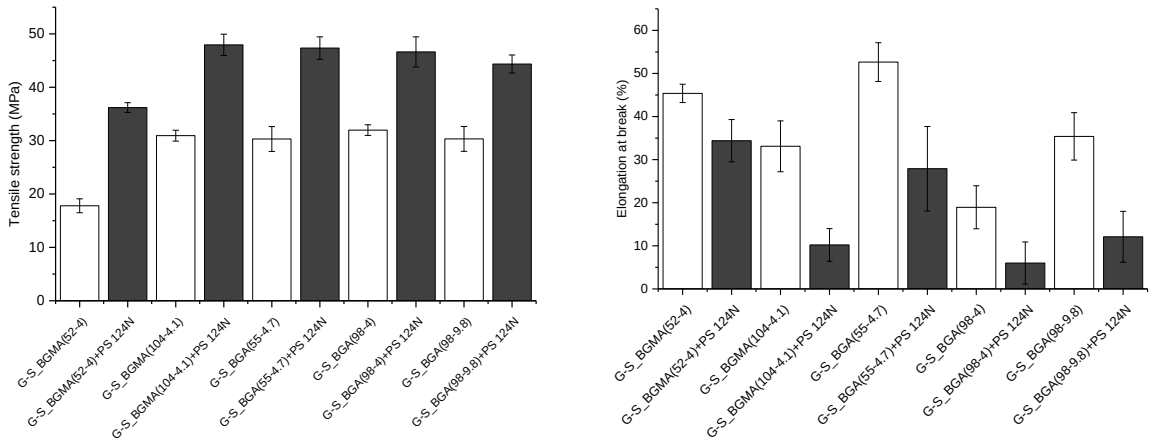

Figure 52. Tensile strength and elongation at break of blends (white) and blends + PS 124N (grey).

The observed trend is similar for all the samples, with an increase of the tensile strength and a decrease of the elongation at break upon addition of PS 124N. However, the amplitude of the gains and losses differs greatly between the samples as showed in Table 31.

Table 31. Gain of tensile strength and loss in elongation at break of blends with addition of PS 124N.

Blends + commercial h-PS	Gain of tensile strength	Loss of elongation at break
G-S_B_{GMA}(52-4) + PS 124N	+102%	-25%
G-S_B_{GMA}(104-4.1) + PS 124N	+55%	-70%
G-S_B_{GA}(55-4.7) + PS 124N	+57%	-47%
G-S_B_{GA}(98-4) + PS 124N	+47%	-68%
G-S_B_{GA}(98-9.8) + PS 124N	+45%	-66%

The variation of tensile strength is greater in case of G-S_B_{GMA}(52-4) compared to other samples, whereas its decrease of elongation at break is the smallest. However, it should be noted that this sample had lower tensile strength in comparison to other samples (see Table 29). Therefore, its large increase upon addition of PS 124N is predictable. All the other samples show an increase of tensile strength of about 50 %. Samples with backbone having M_n of around 100 kg/mol show the lowest increase of tensile strength and the highest decrease of elongation at break. This result indicates that the large backbone length induces stronger phase separation compared to the samples prepared with lower M_n backbone.

The mechanical characteristics of the obtained blends indicate potential for compatibilization behavior with styrenic polymers. As the sample G-S_B_{GMA}(52-4) + PS 124N reached a tensile strength of 35 MPa and elongation at break of 35 %, it could be a suitable candidate for further development. It is expected that the advantage of this block copolymer blend comes from the achieved features of the backbone, as well as the established window of graft copolymerization synthesis conditions.

7. Summary and conclusions in English and German

The synthesis of graft copolymer blends containing PBA-g-PS and h-PS was achieved via two separate routes. Route A uses two steps: (i) polymerization of BA with AMA or DCPA and (ii) copolymerization of PBA-co-AMA or PBA-co-DCPA backbones with styrene yielding PBA-g-PS/h-PS blends. Route B uses three steps: (i) copolymerization of BA with GA or GMA, (ii) polymer analogous reaction of the obtained PBA-co-GA or PBA-co-GMA backbones with AA and (iii) graft copolymerization of the obtained acryloyl-modified backbones with styrene yielding PBA-g-PS/h-PS. Independently of the route used for the graft copolymerization, two methods of synthesis were investigated in terms of the polymerization media: emulsion and solution polymerization.

In route A, the backbone is polymerized by reaction of BA with DCPA or AMA, which can be performed in emulsion or in solution. The synthesis of PBA-co-DCPA and PBA-co-AMA was achieved in emulsion after the reaction conditions in a system with pure PBA were established. The subsequent grafting reaction, also performed in emulsion polymerization, showed clear difference between products copolymerized with AMA- or DCPA-based backbones. In the grafting reactions where PBA-co-DCPA was used as precursor, no grafting occurred, rendering the product opaque and brittle due to the large portion of h-PS and ungrafted backbone. On the contrary, the product of the grafting reaction prepared with PBA-co-AMA showed transparency and flexibility with elongation at break up to 34 % and E modulus around 140 MPa. It is expected, that the lack of high E modulus and elongation at break arises from the synthesis of the backbone itself. It appeared that a substantial fraction of oligomeric chains were produced during the synthesis of the backbone and hindered the properties of the resulting graft copolymer. Using route A, PBA-co-AMA was also synthesized by solution polymerization by dilution of the monomer in the solvent and dosing of the monomer/initiator mixture during the course of the synthesis. The graft copolymerization led to the formation of brittle and opaque products, due to segregation between PS and PBA phase.

Route A, although showing great advantages in the formation of graft copolymer, due to the lower amount of steps required, did not lead to transparent and/or flexible blends. It is expected, that higher amount of AMA moieties in the backbone could increase the grafting efficiency of styrene onto the backbone, enhancing the compatibility between the two phases. However, the synthesis of PBA-co-AMA backbone is more prone to cross-linking due to the higher amount of AMA comonomer.

The results from the emulsion polymerization of styrene in the presence of PBA-co-AMA indicate a higher degree of grafting, suggesting that styrene or polystyrene radicals have superior access to the backbone compared to solution polymerization. However, it is worth noting that emulsion polymerization may lead to an agglomeration effect, resulting in high grafting variations during the reaction and potentially causing non-uniform phase separation in the final polymer product. [106] To circumvent such issues, the use of solution polymerization proves advantageous as it avoids phase segregation and demixion during the copolymer synthesis.

Selecting the appropriate co-monomer during the backbone synthesis plays a crucial role in balancing the reactivity of the functional groups and achieving optimal grafting efficiency. Vinyl acrylate or vinyl methacrylate are viable candidates, as they permit a higher number of reactive sites on the backbone, while reducing the likelihood of cross-linking during synthesis. By tailoring the co-monomer type and employing solution polymerization, it becomes possible to enhance the uniformity and overall quality of the resulting copolymer.

Route B, where BA is firstly copolymerized with GMA or GA, shows a clear advantage. In this method, the synthesis of the backbone is simpler and the risk of cross-linking is essentially reduced. Similarly to route A, the synthesis of the backbone in route B can be carried out in either solution or emulsion polymerization. However, an additional post-modification reaction of the backbone is required, in order to convert the glycidyl functions from GMA or GA into acryloyl function, creating active sites for the subsequent graft copolymerization.

To reduce the probability of cross-linking during the graft copolymerization, a fraction of the initiator and styrene monomer were continuously added to the reaction mixture, providing constant concentration of initiator and dilution of the system. The graft copolymerization product obtained in solution polymerization according to the route B showed elongation at break at 34 %, while the tensile strength reached 35 MPa.

A DoE was performed to establish the influence of a set of factors on the properties of the blend as well as their interaction. The dosing duration of the monomer/initiator mixture, the final concentration of polymer as well as the initiator concentration were set as the studied factors and it was determined that the latter is the primary factor of influence. A clear conclusion arising from the performed statistical analysis was the demonstration of the process repeatability, which showed strong variation in results in term of mechanical properties. As all the experiments were performed under the same

conditions following the principle of DoE, it was concluded that only the starting material was responsible for the observed variation in the mechanical performance of the resulting blends. It was observed that the backbone, produced by emulsion polymerization, had a bimodal distribution of its molecular weight with a portion around 30 kg/mol and another around 1000 kg/mol. Hence, the species with higher molecular weight are bearing higher amount of active sites. Therefore, it was deduced that their presence in the backbone product increases the viscosity of the mixture during the graft copolymerization. As a consequence of their low mobility and high density of active sites, the conditions for cross-linking reaction are promoted.

Therefore, route B was also performed with a backbone polymerized in solution. To establish a parameter window for the synthesis of the PBA-co-GMA and PBA-co-GA backbones, avoiding cross-linking side reactions, the synthesis of pure PBA was studied. The PBA polymer with M_n between 20 and 100 kg/mol and dispersity as low as 2 was obtained by adjusting the concentration of chain transfer agent and initiator, as well as choosing adequately the solvent. The defined parameters were further applied for the synthesis of PBA-co-GMA and PBA-co-GA with varied number of glycidyl groups per chain. NMR spectroscopy and gravimetric analysis showed full conversion of the monomers and the Soxhlet extraction confirmed the absence of cross-linking. The subsequent modification of the glycidyl functionalities in the backbone by polymer analogous reaction with acrylic acid created sites for graft copolymerization. The incorporation of pendant acryloyl groups, as well as the lack of cross-linking was proved by NMR spectroscopy and soxhlet extraction, respectively.

The produced backbones were used as precursor for the graft copolymerization with styrene in solution. It was observed that the NSF in the graft copolymerization product is strongly dependents on the N_{Acr} in case of the modified PBA-co-GMA backbones. The N_{Acr} has to be limited to about 10 per chain in order to avoid extensive cross-linking, causing deterioration of processability and optical properties of the blend. Additionally, the copolymerization course was influenced by the type of the comonomer built into the backbone. The structural differences between GMA and GA monomers determined the reactivity ratio with BA. PBA-co-GMA showed a higher composition drift in comparison to the copolymer containing the GA monomer. As a result, the graft copolymers produced with modified PBA-co-GA backbones have less NSF compared to the materials obtained from GMA based backbones. This effect is particularly visible for backbone with M_n below 50 kg/mol and with Nm below 100.

The morphology of the obtained copolymer blends was examined by TEM in the thermodynamically relaxed state of solvent-cast films. Noticeable differences appear between the synthesized blends depending on M_n of the used backbone. The backbone with M_n around 100 kg/mol led to the formation of distinct PBA phase, whereas backbones with M_n in the range of 50 kg/mol produced more continuous morphology with overlapping phases.

The optical properties can be correlated to the morphology of the prepared copolymer blends. The samples showing low transparency contained large PS domains in the blend, with a size above the wavelength of visible light. On the contrary, blends showing high transparency with haze as low as 15 % varied in the PS domain size from 50-200 nm. No significant correlation was observed between the mechanical performance of the blends and their morphology. Typically, the films were brittle with low elongation at break below 5 % and high tensile strength above 15 MPa. It is well documented, that the size of the domains in PS-based copolymers is crucial in achieving high flexibility and thin layer yielding of the material. The limited flexibility of the produced solvent-cast films is explained by the PS domains size, which is above the critical value of 20 nm. Moreover, SEC deconvolution demonstrated that not more than 30 % of the PS chains were grafted to the backbone. This further explains the low flexibility of the films.

The material treatment through solvent-casting or injection molding processing influences the mechanical and optical behavior of the blend. It was found that the flexibility, as well as the tensile strength of the product, is highly improved in the samples obtained by injection molding. However, no major change in the morphology of the blend was observed between the cast films and the injected specimens. Two hypothesis can explain this effect: an alignment of the domains during injection molding in comparison to the relaxed state of solvent-cast films, or a chemical reaction at elevated processing temperature, leading to the formation of cross-links between copolymer molecules. The later possibility is supported by the increase of NSF after injection molding step in comparison to the solvent-casting procedure.

To demonstrate how the synthesized blends perform as a compatibilizer, their blending behavior was studied with a commercial grade of h-PS, within the mold-processing step. It was found that the tensile strength of the obtained specimens was significantly improved in comparison to the synthesized graft copolymer blends with moderate loss of flexibility. The decrease of elongation at break is minimal for samples based on backbones with M_n around 50 kg/mol, while the tensile strength shows

a major increase. On the contrary, the use of samples based on backbone with M_n around 100 kg/mol resulted in a strong decrease in elongation at break and limited improvement of tensile strength.

In conclusion, the development of free-radical polymerization of PBA-g-PS/h-PS was successfully achieved by a new 3-steps synthetic method. Targeted adjustment of the synthesis parameters and structure of backbones allowed to produce flexible graft copolymer blends with desired morphology, using free-radical polymerization technique. The investigation of the morphology of the copolymer blend revealed the presence of lamellar structures despite the observed low flexibility. To enhance the flexibility of the copolymer blend, it is essential to further reduce the PS domains. Thus, the demonstrated free-radical grafting approach showcased great potential in achieving this objective. Further steps of improving the grafting efficiency and reducing the reactivity of active sites on the backbone, while increasing their quantity, are expected to promote the formation of copolymer products over h-PS. The reactivity of the active sites could be effectively reduced by incorporation of vinyl or allyl functional groups, in contrast to the acryloyl groups utilized in this study. Additionally, efficient methods to separate the copolymer from ungrafted PS would greatly contribute to a deeper understanding of phase separation formation and the role that ungrafted PS plays in the resulting morphology.

In summary, the synthesis approach established in this research provides a practical and efficient means of producing the desired class of products, combining the sought-after performance characteristics with the transparency inherent in styrenic copolymers. The investigation demonstrates how the choice of monomers utilized in both the backbone and side chains of the copolymer drives the properties of the final material. Thus it opens further possibilities for tailored build-up between soft and hard phases in the copolymer. As a consequence, this study has shed light on the importance of strategic monomer design and synthesis, paving way for further advancements and innovations in copolymer material science.

Die Synthese von Pfropfcopolymer-Blends, die PBA-g-PS und h-PS enthalten, wurde über zwei separate Wege erreicht. Route A besteht aus zwei Schritten: (i) der Polymerisation von BA mit AMA oder DCPA und (ii) der Copolymerisation von PBA-co-AMA bzw. PBA-co-DCPA-Rückgraten mit Styrol, was zu PBA-g-PS/h-PS-Blends führt. Route B umfasst drei Schritte: (i) die Copolymerisation von BA mit GA oder GMA, (ii) die polymeranaloge Reaktion der erhaltenen PBA-co-GA bzw. PBA-co-GMA-Rückgrate mit AA und (iii) die Pfropfcopolymerisation der erhaltenen acryloylmodifizierten Rückgrate mit Styrol, was zu PBA-g-PS/h-PS führt. Unabhängig von der gewählten Route für die Pfropfcopolymerisation wurden zwei Synthesemethoden in Bezug auf das Polymerisationsmedium untersucht: Emulsions- und Lösungspolymerisation.

In Route A wird das Rückgrat durch die Reaktion von BA mit DCPA oder AMA polymerisiert, was in Emulsion oder Lösung erfolgen kann. Die Synthese von PBA-co-DCPA und PBA-co-AMA wurde in Emulsion durchgeführt, nachdem die Reaktionsbedingungen in einem System mit reinem PBA etabliert wurden. Die nachfolgende Pfropfreaktion, ebenfalls als Emulsionspolymerisation durchgeführt, zeigte klare Unterschiede zwischen den Produkten, die mit AMA- oder DCPA-basierten Rückgraten copolymerisiert wurden. Bei Verwendung von PBA-co-DCPA als Vorläufer erfolgte keine Pfropfung, was das Produkt opak und spröde machte, aufgrund des großen Anteils an h-PS und unverzweigtem Rückgrat. Im Gegensatz dazu zeigte das Produkt der Pfropfreaktion, das mit PBA-co-AMA hergestellt wurde, Transparenz und Flexibilität mit einer Bruchdehnung von bis zu 34 % und einem E-Modul von etwa 140 MPa. Es wird erwartet, dass das geringe E-Modul und die geringe Bruchdehnung auf die Synthese des Rückgrats selbst zurückzuführen sind. Es schien, dass während der Synthese des Rückgrats eine beträchtliche Menge an oligomeren Ketten erzeugt wurde, die die Eigenschaften des resultierenden Pfropfcopolymers beeinträchtigten.

Die Verwendung von Route A führte zur Synthese von PBA-co-AMA mittels Lösungspolymerisation durch Verdünnung des Monomers im Lösungsmittel und Dosierung der Monomer/Initiator-Mischung während des Verlaufs der Synthese. Die Pfropfcopolymerisation führte zur Bildung von spröden und undurchsichtigen Produkten aufgrund der Auftrennung zwischen der PS- und PBA-Phase.

Route A zeigte zwar Vorteile bei der Bildung des Propfcopolymers aufgrund der geringeren Anzahl von Schritten, führte aber nicht zu transparenten und/oder flexiblen Blends. Es ist davon auszugehen, dass eine höhere Menge an AMA-Einheiten im Rückgrat die Pfropfeffizienz von Styrol auf das Rückgrat erhöhen könnte und die Kompatibilität zwischen den beiden Phasen verbessert. Allerdings ist die

Synthese des PBA-co-AMA-Rückgrats aufgrund des höheren Anteils an AMA-Comonomer anfälliger für Vernetzungsreaktionen.

Die Ergebnisse der Emulsionspolymerisation von Styrol in Gegenwart von PBA-co-AMA deuten auf einen höheren Grad der Pfropfung hin. Dies wird möglicherweise verursacht durch die verbesserte Zugänglichkeit des Rückgrats für Styrol- oder Polystyrolradikale im Vergleich zur Lösungspolymerisation. Es ist jedoch zu beachten, dass die Emulsionspolymerisation zu einem Agglomerationseffekt führen kann, der zu hohen Schwankungen in der Pfropfung während der Reaktion führt und potenziell zu einer ungleichmäßigen Phasentrennung im Endpolymerprodukt führen kann. [106]

Um solche Probleme zu umgehen, erweist sich die Verwendung von Lösungspolymerisation als vorteilhaft, da sie Phasentrennung und Entmischung während der Copolymersynthese vermeidet. Die Auswahl des geeigneten Comonomers während der Rückgratsynthese spielt eine entscheidende Rolle für das Gleichgewicht der Reaktivität der funktionellen Gruppen und die Erzielung optimaler Pfropfeffizienz. Vinylacrylat und Vinylmethacrylat sind geeignete Kandidaten, da sie eine höhere Anzahl reaktiver Stellen am Rückgrat ermöglichen und die Wahrscheinlichkeit der Vernetzung während der Synthese verringern. Durch die Anpassung des Comonomertyps und die Verwendung von Lösungspolymerisation wird es möglich, die Gleichmäßigkeit und Gesamtqualität des resultierenden Copolymers zu verbessern.

Route B, in dem BA zunächst mit GMA oder GA copolymerisiert wird, zeigt einen klaren Vorteil. In dieser Methode ist die Synthese des Rückgrats einfacher und das Risiko der Vernetzung ist deutlich reduziert. Ähnlich wie bei Route A kann die Synthese des Rückgrats in Route B entweder in Lösung oder Emulsionspolymerisation durchgeführt werden. Allerdings ist eine zusätzliche Modifikationsreaktion des Rückgrats erforderlich, um die Glycidylfunktionen von GMA oder GA in Acryloylfunktionen umzuwandeln und aktive Stellen für die nachfolgende Pfropfcopolymerisation zu schaffen.

Um die Wahrscheinlichkeit der Vernetzung während der Pfropfcopolymerisation zu reduzieren, wurde eine Fraktion des Initiators und Styrolmonomers kontinuierlich zur Reaktionsmischung hinzugefügt, um eine konstante Konzentration des Initiators und Verdünnung des Systems zu gewährleisten. Das Pfropfcopolymerisationsprodukt, das in Lösungspolymerisation nach Route B erhalten wurde, zeigte eine Bruchdehnung von 34 % und eine Zugfestigkeit von 35 MPa.

Ein DoE (Design of Experiments) wurde durchgeführt, um den Einfluss einer Reihe von Faktoren auf die Eigenschaften des Blends sowie deren Wechselwirkung zu bestimmen. Die Dosierdauer der Monomer/Initiator-Mischung, die Endkonzentration des Polymers sowie die Initiatorkonzentration wurden als untersuchte Faktoren festgelegt, wobei festgestellt wurde, dass letztere der hauptsächliche Einflussfaktor ist. Eine klare Schlussfolgerung aus der durchgeführten statistischen Analyse war die Demonstration der Prozesswiederholbarkeit, die starke Variationen in den Ergebnissen in Bezug auf die mechanischen Eigenschaften zeigte. Da alle Experimente unter denselben Bedingungen nach dem Prinzip des DoE durchgeführt wurden, wurde geschlussfolgert, dass nur das Ausgangsmaterial für die beobachtete Variation in der mechanischen Leistung der resultierenden Blends verantwortlich war.

Es wurde beobachtet, dass das Rückgrat, das durch Emulsionspolymerisation hergestellt wurde, eine bimodale Verteilung seines Molekulargewichts aufwies, mit einem Anteil von etwa 30 kg/mol und einem anderen von etwa 1000 kg/mol. Daher tragen die Spezies mit höherem Molekulargewicht eine höhere Anzahl von aktiven Stellen. Es wurde daher geschlussfolgert, dass diese aktiven Stellen im Rückgrat die Viskosität der Mischung während der Pfropfcopolymerisation erhöhen. Aufgrund ihrer geringen Mobilität und hohen Dichte an aktiven Stellen werden die Bedingungen für die Vernetzungsreaktion gefördert.

Daher wurde Route B auch mit einem in Lösung polymerisierten Rückgrat durchgeführt. Um einen Parameterraum für die Synthese der PBA-co-GMA- und PBA-co-GA-Rückgrate ohne Vernetzungsreaktionen zu etablieren, wurde die Synthese von reinem PBA untersucht. Das PBA-Polymer mit M_n zwischen 20 und 100 kg/mol und einer Dispersität von mindestens 2 wurde durch Anpassung der Konzentration des Kettenübertragungsmittels und des Initiators sowie durch die Auswahl des Lösungsmittels erhalten. Die definierten Parameter wurden weiterhin für die Synthese von PBA-co-GMA und PBA-co-GA mit variierter Anzahl von Glycidylgruppen pro Kette angewendet. NMR-Spektroskopie und gravimetrische Analyse zeigten eine vollständige Umwandlung der Monomere und die Soxhlet-Extraktion bestätigte das Fehlen von Vernetzung. Die anschließende Modifikation der Glycidylfunktionen im Rückgrat durch polymeranaloge Reaktion mit Acrylsäure schuf Stellen für die Pfropfcopolymerisation. Die Einbindung von Anhängen mit Acryloylgruppen sowie das Fehlen von Vernetzung wurden durch NMR-Spektroskopie bzw. Soxhlet-Extraktion nachgewiesen.

Die hergestellten Rückgrate wurden als Vorläufer für die Pfropfcopolymerisation mit Styrol in Lösung verwendet. Es wurde beobachtet, dass die NSF im Pfropfcopolymerisationsprodukt stark von N_{Acr} abhängt, insbesondere bei modifizierten PBA-co-GMA-Rückgraten. N_{Acr} muss auf etwa

10 pro Kette begrenzt werden, um eine umfangreiche Vernetzung zu vermeiden, die zu einer Verschlechterung der Verarbeitbarkeit und optischen Eigenschaften des Blends führen würde. Darüber hinaus wurde der Verlauf der Copolymerisation durch den Typ des in das Rückgrat eingebauten Comonomers beeinflusst. Die strukturellen Unterschiede zwischen GMA- und GA-Monomeren bestimmten das Reaktivitätsverhältnis mit BA. PBA-co-GMA zeigte eine höhere Änderung der Zusammensetzung im Vergleich zum Copolymer, welches das GA-Monomer enthielt. Als Ergebnis haben die mit modifizierten PBA-co-GA-Rückgraten hergestellten Pfropfcopolymere eine niedrigere NSF im Vergleich zu den Materialien, die aus GMA-basierten Rückgraten hergestellt wurden. Dieser Effekt ist besonders sichtbar für Rückgrate mit M_n unter 50 kg/mol und Nm unter 100.

Die Morphologie der erhaltenen Pfropfcopolymer-Blends wurde im thermodynamisch entspannten Zustand von lösemittelgegossenen Filmen mittels TEM untersucht. Deutliche Unterschiede zeigten sich je nach M_n des verwendeten Rückgrats. Ein Rückgrat mit einem M_n von etwa 100 kg/mol führte zur Bildung einer deutlichen PBA-Phase, während Rückgrate mit einem M_n im Bereich von 50 kg/mol eine kontinuierlichere Morphologie mit überlappenden Phasen erzeugten.

Die optischen Eigenschaften können mit der Morphologie der vorbereiteten Pfropfcopolymer-Blends korreliert werden. Proben mit geringer Transparenz enthielten große PS-Domänen im Blend, deren Größe über der Wellenlänge des sichtbaren Lichts lag. Im Gegensatz dazu variierten Blends mit hoher Transparenz und einer Trübung von nur 15 % in der Größe der PS-Domänen zwischen 50 und 200 nm. Es wurde keine signifikante Korrelation zwischen den mechanischen Eigenschaften der Blends und ihrer Morphologie beobachtet. Typischerweise waren die Filme spröde mit einer geringen Bruchdehnung unter 5 % und einer hohen Zugfestigkeit über 15 MPa. Es ist gut beschrieben, dass die Größe der Domänen in PS-basierten Copolymeren entscheidend ist, um hohe Flexibilität und dünnwandiges Verhalten des Materials zu erreichen. Die begrenzte Flexibilität der hergestellten lösemittelgegossenen Filme wird durch die Größe der PS-Domänen erklärt, die über dem kritischen Wert von 20 nm liegt. Darüber hinaus zeigte die SEC-Dekonvolution, dass nicht mehr als 30 % der PS-Ketten am Rückgrat gepfropft wurden, eine weitere Ursache für die geringe Flexibilität der Filme.

Die Verarbeitung des Materials durch Lösungsgießen oder Spritzguss beeinflusst das mechanische und optische Verhalten des Blends. Es wurde festgestellt, dass die Flexibilität sowie die Zugfestigkeit des Produkts in den durch Spritzguss erhaltenen Proben erheblich verbessert sind. Es wurde jedoch keine wesentliche Veränderung in der Morphologie des Blends zwischen den gegossenen Filmen und den gespritzten Proben beobachtet. Zwei Hypothesen können diesen Effekt erklären: eine Ausrichtung der Domänen während des Spritzgusses im Vergleich zum entspannten Zustand der lösemittelgegossenen Filme oder eine chemische Reaktion bei erhöhter Verarbeitungstemperatur, die zur Bildung von Vernetzungen zwischen den Copolymermolekülen führt. Die letztere Hypothese wird durch den Anstieg der NSF nach dem Spritzguss im Vergleich zum Gießen mit Lösungsmittel unterstützt.

Um zu zeigen, wie sich die synthetisierten Blends als Kompatibilisator verhalten, wurde ihr Mischverhalten mit einer kommerziellen Sorte von h-PS im Rahmen des Formgebungsprozesses untersucht. Es wurde festgestellt, dass die Zugfestigkeit der erhaltenen Proben im Vergleich zu den synthetisierten Pfropfcopolymerblends bei moderatem Verlust an Flexibilität signifikant verbessert wurde. Der Rückgang der Bruchdehnung ist gering bei Proben auf Basis von Rückgraten mit einem M_n von etwa 50 kg/mol, während die Zugfestigkeit einen wesentlichen Anstieg zeigt. Im Gegensatz dazu führte die Verwendung von Proben auf Basis von Rückgraten mit einem M_n von etwa 100 kg/mol zu einem starken Rückgang der Bruchdehnung und einer geringeren Verbesserung der Zugfestigkeit.

Zusammenfassend wurde die Entwicklung der radikalischen Polymerisation von PBA-g-PS/h-PS erfolgreich durch eine neue dreistufige Synthesemethode erreicht. Die gezielte Anpassung der Syntheseparameter und der Rückgratstruktur ermöglichte die Herstellung flexibler Pfropfcopolymerblends mit gewünschter Morphologie mittels radikalischer Polymerisation. Die Untersuchung der Morphologie des Pfropfcopolymerblends zeigte trotz der beobachteten geringen Flexibilität das Vorhandensein von lamellaren Strukturen. Um die Flexibilität des Pfropfcopolymerblends zu erhöhen, ist es entscheidend, die PS-Domänen weiter zu reduzieren. Der gezeigte radikalische Pfropfungsansatz hat großes Potenzial, dieses Ziel zu erreichen. Weitere Schritte zur Verbesserung der Pfropfeffizienz und zur Reduzierung der Reaktivität der aktiven Stellen im Rückgrat, bei gleichzeitiger Erhöhung ihrer Menge, werden erwartet, um die Bildung von Copolymerprodukten gegenüber h-PS zu fördern. Die Reaktivität der aktiven Stellen könnte effektiv durch die Einführung von Vinyl- oder Allyl-Funktionsgruppen reduziert werden, im Gegensatz zu den in dieser Studie verwendeten Acryloyl-Gruppen. Darüber hinaus würden effiziente Methoden zur

Trennung des Copolymers von ungepfropftem PS einen erheblichen Beitrag zum tieferen Verständnis von Phasenseparation und der Rolle, die ungepfropftes PS in der resultierenden Morphologie spielt, leisten.

Zusammenfassend bietet der in dieser Forschung etablierte Syntheseansatz eine praktische und effiziente Möglichkeit zur Herstellung der gewünschten Produktklasse. Dabei werden die erstrebten Eigenschaften mit der inhärenten Transparenz von styrolischen Copolymeren kombiniert. Die Untersuchung zeigt, wie die Auswahl der Monomere, die sowohl im Rückgrat als auch in den Seitenketten des Copolymers verwendet werden, die Eigenschaften des Produkts beeinflusst. Dadurch eröffnen sich weitere Möglichkeiten für eine maßgeschneiderte Ausgestaltung zwischen weichen und harten Phasen im Copolymer. Infolgedessen hat diese Studie die Bedeutung der strategischen Monomerentwicklung und -synthese hervorgehoben und den Weg für weitere Fortschritte und Innovationen in der Materialwissenschaft von Copolymeren geebnet.

8. Experimental part

8.1. Chemicals

Butyl acrylate (BA), allyl methacrylate (AMA), glycidyl methacrylate (GMA), glycidyl acrylate (GA) and styrene were destabilized by being passed through basic aluminum oxide to remove traces of inhibitor. They were kept below 5°C before use. Benzoyl peroxide (BPO) was purified by recrystallization in methanol and kept at -20°C before use. Sodium dodecyl sulfate (SDS), potassium persulfate (KPS), sodium bicarbonate, acrylic acid (AA), triphenylphosphine (TPP), 4-methoxyphenol (MEHQ), tert-dodecanethiol (TDT), toluene, cyclohexane (HPLC grades), and methanol (MeOH) (technical and HPLC grades) were used without any further purification.

Glycidyl acrylate (GA) was supplied by ABCR GmbH. All the other chemicals were supplied by VWR Chemicals.

8.2. Polymerization procedures

8.2.1. Process by emulsion polymerization of the backbone

7.2.1.1. Route A: Synthesis of PBA-g-PS/h-PS in two steps

Backbone synthesis

A 500 mL reactor is charged with 151.5 g of demineralized water, 1.5 g of SDS and 0.2 g of sodium bicarbonate and subsequently evacuated and purge with nitrogen. After heating the reaction vessel to 60°C, 0.18 g of KPS is added to the mixture and the monomer or monomers mixture (BA, BA+DCPA or BA+AMA) is added within 3.5h under constant stirring. After 0.5, 1.5 and 2.5 h a portion of TDT is added. The reaction is continued for another hour.

Graft copolymerization

A 500 mL reactor equipped with a nitrogen inlet, an overhead stirrer and a condenser is charged with 80 g of backbone emulsion (containing 31.44 g of backbone), SDS, sodium bicarbonate and water. The mixture is heated up to 60°C under stirring and KPS is added to the mixture. Styrene is dosed to the reaction mixture continually during 3 h. The reaction is then continued for 3 h. The different amounts of reactants are presented in Table 32.

Table 32. Reactants amounts used for the graft copolymerization using emulsion route A.

Graft copolymer	Styrene	KPS	SDS	$NaHCO_3$	H_2O
	[g]				
G-E_B_{DCPA}(30-1)_01 G-E_B_{AMA}(26-1.4)_01	22.27	0.09	0.2	0.06	50.72
G-E_B_{DCPA}(30-1)_02 G-E_B_{AMA}(26-1.4)_02	125.76	0.50	0.75	0.09	187.24

An aqueous solution containing 1 wt.% of $MgSO_4$ and 0.06 wt.% of H_2SO_4 is prepared and heated up to 50°C. The polymer latex is poured in a minimum of 5-fold of the aqueous acidic solution to coagulate. The polymer is then dissolved in a minimum of THF and precipitated in a minimum of 5-folds of MeOH. The product is filtered and dried in a vacuum oven at 60°C until constant weight.

7.2.1.2. Route B: Synthesis of PBA-g-PS/h-PS in three steps

Backbone synthesis

A 500 mL reactor is charged with 151.5 g of demineralized water, 1.5 g of SDS, 0.2 g of sodium bicarbonate, 0.18 g of KPS and subsequently evacuated and purge with nitrogen. After heating the reaction vessel to 60°C, the monomer or monomers mixture (BA+GMA) is added within 3.5 h under constant stirring. After 0.5, 1.5 and 2.5 h a portion of TDT is added. The reaction is continued for another hour.

An aqueous solution containing 1 wt.% of $MgSO_4$ and 0.06 wt.% of H_2SO_4 was prepared and heated up to 50°C. The prepared latex was poured in a minimum of 5 fold of the aqueous acidic solution to coagulate. The polymer was then filtered and redissolved in THF. The polymer was precipitated in a minimum of 5-folds of MeOH and dried in a vacuum oven at 60°C until constant weight.

Backbone analogous reaction

A 250 mL round-bottom flask equipped with a nitrogen inlet, an overhead stirrer, and a condenser is charged with backbone and solvent. AA, TPP (or TEA) and MEHQ are added at once and the mixture is heated up under stirring. After a defined time, the product is isolated by precipitation in a minimum of 5 fold of a MeOH/water mixture (90/10 V/V), subsequent re-dissolution in THF and further precipitation in the MeOH/water mixture. The process in repeated 2 times. The backbone is then dried

under vacuum at 40°C until constant weight. The different reactions conditions are presented in Table 33.

Table 33. Reaction condition for the polymer analogous reaction of backbone using emulsion route B.

Modification reaction	Backbone	TEA	TPP	AA	MEHQ	Solvent	Solvent	Temperature	Time
	[wt.%]						[type]	[°C]	[h]
#1	11.80	0.21	-	2.15	-	85.84	THF	25	24
#2	11.69	-	0.23	2.34	-	85.74	THF	25	24
#3	11.88	-	0.16	1.58	0.01	86.37	DMF	120	8
#4	26.41	-	1.76	26.41	1.41	44.01	THF	Reflux	16
#5	25.55	1.82	-	25.55	1.46	45.62			16
#6	39.34	-	3.01	18.13	0.18	39.34			16
#7	45.01	-	0.90	9.00	0.09	45.01			60
#8	45.00	-	0.90	9.00	0.09	45.00	Toluene	Reflux	60

Graft copolymerization

A 250 mL reactor flask equipped with an anchor stirrer, a condenser and a nitrogen inlet is charged with 13 g of the post-modified backbone pre-diluted in toluene and heated up to 85°C while stirring at 200 rpm. BPO is dissolved in 52g of styrene and degassed with nitrogen for 15 minutes. This initiator in styrene solution is fed to the reaction mixture for 5 to 15 h. After 24 h, the polymer mixture is allowed to cool down and the polymer is precipitated in MeOH. After filtration, the polymer powder is dried in a vacuum oven at 60°C for 15 h.

Table 34. Reaction condition for the graft copolymerization of post-modified backbone using emulsion route B.

Graft copolymer	BPO	Toluene	Dosing time
	[g]		[h]
G-E_B_{GMA}(28-1.1)	0.52	151.67	10
G-E_B_{GMA}(28-2.0)	0.52	151.67	10
G-E_B_{GMA}(30-2.7)	0.52	151.67	10
#1	0.52	195.00	5
#2	0.52	195.00	15
#3	0.26	195.00	10
#4	0.78	195.00	10
#5	0.26	151.67	5
#6	0.78	151.67	5
#7	0.26	151.67	15
#8	0.78	151.67	15

#9	0.52	151.67	10
#10	0.52	151.67	10
#11	0.52	151.67	10
#12	0.52	120.71	5
#13	0.52	120.71	15
#14	0.26	120.71	10
#15	0.78	120.71	10
#opt1	0.63	186.94	5
#opt2	0.41	188.91	13.4

8.2.2. Process by solution polymerization of the backbone

7.2.2.1. Route A: Synthesis of PBA-g-PS/h-PS in two steps

Backbone synthesis

A 250 mL reactor equipped with a nitrogen inlet, an overhead stirrer and a condenser is charged with 68.6 g of BA, 1.4 g of AMA and 300 g of toluene and heated up to 80°C. 1 g of BPO in a mixture of 29.4 g of BA and 0.6 g of AMA is dosed for 5 h. The reaction is continued for another 15 h. The product is isolated by precipitation in a minimum of 5-fold of a MeOH/water mixture (90/10 V/V), subsequent re-dissolution in THF and further precipitation in the MeOH/water mixture. This process in repeated 2 times. The backbone is then dried under vacuum at 50°C until constant weight.

Table 35. Synthesis condition of backbones using solution-route A.

Backbone	BA	AMA	Toluene
	[g]		
S_B_{AMA}(CL-4)	96	4	100
S_B_{AMA}(CL-2)	98	2	200
S_B_{AMA}(29-2)	98	2	300

Graft copolymerization

A 250 mL reactor flask equipped with an anchor stirrer, a condenser and a nitrogen inlet is charged with 13 g of PBA-co-AMA backbone and toluene (varying amount) and heated up to 85°C while stirring at 200 rpm. 0,52 g of BPO is dissolved in 52g of styrene and degassed with nitrogen for 15 minutes. This initiator in styrene solution is fed to the reaction mixture for 10 h. After 24 h, the polymer mixture

is allowed to cool down and the polymer is precipitated in MeOH. After filtration, the polymer powder is dried in a vacuum oven at 60°C for 15 h.

Table 36 - Synthesis condition of PBA-g-PS using solution route A

Graft copolymer	BPO	Styrene	Toluene
	[g]		
G-S_B_{AMA}(29-2)_01	0.52	52	151.67
G-S_B_{AMA}(29-2)_02	0.52	52	97.5
G-S_B_{AMA}(29-2)_03	0.52	52	65.0

7.2.2.2. Route B: Synthesis of PBA-g-PS/h-PS in three steps

Backbone synthesis

A 250 mL round-bottom flask equipped with a nitrogen inlet, an overhead stirrer, a condenser, and a thermometer is charged with 100 g of monomer or monomers mixture, 100 g of solvent and TDT. The mixture is heated up to 92°C if cyclohexane is used or 100°C if toluene is used, and BPO is added at once. The reaction is continued for 1 h and the mixture is let to cool down to room temperature. The product is isolated by precipitation in a minimum of 5 fold of a MeOH/water mixture (90/10 V/V), subsequent re-dissolution in THF and further precipitation in the MeOH/water mixture. This process in repeated 2 times. The backbone is then dried under vacuum at 60°C until constant weight.

Table 37. Synthesis condition for PBA-co-G(M)A in solution-route B.

Backbone	TDT	BA	GMA/GA	BPO	Solvent
	[g]				[type]
S_B_{BA}(26-0)	1.0	100	0	1.0	Toluene
S_B_{BA}(15-0)	1.0	100	0	0.5	Toluene
S_B_{BA}(20-0)	0.5	100	0	0.5	Toluene
S_B_{BA}(30-0)	1.0	100	0	1.0	Cyclohexane
S_B_{BA}(31-0)	1.0	100	0	1.0	Cyclohexane
S_B_{BA}(38-0)	0.75	100	0	1.0	Cyclohexane
S_B_{BA}(45-0)	0.5	100	0	1.0	Cyclohexane
S_B_{BA}(50-0)	0.25	100	0	1.0	Cyclohexane
S_B_{BA}(98-0)	0.2	100	0	0.1	Cyclohexane
S_B_{GMA}(26-1.9)	0.75	98.1	1.9	1	Cyclohexane
S_B_{GMA}(35-9)	0.75	91	9	1	Cyclohexane
S_B_{GMA}(52-1.1)	0.25	98.1	1.9	1	Cyclohexane
S_B_{GMA}(50-4.7)	0.25	95.3	4.7	1	Cyclohexane
S_B_{GMA}(104-0.6)	0.20	99.4	0.6	0.1	Cyclohexane

S_B_{GA}(55-1.1)	0.25	98.9	1.1	1	Cyclohexane
S_B_{GA}(98-0.5)	0.20	99.5	0.5	0.1	Cyclohexane
S_B_{GA}(98-1.3)	0.20	98.7	1.3	0.1	Cyclohexane

Backbone analogous reaction

A 250 mL round-bottom flask equipped with a nitrogen inlet, an overhead stirrer, and a condenser is charged with a 90 g of a solution of backbone in toluene (50 wt.%). 9.0 g of AA, 0.9 g of TPP and 0.09 g of MEHQ are added at once and the mixture is heated up to reflux under stirring. The reaction is continued for 60 h. The product is isolated by precipitation in a minimum of 5-fold of a MeOH/water mixture (90/10 V/V), subsequent re-dissolution in THF and further precipitation in the MeOH/water mixture. The process in repeated 2 times. The backbone is then dried under vacuum at 40°C until constant weight.

Graft copolymerization

A 250 mL reactor equipped with an overhead stirrer and a condenser is charged with 15 g of post-modified backbone, 60 g of styrene and 60 g of cyclohexane. After heating the reaction mixture to 80°C, 0.1 g of BPO are added to the mixture and 0.4 g of BPO diluted in 3.6 g of styrene is continuously added for 6 h. After 2 h of reaction, 60 g of styrene is continuously added for 4 h. After 6 h of reaction, the product is isolated by precipitation in 5-fold of MeOH. The product is then re-dissolved in THF and precipitated in MeOH. This process is repeated 2 times. The polymer powder is dried in a vacuum oven at 60 °C until constant weight.

8.3. Extraction of non-soluble fraction (NSF)

To quantify the amount of cross-linked material, Soxhlet extraction is performed in toluene for 64 h. The extraction thimble is weighted empty (w_0) and with the polymer powder (w_1). After extraction the thimble is dried for 48 h at 60 °C under vacuum and weighted (w_2). The non-soluble fraction is calculated from the following equation:

$$NS\ [\%] = \frac{w_2 - w_0}{w_1 - w_0} \times 100 \qquad (30)$$

8.4. Processing

Film casting

Films are prepared in 10 cm diameter petri dishes from 20 mL of a 3 wt.% polymer solutions in toluene. Toluene is slowly evaporated by keeping the petri dish in a fume hood for 24 h at room temperature. The resulting films are removed from the petri dish by dipping into deionized water for 2 h. Prior to characterization, the films are dried at 50 °C under vacuum for 24 h. Film thickness is measured with a micrometer caliper. All the films have a mean thickness of 100 ± 10 μm. Dumbbell-shape specimens are punched out from the film for mechanical testing.

Extrusion and injection molding

Extrusion (200 °C, 200 rpm) and injection molding (mold temperature 40 °C) are performed using a co-rotating twin screw micro-extruder MC5 (volume 5 cm^3) and subsequent IM 5.5 injection molder from X-plore. The material is extruded for 2 minutes if pristine and 5 minutes if in a blend with PS 124N before being injected in the mold. The produced dumbbell-shape specimens are used for mechanical testing.

8.5. Analysis

Nuclear magnetic resonance spectroscopy (NMR)

^1H MNR spectroscopy is used to determine the different copolymers composition. Spectra are recorded at room temperature in deuterated chloroform with a Bruker 300 spectrometer operating at 300 MHz. Typical parameters for the proton spectra are a 13.4 μs pulse width, a pulse delay of 5 s, an acquisition time of 2.7 s, a 6 kHz spectral width and 127 scans.

The mole fraction of GMA comonomer in the copolymer (x_{GMA} in mol.%), the mass fraction of GMA in the copolymer (w_{GMA} in wt.%) and the number of comonomer per chain (N_{GMA}) are calculated using the following formulas:

$$x_{GMA} = \frac{\frac{I_{GMA}}{N_{H,GMA}}}{\frac{I_{GMA}}{N_{H,GMA}} + \frac{I_{BA}}{N_{H,BA}}} \quad (31)$$

$$w_{GMA} = \frac{x_{GMA} \times M_{GMA}}{(1 - x_{GMA}) \times M_{BA} + x_{GMA} \times M_{GMA}} \quad (32)$$

$$N_{GMA} = \frac{w_{GMA} \times M_{n(backbone)}}{M_{GMA}} \quad (33)$$

I_{GMA} and I_{BA} represent the NMR integration area of GMA peak at 2.61 ppm and BA peak at 2.25 ppm. $N_{H,\,GMA}$ and $N_{H,\,BA}$ represent the number of hydrogens corresponding to the integrated peaks in GMA and BA. M_{GMA} and M_{BA} represent the molecular mass of GMA (142.15 g/mol) and BA repeating unit (128.17 g/mol). $M_{n(backbone)}$ is the M_n of the backbone determined by SEC analysis.

In a similar manner, the mole and mass fraction of acryloyl comonomer after the post-modification reaction of the backbone as well as the number of acryloyl comonomer per chain are calculated as follows:

$$x_{Acr} = \frac{\frac{I_{Acr}}{N_{H,Acr}}}{\frac{I_{Acr}}{N_{H,Acr}} + \frac{I_{BA}}{N_{H,BA}}} \quad (34)$$

$$w_{Acr} = \frac{x_{Acr} \times M_{Acr}}{(1 - x_{Acr}) \times M_{BA} + x_{Acr} \times M_{Acr}} \quad (35)$$

$$N_{Acr} = \frac{w_{Acr} \times M_{n(Backbone)}}{M_{Acr}} \quad (36)$$

where I_{Acr} represents the integration area of the acryloyl comonomer peak at 6.41 ppm, M_{Acr} and M_{BA} represent the molecular mass of the acryloyl monomer (214.21 g/mol) and BA repeating unit (128.17 g/mol).

The weight fraction of PS in the copolymer is calculated using the following formula:

$$x_{St} = \frac{\frac{I_{St}}{N_{H,St}}}{\frac{I_{St}}{N_{H,St}} + \frac{I_{BA}}{N_{H,BA}}} \quad (37)$$

$$w_{St} = \frac{x_{St} \times M_{St}}{(1 - x_{St}) \times M_{BA} + x_{St} \times M_{St}} \quad (38)$$

where I_{St} represents the integration area of the PS peak at 6.58 ppm, M_{St} and M_{BA} represent the molecular mass of the styrene monomer (104.15 g/mol) and BA repeating unit (128.17 g/mol).

Size exclusion chromatography (SEC)

SEC is performed on an Agilent Series 1100 instrument equipped with a HPLC pump, a series of columns PL gel mixed C (1x 50x4.5 mm and 2x 300x 7.5 mm, Agilent), a refractive index detector and an ultraviolet detector. THF is used as solvent at 35°C with a flow rate of 1 $mL.min^{-1}$ and an injection volume of 100 µL. Calibration is performed with a series of PS standard from PSS polymer (5 samples between 0.580 and 2536 kg/mol).

An important characteristic of the product is the amount of graft copolymer in the system, or the ratio of graft copolymer to h-PS. In order to determine this value, one can use the SEC of produced material and process it through deconvolution. This kind of method was developed with PS/PB system by Huang et al [107].

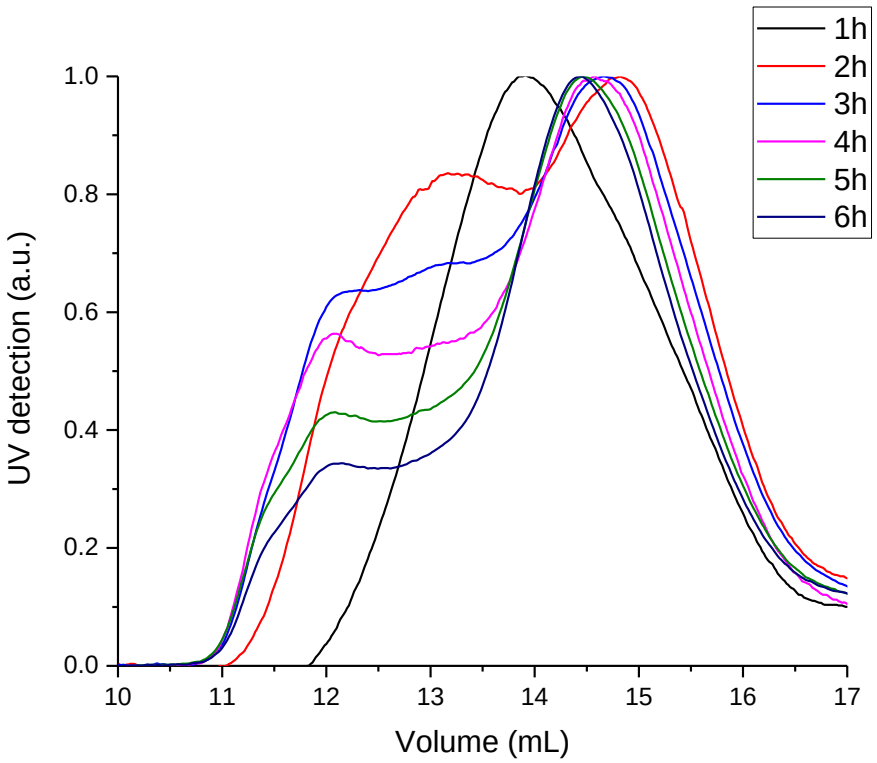

Figure 53. SEC elugram of a copolymerization product through reaction by UV detection after normalization.

Figure 53 shows the typical SEC curve obtained during the graft copolymerization. The elugram consists of two zones: one between 10 and 13.5 mL corresponding to high molecular weight graft copolymer, and another one between 13.5 and 17 mL corresponding to h-PS. The deconvolution method is used to mathematically separate overlapping peaks as depicted in Figure 54. The area under the deconvolution peaks is proportional to the amount of each component in the blend. Therefore, the amount of graft copolymer and h-PS can be determined, and the grafting efficiency of the reaction is calculated for the samples taken out through the reaction course.

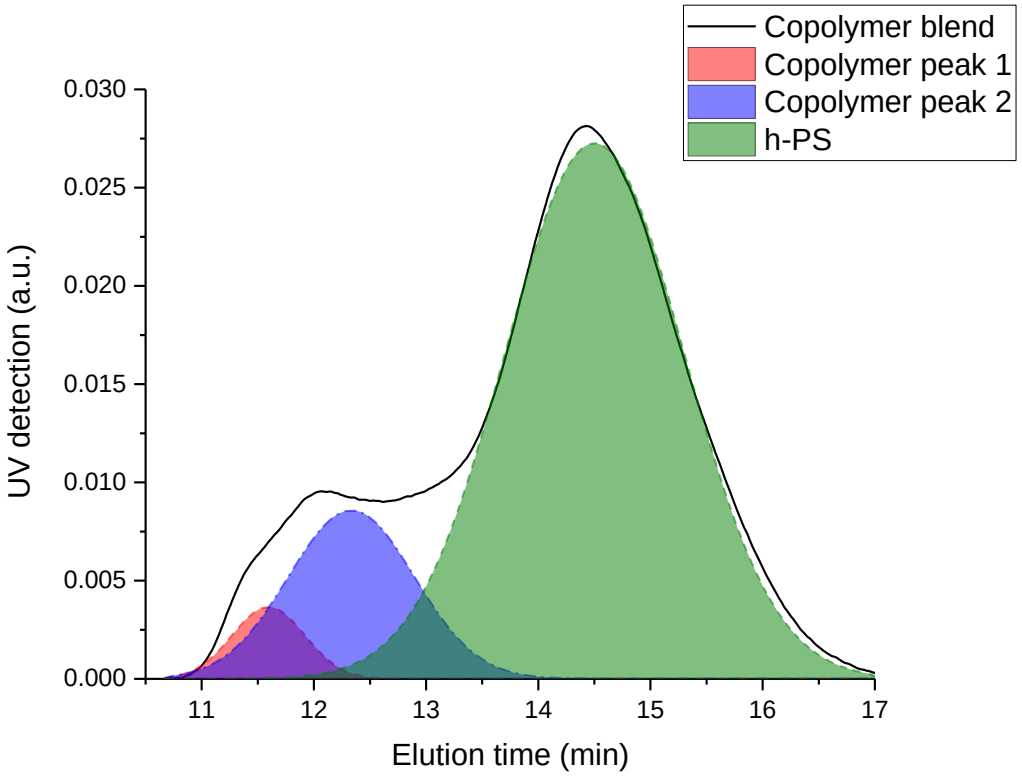

Figure 54. Example of deconvolution on graft copolymerization blend.

The blend is separated in three distinguished peaks corresponding to copolymer and h-PS. The copolymer is split into two separate peaks, as reported for PB-g-PS/PS blends previously by Huang et al. [107] The grafting efficiency is then calculated as:

$$G_{eff} = \frac{Area\ copolymer\ peak\ 1 + Area\ copolymer\ peak\ 2}{Total\ area} \tag{39}$$

8.6. Physical characterization and imaging

Mechanical test

Stress-strain curves are measured using a Zwick Roell Z 2.5 tensile tester at 23 °C and 48 % of relative humidity. The samples are conditioned for 2 days prior to testing. The test is performed at a rate of 0.1 mm/min below 0.25 % of elongation for determining the E modulus. The rest of the test is performed with a rate of 20 mm/min to determine the tensile strength and elongation at break.

Optical characterization

Optical properties including haze, transmittance, and clarity are measured on solvent-cast films using the Haze Gard plus (BYK-Gardner GmbH).

Transmission electronic microscope imaging (TEM)

The morphology of the samples is investigated by transmission electronic microscope (TEM, 60 kV, Zeiss EM10, Carl Zeiss AG). Ultrathin sections of the samples (approximate thickness 40 nm) were microtomed from a specimen (solvent cast films were embedded in epoxy resin) using a UTC ultramicrotomy device (Leica Microsystems). The temperature of the chamber and of the blade was fixed at − 20 °C and the temperature of the sample was − 50 °C.

Differential scanning calorimeter (DSC)

The thermal properties of the polymers are measured using a differential scanning calorimeter (Mettler Toledo DSC 822E) in a nitrogen flow (20 ml/min). The DSC is calibrated periodically with indium and zinc standards. For the measurements, 7 (±0,1) mg of polymer is weighed and sealed in 40 µL aluminum pan. Prior to measurements, the sample is dried for 12 hours at 60 °C in vacuum oven. The data evaluation is carried out with STARe evaluation software form Mettler-Toledo AG.

All samples are measured under nitrogen atmosphere in the temperature range of -100-200 °C. Samples are heated from -100 °C to 200 °C at a rate of 10 °C/min (first heating cycle). After a period of 5 min the sample is cooled at 10°C/min to -100 °C and reheated to 200 °C at a rate of 10°C/min (second heating cycle). In order to evaluate material properties without processing effects, thermograms of the first cooling and second heating cycle are analyzed. From the second heating cycle, glass transition temperature (T_g) is detected.

9. List of abbreviations

Abbreviation	Meaning
μ	Conversion of polymerization
AA	Acrylic acid
ABS	Acrylonitrile butadiene styrene
AIBN	Azobisisobutyronitrile
AMA	Allyl methacrylate
ASA	Acrylonitrile styrene acrylate
ATRP	Atom transfer radical polymerization
BA	Butyl acrylate
BBD	Box-Behnken design
BPO	Benzoyl peroxide
Đ	Dispersity index
DCPA	Dihydrodicyclopentadienyl acrylate
DoE	Design-of-experiments
FTIR	Fourier transform infrared spectroscopy
GA	Glycidyl acrylate
GMA	Glycidyl methacrylate
HIPS	High impact polystyrene
HPLC	High performance liquid chromatography
h-PS	Homo-polystyrene
KPS	Potassium persulfate
M_n	Number average molecular weight
Nacr	Number of acryloyl moieties per backbone chain
NMR	Nuclear magnetic resonance spectroscopy
NSF	Non-soluble fraction
PB	Polybutadiene
PBA	Polybutylacrylate
PBA-g-PS	Polybutylacrylate-graft-polystyrene
PB-g-PS	Polybutadiene-graft-polystyrene
PC	Polycarbonate
PBMA	Polybutylmethacrylate

PMMA	Polymethylmethacrylate
PS	Polystyrene
RAFT	Reversible addition−fragmentation chain-transfer polymerization
RI	Differential refractive index detection
SAN	Styrene acrylonitrile
SEC	Size exclusion chromatography
TDT	Ter-dodecanethiol
TEA	Triethylamine
TEM	Transmission electron microscope
T_g	Glass transition temperature
THF	Tetrahydrofuran
TPP	Triphenyl phosphine
UV	Ultraviolet

10. List of figures

11. List of Tables

12. References

1. Simon, E., *Ueber den flüssigen Storax (Styrax liquidus).* Annalen der Pharmacie, 1839. **31**(3): p. 265-277.
2. Scheirs, J., *Historical Overview of Styrenic Polymers*, in *Modern Styrenic Polymers: Polystyrenes and Styrenic Copolymers*. 2003, John Wiley & Sons, Ltd. p. 1-24.
3. Adhikari, R., et al., *Morphology and micromechanical deformation behavior of SB-block copolymers. II. Influence of molecular architecture of asymmetric star block copolymers.* Journal of Applied Polymer Science, 2002. **85**(4): p. 701-713.
4. Chen, C.C. and J.L. White, *Compatibilizing agents in polymer blends: Interfacial tension, phase morphology, and mechanical properties.* Polymer Engineering & Science, 1993. **33**(14): p. 923-930.
5. Butté, A., G. Storti, and M. Morbidelli, *Living Free Radical Polymerization of Styrene*, in *Modern Styrenic Polymers: Polystyrenes and Styrenic Copolymers*. 2003, John Wiley & Sons, Ltd. p. 111-128.
6. Niessner, N. and H. Gausepohl, *Polystyrenes and Styrene Copolymers – An Overview*, in *Modern Styrenic Polymers: Polystyrenes and Styrenic Copolymers*. 2003, John Wiley & Sons, Ltd. p. 25-42.
7. Listigovers, N.A., et al., *Narrow-Polydispersity Diblock and Triblock Copolymers of Alkyl Acrylates by a "Living" Stable Free Radical Polymerization.* Macromolecules, 1996. **29**(27): p. 8992-8993.
8. Cassebras, M., et al., *Synthesis of di- and triblock copolymers of styrene and butyl acrylate by controlled atom transfer radical polymerization.* Macromolecular Rapid Communications, 1999. **20**(5): p. 261-264.
9. Hawker, C.J., A.W. Bosman, and E. Harth, *New Polymer Synthesis by Nitroxide Mediated Living Radical Polymerizations.* Chemical Reviews, 2001. **101**(12): p. 3661-3688.
10. Dvořánek, L. and P. Vlček, *Anionic polymerization of acrylates.* Polymer Bulletin, 1993. **31**(4): p. 393-399.
11. Vlcek, P., et al., *Anionic Polymerization of Acrylates. 10. Synthesis and Characterization of Block Copolymers with Acrylate Blocks.* Macromolecules, 1995. **28**(21): p. 7262-7265.
12. Dvoranek, L. and P. Vlcek, *Anionic Polymerization of Acrylates. 8. Kinetics of the Anionic Polymerization of Butyl Acrylate Initiated with the Complex Initiator Lithium Ester Enolate/Lithium tert-Butoxide.* Macromolecules, 1994. **27**(18): p. 4881-4885.
13. Portl, T., *NanoHIPS als schlagzähmodifizierter Thermoplast*. 2011, Technischen Universität Darmstadt.
14. McKee, G.E., et al., *Synthesis, Properties and Applications of Acrylonitrile–Styrene–Acrylate Polymers*, in *Modern Styrenic Polymers: Polystyrenes and Styrenic Copolymers*. 2003.
15. HH., K., *Polymer fracture. 2nd ed.* . 1987: Heidelberg-Berlin: Springer.
16. Mark, J.E., *Mechanical Properties of Polymers Based on Nanostructure and Morphology. Edited by Georg H. Michler and Francisco J. Balta'-Calleja.* Angewandte Chemie International Edition, 2006. **45**(37): p. 6080-6080.
17. Kausch, H.H., *Crazing in Polymers*. Vol. 1. 1983: Springer-Verlag Berlin Heidelberg.
18. Wu, S., *Chain structure, phase morphology, and toughness relationships in polymers and blends.* Polymer Engineering & Science, 1990. **30**(13): p. 753-761.
19. Adhikari, R., *Correlation between Molecular Architecture, Morphology, and Deformation Behaviour of Styrene/Butadiene Block Copolymers and blends*. 2001, Martin-Luther-Universität Halle-Wittenberg: Halle, Germany.

20. Adhikari, R., et al., *Relationship between nanostructure and deformation behavior of microphase-separated styrene/butadiene systems.* Journal of Applied Polymer Science, 2006. **101**(2): p. 998-1006.
21. Michler, G.H., H.H. Kausch, and R. Adhikari, *Modeling of Thin Layer Yielding in Polymers.* Journal of Macromolecular Science, Part B, 2006. **45**(5): p. 727-739.
22. Michler, G.H., et al., *Morphology and micromechanical deformation behavior of styrene/butadiene-block copolymers. I. Toughening mechanisms in asymmetric star block copolymers.* Journal of Applied Polymer Science, 2002. **85**(4): p. 683-700.
23. van der Sanden, M.C.M., H.E.H. Meijer, and P.J. Lemstra, *Deformation and toughness of polymeric systems: 1. The concept of a critical thickness.* Polymer, 1993. **34**(10): p. 2148-2154.
24. van der Sanden, M.C.M., H.E.H. Meijer, and T.A. Tervoort, *Deformation and toughness of polymeric systems: 2. Influence of entanglement density.* Polymer, 1993. **34**(14): p. 2961-2970.
25. Hartmann, L., et al., *Molecular dynamics in thin films of isotactic poly(methyl methacrylate).* Eur. Phys. J. E, 2002. **8**(2): p. 145-154.
26. Wang, X. and W. Zhou, *Glass Transition of Microtome-Sliced Thin Films.* Macromolecules, 2002. **35**(18): p. 6747-6750.
27. Möginger, B., G.H. Michler, and H.C. Ludwig, *ABS — Sprödbruch-Untersuchungen der Morphologie-Versagens-Beziehung*, in *Deformation und Bruchverhalten von Kunststoffen*, W. Grellmann and S. Seidler, Editors. 1998, Springer Berlin Heidelberg: Berlin, Heidelberg. p. 301-318.
28. Thomas, E.L., et al., *Phase morphology in block copolymer systems.* Philosophical Transactions of the Royal Society of London. Series A: Physical and Engineering Sciences, 1994. **348**(1686): p. 149-166.
29. Calleja, F.J.B. and Z. Roslaniec, *Block Copolymers*. 2000, New York: Marcel Dekker Publishers.
30. Bates, F.S. and G.H. Fredrickson, *Block copolymers-designer soft materials.* Physics Today, 1999. **52**(2): p. 32-38.
31. Hamley, I.W., *The Physics of Block Copolymers*. 1998, Oxford: Oxford Science Publications.
32. Matshuhita, Y., *Block and graft copolymers*, in *Structures & Properties of Multiphase Polymeric Materials* 1998, Marcel Dekker Inc.
33. Hamley, I., *The Physics of Block Copolymers*. 1998: Oxford Science Publications.
34. Sakurai, S., *Control of morphology in block copolymers.* Trends in Polymer Science, 1995. **3**: p. 90-98.
35. Hasegawa, H. and T. Hashimoto, *14 - Self-assembly and Morphology of Block Copolymer Systems*, in *Comprehensive Polymer Science and Supplements*, G. Allen and J.C. Bevington, Editors. 1996, Pergamon: Amsterdam. p. 497-539.
36. Adhikari, R. and G.H. Michler, *Nanostructures of two-component amorphous block copolymers: Effect of chain architecture*. 2005. p. 81-130.
37. Adhikari, R., et al., *Correlation between Molecular Architecture, Morphology, and Deformation Behaviour of Styrene/Butadiene Block Copolymers.* Macromolecular Chemistry and Physics, 2003. **204**(3): p. 488-499.
38. Cowie, J.M.G., *Developments in block copolymers-I*, ed. I. Goodman. 1982, London: Applied Science Publishers.
39. Khandpur, A.K., et al., *Polyisoprene-Polystyrene Diblock Copolymer Phase Diagram near the Order-Disorder Transition.* Macromolecules, 1995. **28**(26): p. 8796-8806.
40. Woodward, A.E., *Atlas of polymer morphology*. 1988, Munich: Hanser Publishers.

41. Hajduk, D.A., et al., *The Gyroid: A New Equilibrium Morphology in Weakly Segregated Diblock Copolymers.* Macromolecules, 1994. **27**(15): p. 4063-4075.
42. Hajduk, D.A., et al., *A Reevaluation of Bicontinuous Cubic Phases in Starblock Copolymers.* Macromolecules, 1995. **28**(7): p. 2570-2573.
43. Stadler, R., et al., *Morphology and Thermodynamics of Symmetric Poly(A-block-B-block-C) Triblock Copolymers.* Macromolecules, 1995. **28**(9): p. 3080-3097.
44. Mogi, Y., et al., *Superlattice Structures in Morphologies of the ABC Triblock Copolymers.* Macromolecules, 1994. **27**(23): p. 6755-6760.
45. Abetz, V. and T. Goldacker, *Formation of superlattices via blending of block copolymers.* Macromolecular Rapid Communications, 2000. **21**(1): p. 16-34.
46. Breiner, U., et al., *Structural Characterization of the "Knitting Pattern" in Polystyrene-block-poly(ethylene-co-butylene)-block-poly(methyl methacrylate) Triblock Copolymers.* Macromolecules, 1998. **31**(1): p. 135-141.
47. Mogi, Y., et al., *Preparation and morphology of triblock copolymers of the ABC type.* Macromolecules, 1992. **25**(20): p. 5408-5411.
48. Mogi, Y., et al., *Tricontinuous morphology of triblock copolymers of the ABC type.* Macromolecules, 1992. **25**(20): p. 5412-5415.
49. Shibayama, M., et al., *Microdomain structure of an ABC-type triblock polymer of polystyrene-poly[(4-vinylbenzyl)dimethylamine]-polyisoprene cast from solutions.* Macromolecules, 1982. **15**(2): p. 274-280.
50. Milner, S.T., *Chain Architecture and Asymmetry in Copolymer Microphases.* Macromolecules, 1994. **27**(8): p. 2333-2335.
51. Matsen, M.W., *Equilibrium behavior of asymmetric ABA triblock copolymer melts.* The Journal of Chemical Physics, 2000. **113**(13): p. 5539-5544.
52. Lee, C., et al., *H-shaped double graft copolymers: Effect of molecular architecture on morphology.* The Journal of Chemical Physics, 1997. **107**(16): p. 6460-6469.
53. Knoll, K. and N. Nießner, *Styrolux+ and styroflex+ - from transparent high impact polystyrene to new thermoplastic elastomers: Syntheses, applications and blends with other styrene based polymers.* Macromolecular Symposia, 1998. **132**(1): p. 231-243.
54. Hadjichristidis, N., et al., *Asymmetric Star Polymers: Synthesis and Properties*, in *Branched Polymers I*, J. Roovers, Editor. 1999, Springer Berlin Heidelberg: Berlin, Heidelberg. p. 71-127.
55. Hadjichristidis, N., et al., *Morphology and miscibility of miktoarm styrene-diene copolymers and terpolymers.* Macromolecules, 1993. **26**(21): p. 5812-5815.
56. Knoll, K., *Anionische Blockcopolymere*, in *Kunststoff-Handbuch: 4. Polystyrol*, H.G.e. al., Editor. 1996, Hanser Verlag, München. p. 145-166.
57. Aggarwal, S.L., *Introduction and overview* in *Processing, structure and properties of block copolymers*, M.J. Folkes, Editor. 1986, Elsevier Applied Publishers: London. p. 125-164.
58. Holden, G., *Understanding thermoplastic elastomers*. 2000, Carl Hanser Verlag: Munich. p. 15-35.
59. Holden, G., *Application of Thermoplastic Elastomers*, in *Thermoplastic Elastomers, 2nd Edition*, N.R.L. G. Holden, R.P. Quirk and H.E. Schroeder, Editor. 1998, Hanser Publishers: Munich. p. 574-601.
60. Folkes, R.G.C.A.a.M.J., *Block copolymers and blends as composite materials* in *Processing, structure and properties of block copolymers*, M.J. Folkes, Editor. 1986, Elsevier applied science publishers: London. p. 125-164.

61. Hashimoto, H., et al., *Domain-boundary structure of styrene-isoprene block copolymer films cast from solutions. 7. Quantitative studies of solubilization of homopolymers in spherical domain system.* Macromolecules, 1981. **14**(3): p. 844-851.
62. Hashimoto, T., H. Tanaka, and H. Hasegawa, *Ordered structure in mixtures of a block copolymer and homopolymers. 2. Effects of molecular weights of homopolymers.* Macromolecules, 1990. **23**(20): p. 4378-4386.
63. Koizumi, S., H. Hasegawa, and T. Hashimoto, *Ordered structure of block polymer/homopolymer mixtures, 4. Vesicle formation and macrophase separation.* Makromolekulare Chemie. Macromolecular Symposia, 1992. **62**(1): p. 75-91.
64. Koizumi, S., H. Hasegawa, and T. Hashimoto, *Spatial Distribution of Homopolymers in Block Copolymer Microdomains As Observed by a Combined SANS and SAXS Method.* Macromolecules, 1994. **27**(26): p. 7893-7906.
65. Koizumi, S., H. Hasegawa, and T. Hashimoto, *Ordered Structures of Block Copolymer/Homopolymer Mixtures. 5. Interplay of Macro- and Microphase Transitions.* Macromolecules, 1994. **27**(22): p. 6532-6540.
66. Feng, H., Z. Feng, and L. Shen, *Miscibility, Microstructure, and Dynamics of Blends Containing Block Copolymer. 2. Microstructure of Blends of Homopolystyrene with Styrene-Butadiene Block Copolymers.* Macromolecules, 1994. **27**(26): p. 7835-7839.
67. Feng, H., Z. Feng, and L. Shen, *Miscibility, Microstructure, and Dynamics of Blends Containing Block Copolymer. 3. Molecular Motion in Homopolystyrene and Polystyrene/Four-Arm Styrene-Butadiene Star Block Copolymer Blends.* Macromolecules, 1994. **27**(26): p. 7840-7842.
68. Feng, H., et al., *Miscibility, Microstructure, and Dynamics of Blends Containing Block Copolymer. 1. Miscibility of Blends of Homopolystyrene with Styrene-Butadiene Block Copolymers.* Macromolecules, 1994. **27**(26): p. 7830-7834.
69. Fujimura, M., T. Hashimoto, and H. Kawai, *Structural Change Accompanied by Plastic-to-Rubber Transition of SBS Block Copolymers.* Rubber Chemistry and Technology, 1978. **51**(2): p. 215-224.
70. Kawai, H., et al., *Microdomain structure and some related properties of block copolymers. II. Plastic deformation mechanisms of the glassy component in rubber-toughened plastics.* Journal of Macromolecular Science, Part B, 1980. **17**(3): p. 427-472.
71. Hashimoto, T., et al., *Strain-Induced Plastic-to-Rubber Transition of a SBS Block Copolymer and Its Blend with PS*, in *Multiphase Polymers*. 1979, AMERICAN CHEMICAL SOCIETY. p. 257-275.
72. Sakurai, S., et al., *Preferential Orientation of Lamellar Microdomains Induced by Uniaxial Stretching of Cross-Linked Polystyrene-block-polybutadiene-block-polystyrene Triblock Copolymer.* Macromolecules, 2001. **34**(11): p. 3672-3678.
73. Cohen, Y., et al., *Deformation of Oriented Lamellar Block Copolymer Films.* Macromolecules, 2000. **33**(17): p. 6502-6516.
74. Michler, G.H., R. Adhikari, and S. Henning, *Micromechanical properties in lamellar heterophase polymer systems.* Journal of Materials Science, 2004. **39**(10): p. 3281-3292.
75. Cohen, Y., M. Brinkmann, and E.L. Thomas, *Undulation, dilation, and folding of a layered block copolymer.* The Journal of Chemical Physics, 2001. **114**(2): p. 984-992.
76. Huy, T.A., R. Adhikari, and G.H. Michler, *Deformation behavior of styrene-block-butadiene-block-styrene triblock copolymers having different morphologies.* Polymer, 2003. **44**(4): p. 1247-1257.
77. Rosenau, B., Kunststoffe, 1995. **85**: p. 805.
78. Zahn, A., Kunststoffe, 1997. **87**: p. 314.

79. Weidisch, R., et al., *Mechanical properties of weakly segregated block copolymers: 1. Synergism on tensile properties of poly(styrene-b-n-butylmethacrylate) diblock copolymers.* Polymer, 1999. **40**(5): p. 1191-1199.
80. Weidisch, R., G.H. Michler, and M. Arnold, *Mechanical properties of weakly segregated block copolymers 2. The influence of phase behaviour on tensile properties of poly(styrene-b-butylmethacrylate) diblock copolymers.* Polymer, 2000. **41**(6): p. 2231-2240.
81. Weidisch, R., et al., *Mechanical Properties of Weakly Segregated Block Copolymers. 3. Influence of Strain Rate and Temperature on Tensile Properties of Poly(styrene-b-butyl methacrylate) Diblock Copolymers with Different Morphologies.* Macromolecules, 1999. **32**(3): p. 742-750.
82. Weidisch, R., et al., *Mechanical properties of weakly segregated block copolymers Part IV Influence of chain architecture and miscibility on tensile properties of block copolymers.* Journal of Materials Science, 2000. **35**(5): p. 1257-1268.
83. *Radical Chain Polymerization*, in *Principles of Polymerization*. 2004. p. 198-349.
84. *Emulsion Polymerization*, in *Principles of Polymerization*. 2004. p. 350-371.
85. Cowie, J.M.G., *3 - Block and Graft Copolymers*, in *Comprehensive Polymer Science and Supplements*, G. Allen and J.C. Bevington, Editors. 1996, Pergamon: Amsterdam. p. 33-42.
86. Schierholz, J.U. and G.P. Hellmann, *In situ graft copolymerisation: salami morphologies in PMMA/EP blends: part I.* Polymer, 2003. **44**(7): p. 2005-2013.
87. Huang, N.-J. and D.C. Sundberg, *Fundamental studies of grafting reactions in free radical copolymerization. I. A detailed kinetic model for solution polymerization.* Journal of Polymer Science Part A: Polymer Chemistry, 1995. **33**(15): p. 2533-2549.
88. Huang, N.-J. and D.C. Sundberg, *Fundamental studies of grafting reactions in free radical copolymerization. II. Grafting of styrene, acrylate, and methacrylate monomers onto cis-polybutadiene using AIBN initiator in solution polymerization.* Journal of Polymer Science Part A: Polymer Chemistry, 1995. **33**(15): p. 2551-2570.
89. Huang, N.-J. and D.C. Sundberg, *Fundamental studies of grafting reactions in free radical copolymerization. III. Grafting of styrene, acrylate, and methacrylate monomers onto cis-polybutadiene using benzoyl peroxide initiator in solution polymerization.* Journal of Polymer Science Part A: Polymer Chemistry, 1995. **33**(15): p. 2571-2586.
90. Huang, N.-J. and D.C. Sundberg, *Fundamental studies of grafting reactions in free radical copolymerization. IV. Grafting of styrene, acrylate, and methacrylate monomers onto vinyl-polybutadiene using benzoyl peroxide and AIBN initiators in solution polymerization.* Journal of Polymer Science Part A: Polymer Chemistry, 1995. **33**(15): p. 2587-2603.
91. Zammit, M.D., et al., *Evaluation of the Mode of Termination for a Thermally Initiated Free-Radical Polymerization via Matrix-Assisted Laser Desorption Ionization Time-of-Flight Mass Spectrometry.* Macromolecules, 1997. **30**(7): p. 1915-1920.
92. H. F. Mark, N.M.B., C. G. Overberger, and G. Menges, *Encyclopedia of Polymer Science and Engineering*. 1985, New York: Wiley-Interscience.
93. Dhal, P.K., M.S. Ramakrishna, and G.N. Babu, *Copolymerization of glycidyl methacrylate with alkyl acrylate monomers.* Journal of Polymer Science: Polymer Chemistry Edition, 1982. **20**(6): p. 1581-1585.
94. Roos, S.G., A.H.E. Müller, and K. Matyjaszewski, *Copolymerization of n-Butyl Acrylate with Methyl Methacrylate and PMMA Macromonomers: Comparison of Reactivity Ratios in Conventional and Atom Transfer Radical Copolymerization.* Macromolecules, 1999. **32**(25): p. 8331-8335.

95. Yokota, K., M. Kani, and Y. Ishii, *Determination of propagation and termination rate constants for some methacrylates in their radical polymerizations.* Journal of Polymer Science Part A-1: Polymer Chemistry, 1968. **6**(5): p. 1325-1339.
96. Bakhshi, H., et al., *Spectral and chemical determination of copolymer composition of poly (butyl acrylate-co-glycidyl methacrylate) from emulsion polymerization.* Polymer Testing, 2009. **28**(7): p. 730-736.
97. Lovell, P., T. Shah, and F. Heatley, *Correlation of the Extent of Chain Transfer to Polymer with Reaction Conditions for Emulsion Polymerization of n -Butyl Acrylate*. 1992. p. 188-202.
98. Ahmad, N.M., F. Heatley, and P.A. Lovell, *Chain Transfer to Polymer in Free-Radical Solution Polymerization of n-Butyl Acrylate Studied by NMR Spectroscopy.* Macromolecules, 1998. **31**(9): p. 2822-2827.
99. Dotson, N.A., et al., *Polymerization Process Modeling*, in *Polymerization Process Modeling*. 1996, VCH Publishers, Inc. p. 260–279.
100. Odian, G., *Radical Chain Polymerization*, in *Principles of Polymerization*. 2004. p. 198-349.
101. Siołek, M. and M. Matlengiewicz, *Reactivity Ratios of Butyl Acrylates in Radical Copolymerization with Methacrylates.* International Journal of Polymer Analysis and Characterization, 2014. **19**(3): p. 222-233.
102. M. Catala, J., et al., *Radical copolymerization of 2-hydroxyethylacrylate with alkylacrylate*. Vol. 15. 1986. 311-315.
103. Le, A.N., R. Liang, and M. Zhong, *Synthesis and Self-Assembly of Mixed-Graft Block Copolymers.* 2019. **25**(35): p. 8177-8189.
104. Sperling, L.H., *Introduction to physical polymer science, 2nd Edition*. 1992, Wiley-Interscience Publication. p. 122-150.
105. Andrews, R.G., EA., *Glass Transition Temperatures of Polymers*, in *The Wiley Database of Polymer Properties*. 1999.
106. Shen, K., et al., *Poly(styrene–isoprene–butadiene-g-SAN) graft copolymers: Size-controllable synthesis and their toughening properties.* Colloids and Surfaces A: Physicochemical and Engineering Aspects, 2015. **467**: p. 216-223.
107. Huang, N.-J. and D.C. Sundberg, *A gel permeation chromatography method to determine grafting efficiency during graft copolymerization.* Polymer, 1994. **35**(26): p. 5693-5698.

Erklärungen

§8 Abs. 1 lit. c der Promotionsordnung der TU Darmstadt

Ich versichere hiermit, dass die elektronische Version meiner Dissertation mit der schriftlichen Version übereinstimmt und für die Durchführung des Promotionsverfahrens vorliegt.

§8 Abs. 1 lit. d der Promotionsordnung der TU Darmstadt

Ich versichere hiermit, dass zu einem vorherrigen Zeitpunkt noch keine Promotion versuchtwurde und zu keinem früheren Zeitpunkt an einer in- oder ausländischen Hochschuleeingereicht wurde. In diesem Fall sind nähere Angaben über Zeitpunkt, Hochschule,Dissertationsthema und Ergebnis dieses Versuchs mitzuteilen.

§9 Abs. 1 der Promotionsordnung der TU Darmstadt

Ich versichere hiermit, dass die vorliegende Dissertation selbstständig und nur unterVerwendung der angegebenen Quellen verfasst wurde.

§9 Abs. 2 der Promotionsordnung der TU Darmstadt

Die Arbeit hat bisher noch nicht zu Prüfungszwecken gedient.

Darmstadt, 14 Dezember 2023

Julien Fage